Max-Planck Institut für Kolloid- und Grenzflächenforschung

Heterogeneous Catalysis for the Conversion of Fructose to Chemicals and Fuel in a Continuous Flow Process

Dissertation

zur Erlangung des akademischen Grades
"doctor rerum naturalium"
(Dr. rer. nat.)

in der Wissenschaftsdisziplin „Kolloidchemie“
eingereicht an der
Mathematisch-Naturwissenschaftlichen Fakultät
der Universität Potsdam

von
Max Braun

geboren am 29.01.1989 in Würzburg

Potsdam, September 2017

Published online at the
Institutional Repository of the University of Potsdam:
URN urn:nbn:de:kobv:517-opus4-410370
http://nbn-resolving.de/urn:nbn:de:kobv:517-opus4-410370

Table of Contents

1. Introduction

1.1. Motivation

In July 2016 the EU published a report named “A Study on Oil Dependency in the EU”.[1] This report summarizes how addicted all 28 members of the union were on oil in 2016, including import statistics, price as well as future developments. The overall conclusion drafted shows an 88 % import dependency, mostly on countries, in which the political situation is tense or does not correlate with the general understanding on which the EU is based. If this dependency stays as high as it was in 2016, and it is even predicted to rise in the near future, as it was rising about 10 % since the year 2000, the whole petrochemical as well as chemical industry can become a cue ball of other countries or at least become vulnerable in terms of the supply chain. Almost every product synthesized, speaking mostly of transportation fuel, but also of consumables or even food products are directly or indirectly depended on raw oil. This dependency started basically with the industrial revolution in the 19th century, with having access to cheap energy, what enabled the industry to produce consumables and other products in mass production scale.[2] Our addiction is therefore historically grown and almost all bulk chemicals are produced out of, or with oil.[3] This dependency is nowadays hard to fight, not at least because of missing alternative production routes of chemicals[4], currently derived from oil. To overcome this lack of knowledge and to direct the research in meaningful channels, the US Department of Energy published a list of 12 chemicals in 2004, which are believed to play an important role in the future and can be produced out of biomass.[5] Among these chemicals someone can find 2,5-furandicarboxylic acid as well as levulinic acid. In terms of synthesis, 5-hydroxymethylfurfural goes ahead as a precursor in both cases[6], which can be converted from sugar and therefore theoretically from cellulose.[7]

Seeing petroleum as a product of biomass, stored under pressure and temperature for millions of years, it is easy to understand that also fresh biomass can theoretically be converted to the already known chemicals and fuels derived from crude oil[8]. The carbon cycle[9] and the release of CO_2 is theoretically closed for fuels when using fresh biomass. Biofuels can help to end the enrichment in the atmosphere to stop the increase of

temperature and soften the greenhouse effect. The plant uses the released CO_2 again for building up sugars with the energy of sunlight ($nCO_2 + nH_2O \rightarrow (CH_2O)_n + nO_2$).

The previously existing knowledge of biorefinery and technology experienced a damper during the 19th and 20th century, when the cheap and available oil became present everywhere, and more and more oil fields were made accessible.[10] Also nowadays the access to coal and especially gas is promoted again, thinking of new techniques like fracking[11] or strip mining[12]. The knowledge and science of biorefinery research was on the rise before the cheap oil came onto the market. Even automobiles could be fueled by an integrated gasification system of wood, what is mostly forgotten nowadays.[13] The reestablishment of this refinery using biomass, and the understanding, together with the enhancements today is necessary to fight the subjection on fossil resources in terms of energy and chemicals. One abundant biomass molecule, which conserves the energy of the sunlight and acts as power-storage in plants is a carbohydrate named glucose. This molecule is often polymerized (also with other sugars) to cellulose and hemicellulose.[14] The composition of biomass (mainly hemicellulose, cellulose and lignin) was soon discovered, and the separation and break down techniques like saccharification for cellulose were already well established in the 19th century, while also the molecular mechanisms were known.[15] As lignin represents a source for aromatic molecules[16], cellulose can be converted to mostly glucose, a hexose sugar, whereas hemicellulose can be broken down to mainly xylose, a pentose carbohydrate, in a first depolymerization step. These different carbohydrates and their isomers like fructose contain promising properties, which makes them suitable for further upgrade.[17]

Considering that industry is not highly interested in lab mode and batch processes, continuous approaches need to be researched on more intense, as they are more cost effective in terms of labor, maintenance and economy.[18] With additionally respecting the twelve principles of green chemistry[19], a sustainable and stable future for the chemical industry can be realized. One major aspect is the development of continuous processes for biomass upgrade, as well as the investigation of inserting biomass and biorefinery into the already existing chemical landscape. Addressing all these points, together with using raw materials from non-food derived sources, can hold the future for “green” transportation fuel as well as chemicals. Additionally the usage of biomass need to consider the full chain of

products and cannot just focus on a single one. Managing "waste streams"[20] and finding applications for additionally produced molecules can make the upgrade as a whole profitable already in the near future, even when compared to traditional (petro)-chemical industry.

Glucose and its isomer fructose are theoretically available by saccharification of wood and other biomass[21]. A further upgrade towards 5-hydroxymethylfurfural (HMF) or ethyllevulinate (EL) is necessary, addressing the need of a continuous production of fuel and chemicals out of sugar. Furanic molecules are seen as a possible alternative entry into fuel production (DMF)[22] [23], polymerization (FDCA)[6a] or furan based chemicals, which are often considered as the "sleeping giants", because of their big variety of application.[24] EL can be used as a biofuel additive in fuel blends and therefore also contributes to the concept of "green" fuels.[25] As already mentioned, the saccharification of wood is already known since the 19th century and was used to produce mainly ethanol by fermentation[26] with microorganisms. The acidic breakdown of glycosidic bonds does not only result in pure sugar solutions, but also in harmful and dangerous products for the human health by consecutive reactions. Therefore the sugar products cannot be used for food or even feed production from wood, what was the primary purpose during war times and hunger crises.

These days the catalytic process is mostly relying on the homogeneous catalysis with strong acids like sulfuric acid[27], what makes the whole approach difficult to use in continuous systems, due to the difficult recyclability as well as corrosion effects. Another disadvantage is the already mentioned manifold product distribution that arises during the process. The selectivity towards one or two desirable products is not easy and can mainly be achieved by using specifically designed catalysts. Glucose as well as fructose are considered as cheap entry molecules for a further continuous upgrade towards HMF, using heterogeneous catalysts. 5-Hydroxymethylfurfural itself consists of a furanic ring as backbone, on which an alcohol as well as an aldehyde functional group are located at the C_2 and C_6 position. This characteristic makes it suitable for further functionalization as well as offers opportunity for modification. [28]

HMF is already a highly valuable product, in terms of further upgrade and a brought variety of possible usage.[29] HMF (boiling point: 291 °C) itself does not offer sufficient fuel properties, as it still contains three oxygen atoms. This increased oxygen amount is typical

for biomass-derived molecules. The high oxygen content brings disadvantages during a combustion process[30], like a decreased energy density, high boiling points as well as an incomplete combustion. The resulting molecules can contaminate the engine and carbon formation on the motor chamber walls can be observed. When the research octane number (RON) is too low, the fuel tends to combust already too early when no optimal conditions in the chamber are reached. This phenomenon is known as engine knocking.[31] Therefore, the upgrade towards molecules with a higher H / O ratio is desirable.[32] A schematic comparison and examples of different molecules obtained from fructose with diverse hydrogen to oxygen ratios in comparison to their boiling points and RONs are shown in figure 1.

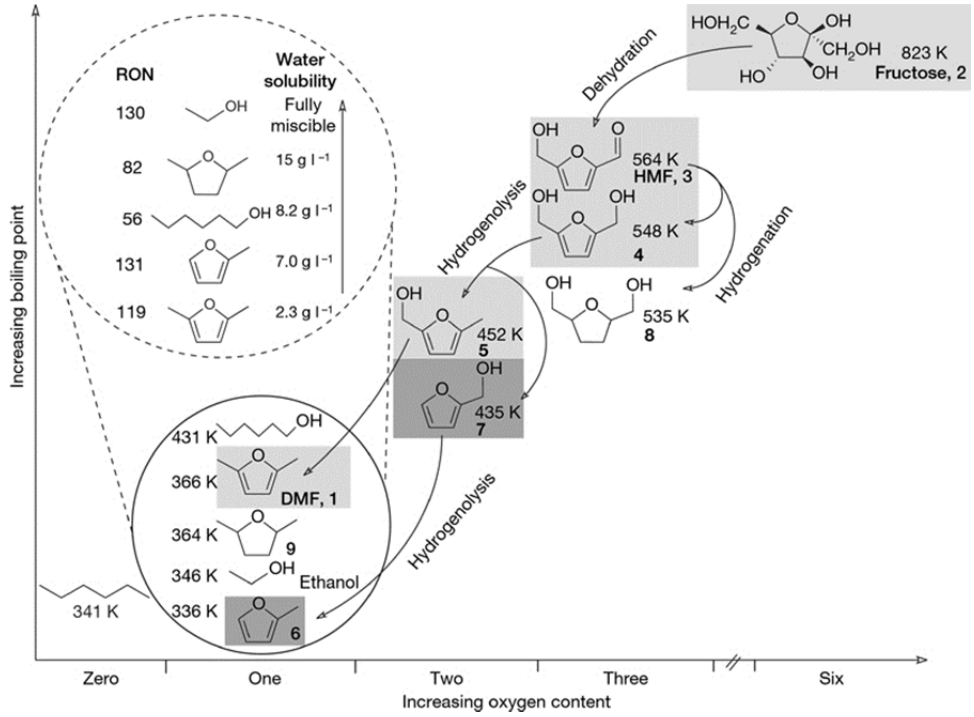

Figure 1: Dependency of oxygen content to the boiling point. The RON as well as the water solubility are as well given for diverse possible products from the dehydration and hydrogenolysis of fructose. (Adapted from Roman-Leshkov et al) [33]

For producing a biofuel valuable enough to compete on the market today, several criteria are necessary. First of all, the molecule should bring a high internal energy, which can be released during the combustion process. The main goal should be the storage of as much energy in the molecule´s structure and bonds as possible to improve the overall energy what can be released during the combustion. The oxidation will break down the molecule and releases the stored energy, until in the best case only CO_2 and water are left. On the

background of the highly praised biodiesel, but by realizing the manipulation by many combustion engine car manufacturers, a real “green” alternative is desirable to be found. Additionally the awareness of the production conditions of fuels is rising. People start understanding, that clearing the forest for growing palm oil for biofuel[34], as well as the bad energy balances for bioethanol[35] (Gasoline E10, 10 % ethanol / fuel blend, Germany) cannot be sustainable, when energy even gets lost during the production process. The overall energy balance of fructose to DMF conversion on the other hand shows the storage of nearly 90 % of the energy transferred by the sun during the photosynthesis process, when upgraded by hydrogenation. This fact, as well as the additional immiscibility with water (2.3 g L^{-1}, figure 1) can make DMF a good candidate for an alternative biofuel[36]. The high RON of 119[37] is almost in the same range of methane with 120[38], whereas DMF is not a gas under atmospheric conditions, but a liquid. Race fuels typically have RONs higher than 110, which underline the potential of the DMF molecule as a high performance liquid fuel.[39] Another issue is the usage of already existing infrastructure. As DMF is in liquid form under normal atmospheric conditions, it can be handled in a similar way as we handle gasoline at the moment. The very low miscibility with water is a great advantage compared to for example bioethanol, whose volumetric energy density is only 2 / 3 of the one of gasoline, as well as a full miscibility with water is possible.

In context to all these promising facts, we believe DMF and EL can be a sustainable alternative to fuels (and chemicals), mainly obtained from fossil feedstocks at the moment. The development of a continuous catalytic system, using suitable heterogeneous catalysts will be the key for their profitable production.

1.2. Current status, potential and basic concepts of biorefinery

Today we define biorefinery as a process converting biomass to highest extents into valuable products such as chemicals, fuels, power and heat.[40] The entire processes and methods are orientated on the processes used in the (petro)-chemical industry and refining. Flow methods and catalysis systems in biorefinery are similar and are tried to become implemented into the existing flow and production sites. By having these similarities, it is also tried to substitute some of the fossil feedstocks with biomass or at least to complement it into running plants and sites. Some studies have already shown promising and beneficial results, adding biomass derived molecules directly into the process flow together with fossil compounds.[41]

The basic idea of biorefinery is always the usage of nature´s synthesis capability and keeping the complexity or stored energy in the final product. Nature developed several highly efficient pathways to produce complex molecules using mainly sunlight as direct or indirect power source. The overall photosynthetic efficiency is in fact only 4 to 6 %[42], whereas nevertheless about 170 billion tons of biomass are growing each year. 75 % of this biomass is allotted to carbohydrates, by which only 3-4 % are dispensed with human´s nutrition and secondary use. The rest of the carbohydrates are viewed as feedstock for green chemistry.[43] Anyway these processes are efficient enough to build up cellulose with an amount of approximately 10^{11} to 10^{12} tons per annum, which is therefore the most abundant renewable polymer worldwide.[44] The synthesized glucose chains can be used directly, but also enhancement is explored, using genetic engineering of plants in order to improve their properties.[45] Furthermore on basis of all these molecules from nature, biorefinery aims to purify and further upgrade the products of conversion into valuable chemicals and materials.

After the extraction of all useful material and substances, the rest of the biomass is simply burned for power und heat at the moment. But because more and more research is focused onto the usage of raw biomass, more ways are discovered to also utilize molecules that were not usable before. In this context lignin is a good example.[46] The rigid and resistant polymeric molecule is not easy to break and therefore not easy to utilize in a chemical sense.[47] The ether and internal bonds are holding the aromatic monomers strongly together, making it difficult for concerted breakage. Recent research investigates how

homogeneous and heterogeneous catalysis can achieve the aim of a more selective breakage, obtaining aromatic bulk chemicals. By using for example nickel-based heterogeneous catalysts, it is possible to selectively cleave the ether bonds, as recently shown by Molinari et al.[16] These nickel catalysts are non-noble and therefore cheap and abundant alternatives for heterogeneous hydrogenation, also used for the upgrade of cellulose and hemicellulose derived molecules.[48]

Cellulose and hemicellulose are polymers of sugar molecules, whereas cellulose is build-up of beta(1-4)-glycosidic connected D-glucose molecules. These six carbon chain sugars are able to be converted to chemicals and building blocks like alcohols[49], sugar acids[50] or furanic molecules.[51] The C_5 sugars extracted from hemicellulose can be converted to furanic-ring molecules, whereas furfural[52] or solvents like 2-methyltetrahydrofuran[53] represent the most promising products. All processes make use of fermentation or direct chemical conversion. Figure 2 summarizes the possible sources and products possible, when hexoses (C_6) and pentoses (C_5) are converted.

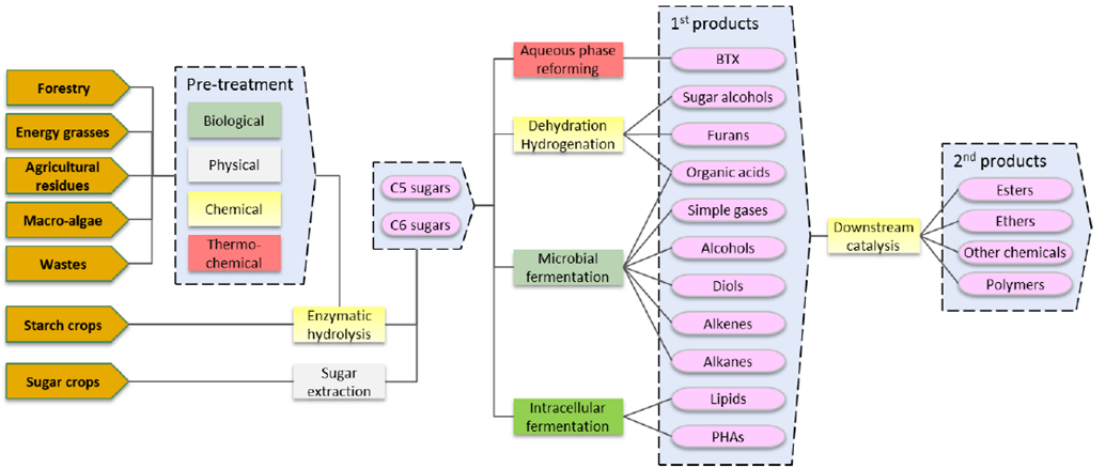

Figure 2: Illustration of possible reaction pathways, starting from starch and sugar crops, as well as other biomasses.[54] This figure summarizes the pre-treatment method, as well as catalysis and fermentation, possible to synthesize different groups of products. Adapted from reference 54.

1.2.1. Basic concepts of catalytic conversion

Thermodynamically all reactions strive for a minimum in energy, meaning all chemical bonds and molecules represent the locally stable form, possible under the current conditions. Molecules contain energy stored in different chemical bonds, but are stable as long as the activation energy to overcome the energy barrier towards even more stable structures is not reached. This activation energy can sometimes be so high (Figure 3, black line), that temperatures and pressures have to be reached, which are beyond to be called economical. In this case, a catalyst can help to lower this activation energy by offering intermediate states (red line). Catalysis therefore accelerates the reaction without touching the reaction equilibrium.[55] This description is summarized in figure 3.

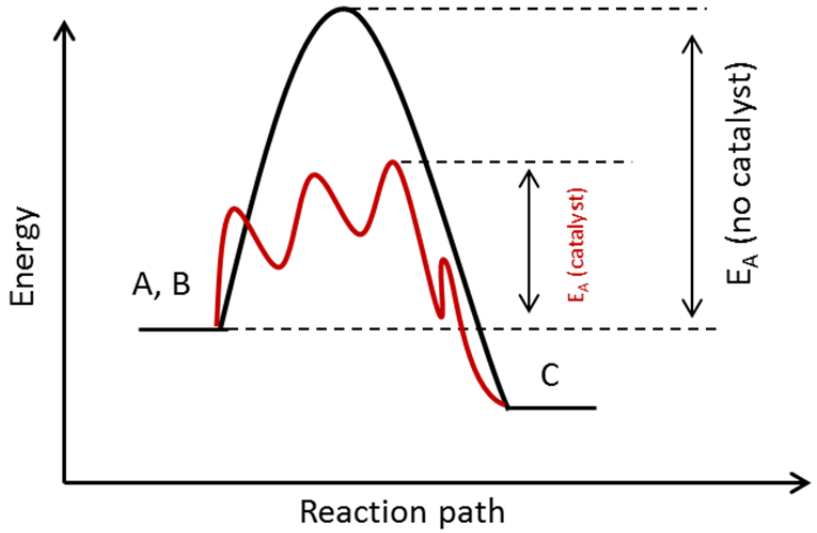

Figure 3: Schematic reaction pathways with (red line) and without (black line) a catalyst. The molecule strives for a minimum energy position, but needs to overcome a certain energy barrier to reach this equilibrium.

For overcoming the first reaction energy barrier (red line) the catalyst´s surface offers active sites, on which molecules can adsorb. These intermediate forms would not be possible without the catalyst.[56] The amount of energy needed towards a next intermediate stage is therefore lower compared to the amount of energy necessary to run the whole reaction (A, B -> C) without a catalyst. Two forms of catalysis can be differentiated:

A catalytic process can be called homogeneous or heterogeneous[57], depending on the solubility of the catalyst in the solvent. If the catalyst is in the same phase as the reactants, speaking in our case of a solution, it is called homogeneous (e.g. sulfuric acid). Is the catalyst

existent in another phase (e.g. a solid in liquid, solid acid catalysts) the reaction is called heterogeneous. Hereby, the borders between these two categories are often not clear, as for instance slight leaching of heterogeneous catalysts can occur. This small dissolving process provides ions, which are solubilized and can act as homogeneous catalysts. In recent years, nanocatalysis bridges the gap between homogeneous and heterogeneous catalysts, as the particle size is made up of only a few atoms. To draw a clear line between nanocatalysis and homogeneous catalysis is also difficult and it is sometimes spoken of a cocktail like catalysis[58], whereas both nanoparticles as well as homogeneous active molecules are existing next to each other. In this study the main focus is on heterogeneous / nanocatalysis. Two advantages that arise from the smaller particles are a high surface area as well as a different electronic surface structure.[59] The surface area increases and with it the number of active sites. With nano-sized particles the atoms in the center of the particle start getting statistically closer to the surface and therefore take influence on the reactivity.[60] This interaction on small scale level can also be observed by using the same (e.g. nickel) nanoparticles, but different supports.[61] The particles interact differently with the scaffold; for example share electrons or the support brings different active sites, whereas different interactions at the interface are possible.[62] Often a so called spillover effect can be observed, using a combination of two materials. The molecules adsorbed can be dissociated on the one material and be shared with the second one. This effect can bring different reactivity, often connected to a specific selectivity at the interface. Bimetallic catalysts make use of this phenomena and a so called synergistic effect can be observed.[63] In here not only the energy of the Lowest Unoccupied Molecular Orbital (LUMO) of the catalyst (e.g. nickel) will be lowered, but also the energy of the Highest Occupied Molecular Orbital (HOMO) of the reactant (e.g. hydrogen) can be lifted. The resulting energy barrier is therefore decreased. Interactions cannot only take place between the reactant and the catalysts, but also between the solvent and the catalytic surface.[64] The solvent molecules are able to cover certain areas and therefore block specific active sites, changing the activity and selectivity. This phenomenon is often observed with ionic liquids, promising solvents for biomass, which also offers catalytic activity.[65]

Next to chemical, also physical parameters are one major point what need to be addressed in catalysis. Each selected conditions are responsible for bringing the (activation) energy into the reaction system. By adjusting mainly temperature and pressure as well as residence

time, the drive of molecules towards the active sites and their conversion can be influenced or even controlled.[66] With higher energy input, a reaction can be accelerated and the distribution of products can be changed respectively. In hydrogenation reactions the catalyst can dissociate more or less hydrogen molecules on the catalysts surface, depending on the partial pressure of the gas. With more hydrogen (without full coverage at lower pressure) the probability of a reaction gets higher, because the molecules are more likely to meet. Also depending on the principle of Le Chatelier[67] and the reaction towards bulkier or even gas phase molecules, the chemical equilibrium can be influenced in favor of the less expanded phase. With an optimization of the chemical reaction in terms of a higher selectivity, a purer solution can be obtained, easier to separate and hence helping to save money, as "waste streams" can make up a huge amount of the costs.[68] Because biomass is a complex mixture of different molecules and structures, someone should always be aware of its composition, as well as possible compounds.

1.2.2. Carbohydrates and lignin

In order to predict possible and useful product molecules, the general composition of the reactants need to be known. Every catalyst has its activity and selectivity towards certain chemical bonds. Molecules in heterogeneous catalysis always first adsorb on the surface before a reaction can take place. These active sites can be cracks or interfaces between two different materials as in bimetallic catalysis or faulting and defects within a particular matter.[69] These adsorption sites need to be reachable by the reactants, which can therefore be one reason of a not occurring reaction. When the molecules are too bulky, or their adsorption properties do not fit to the offered active sites of the catalyst, the reaction will not take place. Cellulose, hemicellulose and lignin are indeed molecules of a polymeric type with high molecular masses and different properties (Figure 4).

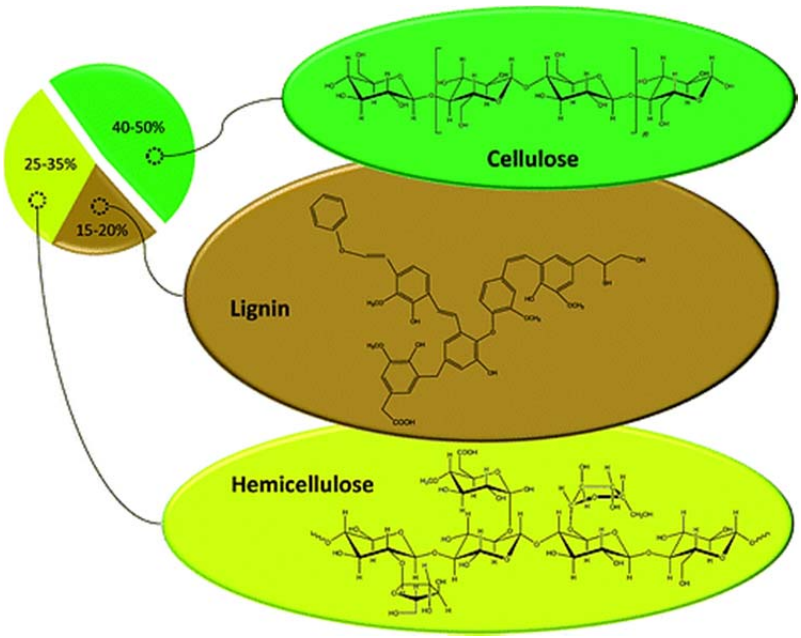

Figure 4: Schematic illustration of the composition of biomass, showing the main types of components. Hemicellulose as well as cellulose are the most abundant molecules, whereas lignin is the one with the lowest proportion in comparison. Adapted from David Martin Alonso et. al.[17]

Lignin is a biosynthesis product obtained from coniferyl, sinapyl and p-coumaryl alcohol in a random radical polymerization.[70] These monomers are randomly polymerized and result in a complex and aromatic structure, having mostly carbon-carbon as well as carbon-oxygen bonds. Various linkages as well as functional groups are observed, wherein ether bonds

represent the most frequent ones. Depending on the plant, lignin has a proportion of around 15-25 % and represents the molecule with the least percentage on the total amount compared to cellulose and hemicellulose.[71] Lignin is the only renewable source for aromatic molecules in nature and has the potential of playing an important role in using its aromatic monomers as bulk chemicals.[72] To break down this complex polymer, homogeneous catalysis or nano-catalysis needs to be taken into account, considering the bulky material cannot come close enough to the catalyst´s surface. Catalytically active molecules or nanoparticles are more suitable to expand into the regions for specific bond cracking.

The molecule with the second highest proportion in the comparison is hemicellulose. 20 % to 40 % (depending on the biomass) of the total amount of a plant is made up by this heteropolymer[73]. It represents a chain of hexose and pentose sugars, randomly cross-linked by alpha- and beta - glycosidic bonds. By having these inter-connections, an amorphous structure is obtained. These internal bonds are strong, whereas the molecule cannot be cut into its monomers in an easy way, using acids or base for instance. The most common and abundant sugar after depolymerization is xylose, but also mannose or galactose can be found.[74]

The most abundant organic polysaccharide is cellulose, linked via beta(1-4) glycosidic bonds. It consists of a linear chain of thousands of exclusively beta-D-glucose molecules (Figure 5).[21]

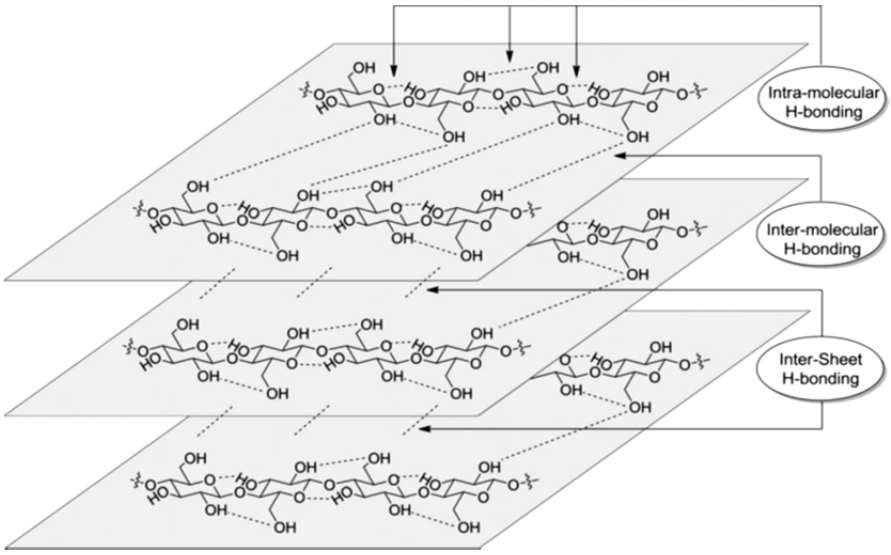

Figure 5: Schematic illustration of cellulose with its inter - and intra – molecular bonds, forming crystal structures. (Adapted from Murzin et al.)[75]

Mammals like humans are not able to digest this polymer, as we do not have enzymes to break this beta(1-4)-glycosidic bonds. On the other hand, insects like termites, fungi or bacteria developed special biocatalysts to crack these strong internal bonds and to make use of the released carbohydrates. Cellulose is therefore not considered as a possible food source for humans, even if the monomers are very important for daily nutrition. On the other hand, starch, what is a mixture of amylose and amylopectin, is digestible. The only difference is the structure of the glucose, which is the alpha form and a therefore alpha-(1-4)-glycosidic bonding is present. Amylopectin shows the same basic structure, but is branched with an alpha-(1-6)-glycosidic bond every 20-30 monomers. This slight difference can therefore have an enormous impact on the stability and influence the decision to not get in conflict with the "food vs. fuel dilemma". In cellulose, every chain interacts within the chain itself by intra-molecular hydrogen-bonds, but does not fold or bend, and therefore keeps its linearity. Hydrogen bonds are also forming between the single chains, as the linear D-glucose strings are kept together via inter-molecular hydrogen-bonds. A third interaction is represented by the inter-sheet interactions, which ensure an ordered stacking. Such regular arrangement result in a crystalline structure, which is way harder to break compared to the heteropolymer hemicellulose. By using acid or base, these hydrogen bonds, as well as the glycosidic bonds can be broken.[76] The resulting glucose and fructose have the same chemical formula: $C_6H_{12}O_6$, whereas the 3D-structure is very different. The isomerization is a known process, used in industry.[77]

Fructose itself is not only present in one form, but can exist as an open structure, what enables two different ring closing mechanisms, shown in figure 6. [78]

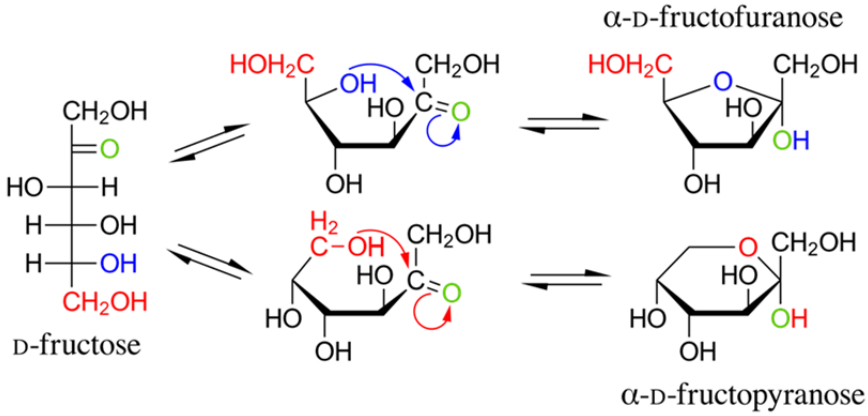

Figure 6: Illustration of different forms of fructose equilibrated according to the conditions pending.

The alpha - D - fructofuranose is formed by direct interaction of the alcohol group of the C_5 atom with the C_2 atom. During this process a heterocyclic compound is formed, which already contains the basic structure of HMF. The alpha-D-fructopyranose is obtained by the direct interaction of the alcohol bound to the C_6 atom with the C_2. Here the C_6 carbon is part of the build ring system and represents therefore a pyranose. Depending on the conditions, one or the other form is preferred, whereas all structures are in equilibrium (ring chain tautomerism). In aqueous solution the fructopyranose form is dominant. For the reaction towards HMF a five-ring system is favorable, what is the case in furanose.

Before the usage of glucose or fructose is possible, these monomers need to be obtained first. The separation of cellulose, hemicellulose and lignin is mainly done by chemical fractionation, making use of different interactions and therefore solubility in selected solvents, as well as breakage of the interconnections between the three main components.[79] The development of these processes already started in the 19th century as already mentioned, and first bigger companies were trying to make use of chemical or enzymatic treatment in the 20th century. Nevertheless the saccharification of wood and the extraction of the components as well as the further upgrade is, till now, just a niche industry.[80] The cheap and abundant fossil resources still suppress the economic development of using biorefinery processes in the energy sector and especially for chemicals. The market for biorefinery starts growing again recently, and companies start investing money in promising conversion routes. The usage of the so called “Scholler treatment”[81] is one of the main used methods and was exploited in Germany, Switzerland or the UDSSR. During this treatment, wood and saw dust is pressed together under moderate pressure and temperature of 130 °C, using steam. A sulfuric acid solution is pumped through the reactor under pressure, before a dilute sugar solution can be withdrawn after several minutes. All bigger plants were shut down sooner or later, because of several disadvantages occurring during the production. Considering the usage of high temperatures, in combination with sulfuric acid, creates a highly corrosive environment. This fact applies for batch processes, as well as for continuously organized flow systems using metal tubing. By additionally using pressure, the stainless steel, which is commonly used is not suitable, thinking of homogeneous catalysis.[82] The “Bergius-Rheinau-treatment”[83] makes use of hydrochloric acid under atmospheric pressure, but struggles from the same problems of corrosion and complex separation of the used acid. Biorefinery can therefore

contribute to a clean production of for example DMF and EL by using heterogeneous acid catalysts. The corrosion is not completely avoided by keeping the acid groups bound to a support, but the proton is hindered to be washed out, as long as there is no cation exchange happening. Using raw biomasses instead of pure compounds often contain salts and other ions, able to exchange and therefore poison the (solid acid) catalyst.[84] Nevertheless, research is investigating more and more pathways, which are robust and therefore promising, even when the basic research still relies on pure compounds in order to clarify the exact catalytic reaction mechanisms.

After the decomposition and separation of the biomass, the upgrade to bulk and fine chemicals can be done using heterogeneous catalysis. In order to give more insight into the selection of acid as well as metal-based catalysts, the different possible catalytic pathways in dehydration and hydrogenation will be roughly discussed.

1.2.3. Alternatives to homogeneous catalysis: heterogeneous catalysts

Whereas in previous processes the decomposition of cellulose and further saccharification was mainly done by homogeneous catalysis, heterogeneous / nano-structured catalysts offer a greener and eco-friendly possibility.[85] Whereas homogeneous catalysts are one limiting factor when it comes to the selection of the reactor material, due to corrosion and leaching, solid acid catalysts are much easier to handle and can be hold in place by a filter membrane. This usually sintered material prevents the catalyst to be flushed out. The reactive material is made of a solid support, on which active catalytic sites are anchored. In this sense it is clear, that the material needs to provide a sufficient surface area as well as a certain kind of porosity in order to be sufficiently active.

Furthermore, the lifetime of the catalyst is one of the most important factors when working in a commercial fashion. Also heterogeneous catalysts cannot be used for an unlimited amount of time, but can have a life span of years depending on the material.[86] By making use of nano-catalysis on an appropriate support, new possibilities arise in terms of reactivity, but also in terms of a reduced back pressure. Choosing materials with porous structure enables the adjustment of using continuous flow application without high energy input in terms of pressure issues.

The overall advantage of solid acid catalysts is the easy handling, filling the solid material into a reactor column and keeping the matter inside. By keeping the material fixed, the separation of products is easily possible as well as high purity and selectivity can be achieved.[87] By the development of such catalytic material, two main criteria need to be addressed. The usage of the catalyst over a long time can only be profitable, when the catalyst shows activity for the reaction which is aimed for, but is also addressing the selectivity. The third pillar is represented by the stability of the material. All three components interplay and are affected by each other using solid acid catalysts. (Figure 7)

Figure 7: The interplay of heterogeneous catalysis in terms of activity, selectivity and stability. All three components distinguish a good catalyst.

By having a high throughput and therefore forces affecting the material throughout the packed bed, the interest in having an active catalyst strongly bound to the support is high. By using for instance comparably cheap nickel in nanoparticle form, distributed over an active supportive material, can offer a great benefit in terms of a reduced back pressure, leaching or reduced Ostwald ripening. The more stable the nanoparticles are bound to the scaffold, and the more the particles interact on an electronic level, the less movement of the particles occurs on the surface during reaction. By using new and continuously improved in-situ approaches, the unique interplay between morphology, grain and crystallite size as well as composition was also explored in our group in more details recently.[88] Already a single microscopy picture at the beginning and at the end of a chemical reaction can bring important details to the front, even if the information is limited on how the catalyst behaves during a reaction. By using dynamic and in-situ techniques, these new studies show a huge impact of conditions, interplay with the surface and the consequential change in composition of the catalyst. This online view during the reaction will to my opinion play a more important role in the future.[89]

Nano-catalysis has to discuss the interaction of these small particles on which they are deposited. In nanometer scale, electronic interactions gain more significance. By using metal nanoparticles in combination with other semi-(metal) particles, a metal-metal heterojunction can be initiated in which electrons are transferred from one to the other material.[62] In which direction the charge is shifted, depends among other things on

electronegativity or on the concept of standard electrode potential. The transmission of electrons activates the catalyst and can influence the reactivity tremendously. Choosing the right material on which the active catalyst is deposited is as important as to select the best and optimum conditions for the appropriation of the activation energy.

In addition, catalytic material does not necessarily need to make use of metal (nanoparticles). By using solid acid catalysts for instance, the material itself already contains the active acid sites, necessary to convert and dehydrate the reactants.[90] Acid catalysis is one of the most important catalysis applications and appropriate solid acid catalysts are known.[91] Active sites of acid catalysts are typically characterized by Lewis or Brønsted theories as well as strength or number of acid sites. Typical solid acids are based on silica, zeolites, polymers, resins or carbons. The acidic active sites are anchored to this support or are brought into the material by a salt, like zinc or aluminum chloride. Additionally relatively new research is focusing on avoiding metals as catalyst. As noble metals are rare and expensive, non-noble metals also have some disadvantages in terms of availability or sustainability. Therefore, recent discoveries are quite promising, suggesting carbon material (e.g. graphene and graphene oxides) as active (carbo-)catalysts.[92]

Besides choosing the right material for providing sufficient activity, flow conditions in heterogeneous catalysis play a major role. Using wet-chemical conversion of reactants in combination with a solid surface, a stagnant layer of liquid needs to be considered, forming around the particle (Figure 8). This layer can just be overcome by diffusion and depicts a limiting criterion for a successful conversion in time. Homogeneous catalysis does not suffer from this problem, whereas the molecules are freely movable in the liquid and no stagnant layer needs to be overcome. Additionally, hydrogenation reactions need to consider the usage of hydrogen in gas form, when not performed as transferhydrogenation. Therefore the solubility of gas into the liquid plays another crucial role. Transferhydrogenations on the other hand can offer opportunities to avoid high pressure vessels and therefore increase the safety of a system. By using molecules like formic acid, isopropanol or dihydroanthracene, the hydrogen can directly be provided by a chemical reaction and being transferred to the substrate.[93] As hydrogen gas is more efficient for hydrogenation reactions, transferhydrogenations are not often used in applications nowadays.

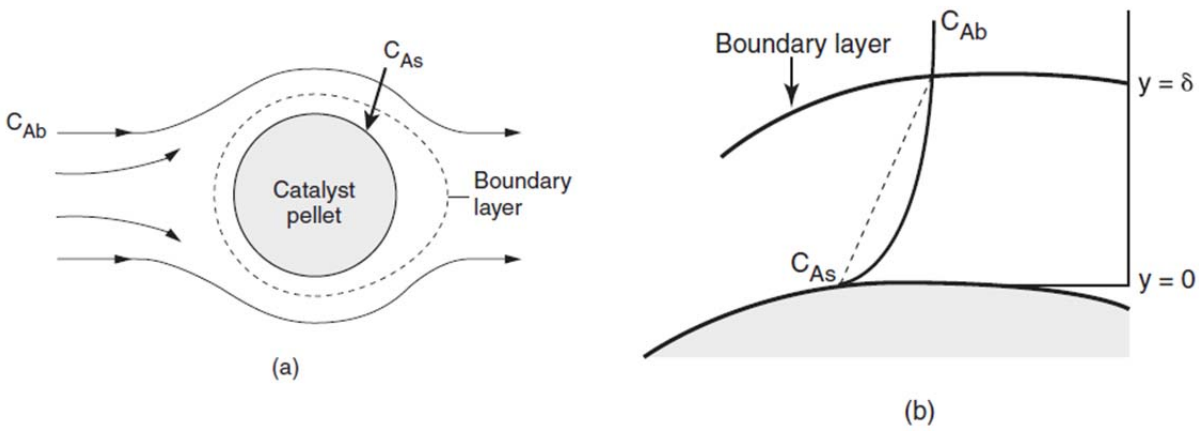

Figure 8: Stagnant layer of liquid surrounding a solid catalyst surface. The stagnant layer thickness at each side depends on the convection applied. The concentration of reactant is depended on the diffusion. (a) Shows the flow over a catalyst pellet, (b) focuses on the boundary layer around the pellet. Adapted from Fogler.[94]

The thicker the layer, the more diffusion limited and therefore the more the whole synthesis depends on this relatively slow process. Flow regimes need to be considered and ideal mixing over the catalyst is necessary and meaningful. The more mixing occurs, the more swirls are forming, which ensures a good blending. Due to wall effects and an interaction of the wall with the near liquid, the flow is slowed down and a laminar flux is established, most obvious in empty columns (Figure 9, 1).

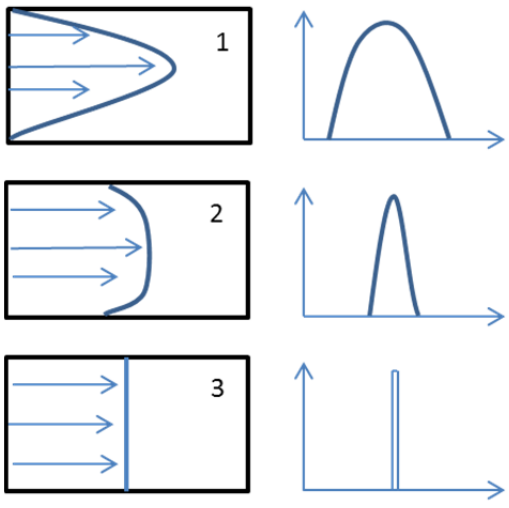

Figure 9: Laminar (1), turbulent (2) and plug flow (3) in a tubular reactor. Laminar flow is most likely to occur in empty tubes, whereas plug flow represents the ideal flow profile for reactions. Turbulent flow (2) is mostly achieved by filling the reactor column with material responsible for swirl formation. The elution profile for each tube is given additionally.

A straight forward plug (3) or turbulent (2) flow over the cross section represents the ideal flow for catalysis. This flow regime is enabled by filling materials like heterogeneous catalysts, which cause swirling. A turbulent flow is established, resulting in a more sharp signal of products, as the reactants are traveling in a more ordered front, which elutes more simultaneously form the column. The product signal results in an elution peak, giving information about the packing of the catalyst. This property can theoretically be expressed in the so called theoretical plate number.[95]

1.2.3.1. Hydrogenation over metal based catalysts

The above mentioned hydrogenation reactions are nowadays typically done, using a metal catalyst, bearing the ability to activate hydrogen. The active sites on the metal surface adsorb and dissociate hydrogen. This property is specific for metal nanoparticles and offers, by using materials like palladium, tungsten carbide or nickel great potential for hydrodeoxygenation of biomass-derived molecules.[96] The usage of hydrogen for the removal of oxygen from a molecule is attractive, as the hydrogen adds heating value to the resulting molecule. Typical catalysts used for hydrogenation reactions are platinum, palladium, rhodium or ruthenium. These catalysts are known for their high activity under relatively mild conditions. The metals can be used in homogeneous as well as in heterogeneous catalysis. In homogeneous catalysis, the metal atoms are bound in a certain structure, offering ligands and sites, which influence the particular catalytic reactivity. The ligands can offer specific electronic properties, creating a specific environment being selective in reactions. These functional groups, in which the molecule is organized, also fulfill the function of shielding the metal atom and offer special accessibility.

In heterogeneous catalysis, the metals are for example organized in small clusters of several thousand atoms, instead of being existent in a bulk material (Figure 10).

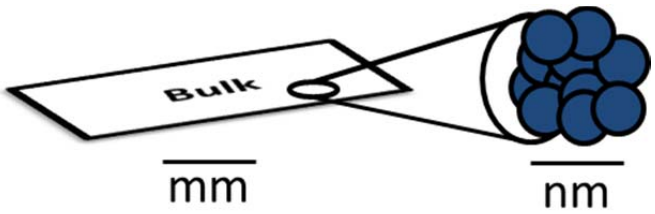

Figure 10: Schematic illustration of the difference of a bulk material (mm) and the same material as a nanoparticle (nm), typically organized as a cluster of a specific amount of atoms.

The principle of breaking a bulk material down to nanoparticle size, as well as using the "bottom up method" for synthesizing nanoparticles out of solution, is working for almost all metals, using their salts. By doing so, the surface area can be massively increased and therefore the reactivity can be influenced. A cheap alternative to noble metals is for example nickel.[97] This metal is less active for hydrogenation and typically requires harsher conditions

like higher pressure and temperatures, in order to dissociate hydrogen on its surface with the same efficiency as noble metals do. Every atom present in such a particle interacts with its environment and the neighboring atoms to form a crystal or an amorphous structure. Whereas catalytic reactions happen at the surface of a heterogeneous catalyst, it is clearly obvious, that the composition and structure has a huge impact on the reactivity.

Metal nanoparticles consist of crystals, forming out of several well-ordered atoms. These structures are mainly important for the reactivity. Several crystals make up a particle, whereas the particle can hence consist of different crystals. And finally several particles can form a grain, what makes up the overall morphology.

1.2.4. Catalytic flow concepts

Pellets and catalysts can be packed in mainly three different ways, shown in figure 11. Thinking of a two stage reaction, like it will be discussed for the upgrade of fructose, a first dehydration[98] and a second hydrogenation[99] are important. The first approach is a combination of columns and therefore a complete separation of reactions. The converted products of column number one are directed into the second column, in order to undergo a further conversion, uncoupled from the first stage. This set-up can bring benefit, if the reactions or catalysts would negatively interact, causing for instance unwanted consecutive reactions or catalyst poisoning. Disadvantages arise from the fact, that reactive products from the first conversion are not instantly converted to less reactive molecules. This thought is used in the second approach (2). By mixing the catalysts in one column, the products can immediately be converted further. The active sites are still separated but the time between the first and the second reaction is massively reduced, due to its areal closeness. This time can only be reduced further, if the catalyst itself is modified, carrying both reactive sites on its surface (3). Whereas the first two approaches are packing and engineering tools, the third one is material and catalyst modification.

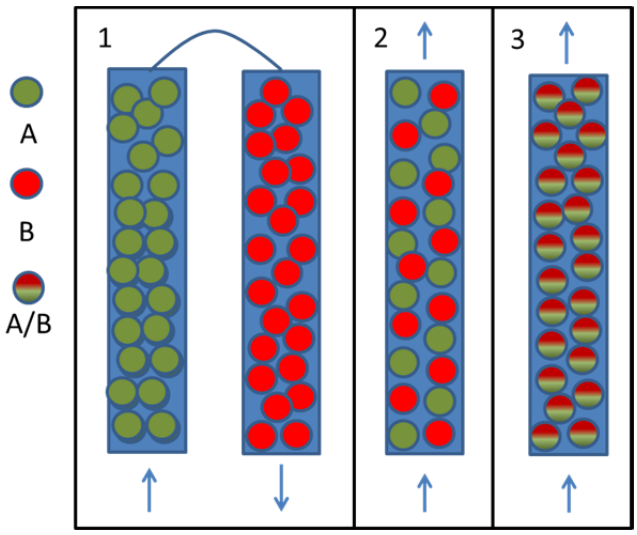

Figure 11: Schematic illustration of packed reactor columns for a two-step reaction. Number one represents a two-column packing, number two and three are one-column approaches. In two the catalysts are simply mixed, in number three, the catalyst itself offers both active sites on its surface.

The residence time, another important factor when speaking about reactions and kinetics, can be adjusted by the flow rate. It can be calculated with the particular equations:

$$\tau = V_{(void)} / Q$$

$$V_{void} = V_{column} - V_{catalyst}$$

$$V_{catalyst} = \frac{m_{catalyst}}{\rho_{catalyst}}$$

The residence time τ is the ratio between the volume V of the cartridge or the void volume V_{void} of the filled cartridge and the volume stream Q of the reactants. The volume of the catalyst is accessible by the division of the mass of the filled catalyst $m_{catalyst}$ and its density $\rho_{catalyst}$. As the density of all the different manufactured catalysts is not easily accessible, an estimation is necessary. The density of tungsten carbide is about 16 g cm^{-3}, the density of carbon was approximated to around 0.264 g cm^{-3} (datasheet, Cabot Vulcan Carbon, VXC72R, in thesis stated as Carbon Black). Depending on the mass filled in each cartridge, the residence time can be appraised.

For applying the knowledge of the catalysts used for dehydration or hydrodeoxygenation, a continuous fixed bed flow system needs to be established, offering appropriate conditions for conversion. The wet-chemistry based reaction solutions need to be directed through the plant, as already shown in figure 11. Hydrogen needs to be provided and residence times need to be adjusted accordingly. The flow concept of continuous applications can be therefore mainly divided in reactivity and applicability. One important property is the back pressure, which appears as a crucial parameter for building up a profitable flow reactor. A schematic drawing of the pressures, occurring in a continuous column can be seen in figure 12.

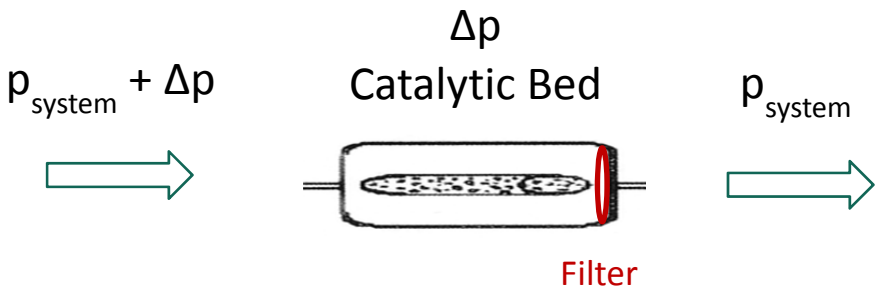

Figure 12: Schematic illustration of a continuous flow application, using a stainless steel column filled with the catalyst powder. The material is trapped inside the column by filters and therefore builds up a back pressure (Δp) when a liquid flow is applied.

Thinking of nano-catalysis and fine carbon material, the limits for the application in flow processes are obvious. By flowing through the catalytic bed, the solvent carrying the reactant is hindered by the powder, creating a flow resistance throughout the bed. The resistance is bigger, the closer the particles are packed. The liquid needs to be pressed through the small residual spaces and creates a back pressure which is much higher the smaller the particles and hence the free spaces are. The viscosities as well as the wettability are just some of the physical parameters which need to be addressed. An optimum heterogeneous catalyst offers a high surface area (porosity) as well as is still in a range of a particle / agglomerate size through which the reactants can flow without a huge pressure drop. The size of the granulate depends on the scale of the reactor, wherefore bigger scales (industry) and for easier handling, the catalysts are typically pressed into porous pellets. Powders and fine material are good for research in lab-scale and at small batch size scales. Powders offer a huge surface area; nano-catalysts can offer specific activity.

The pressure drop in such packed beds is theoretically accessible using the modified Ergun equation[100] [101]

$$\Delta p = \frac{2\, f_p\, L\, \rho\, v^2}{D_p}$$

,which correlates the friction factor of the equivalent spherical diameter of the particles, the density and the void fraction of the bed as well as the length of the bed and the velocity at which the liquid flows through the column.

In this modified equation, several parameters are identified, which are important and contribute to the pressure drop, occurring over a packed bed. The parameters can be divided in bed properties as well as fluid properties. In terms of the fluid medium, it can be stated that the denser the fluid, speaking mostly of parameters like density (ρ) and viscosity, the more difficult it is to pass through small channels. The velocity of the fluid is a quadratic term (v^2) and contributes therefore correspondingly. This modified Ergun equation additionally respects a friction factor (f_p), which is a description of how much friction occurs between the liquid and the solid material. The longer the packed bed (L), the more distance has to be overcome by the fluid and the higher the friction. On the other hand, the void fraction represents the ratio between the void volume in relation to the total volume, whereas this term is included in the friction factor. In other words: If there is a lot of free space between the catalyst particles, where the liquid is able to pass, or there is a huge internal and interconnected porosity, the pressure drop is less significant. The last parameter now missing is the particle diameter (D_p). But by seeing the particle size through engineer's eyes, dealing with back pressure in continuous systems, a smaller particle size contributes directly to the pressure increase. For our flow applications, it is desirable to work with particle sizes / agglomerates in the micrometer range, whereas the bigger the particles / agglomerates, the easier the flow. On the other hand a sufficient active site density is necessary for the reactivity. Nanoparticle applications therefore need to consider immobilizing particles on a support, big enough to keep the particles stable, but also to offer enough porosity and space for the liquid to pass.

The use of wet-chemistry processes for biomass conversion is most promising, as it offers an easy approach with a high density of reactants. The solubility of the hydrogen depends on temperature and the pressure, whereas the partial pressure of the hydrogen is specific for solvents. By choosing an appropriate solvent, the solubility can be improved and the gas, reactant and the catalyst can come close enough. The solubility of hydrogen is slightly bigger in alcohols than it is in water. In pure gas phase reactors the safety and control equipment needs to be checked carefully and the system gets more complicated in terms of plant controlling.

1.2.4.1. Overcoming batch mode: Issues, which need to be addressed

In terms of realizing such a set-up, batch mode can bring some awareness and knowledge about the properties of the catalyst. The final engineering needs to be done in a continuous system, addressing an industrial application. In here the control of temperature, pressure and residence times are the most crucial. All these parameters are responsible for the conversion as well as selectivity.

Chemical production plants can be divided into two main categories. One is the batch mode process, whereas the continuous or modularized synthesis is found on the other side. Batch mode is mainly used in older processes, or in the production of molecules, which are of high quality, but low quantity. When having high throughput and producing high quantities, continuous plants are preferred. As the chemical industry needs to adapt to the increasing competition from countries like China or India, also flexibility of the production line is of value. By developing a continuous flow process, which is in addition also modularized, a new combination of applications is thinkable. Flexibility in production, especially in customized specialty chemicals is necessary and cannot be achieved with batch systems. By the development of different catalysts for different kind of reactions, and their optimization in high throughput applications, it is possible to simply combine different columns and therefore modules to avoid the need of optimization and scale-up of all the different small parts, what is usually time-consuming. When it comes to reactions, which are accomplished very fast, or are very exothermic, as well as require special safety in terms of health risk, they can be controlled more easily in a closed system, so no human contacting is necessary. The production of fuels and chemicals like DMF or EL in this sense is such a multiple step process, which needs different conditions for saccharification of wood, dehydration of sugars and hydrodeoxygenation of the intermediates. In terms of the extension to rawer biomass or the production to even more fine and specialty chemicals, it can be realized by placing another module directly after another. A more complicated flow can be realized, it can be automated in more efficient ways, with minimal impact on the environment and health. During the upgrade of sugars, strong acids as well as hydrogen will be used. Both chemicals need to be handled with care. The acid can harm staff, if not handled in a correct way, as well as damage equipment by corrosion. To keep the reactor constantly under

pressure does not stress the material as much as when opening the reactor all over again. Additionally, hydrogen is costly[102], as the small molecule is diffusing through a lot of commonly used material. The direct production by reforming or electrolysis is recommended and meaningful to avoid hydrogen embrittlement, damaging store tanks mainly made out of steel. Because biorefinery attract more and more attention in the last years, chemists and engineers work together to develop reasonable flow processes.

One example of a successful integration of biorefinery and the production of succinic acid as well as 1,4-butanediol was done by the company Bioamber. The here developed flow concept is based on an integration and a meaningful chain of different compartments from corn treatment and dextrose extraction over fermentation to a catalytic conversion of succinic acid to 1,4 butanediol.[103] Other than the publication of the US Department of Energy in 2004, also the European Commission published a report on sugar based chemicals, to give an overview and direction where European research on behalf of sugar conversion needs to invest.[54] In here 25 promising chemicals and products out of sugars are listed. Among the chemicals and their development stage, also 5-hydroxymethylfurfural, 2,5-furandicarboxylicacid, levulinic acid or p-xylene are mentioned in the research or pilot plant sector. All of these products are thinkable out of the conversion of fructose, but are still not produced efficient enough so that it is worth to invest time and money.

By addressing the overall cost for a continuous production plant, upgrading fructose towards DMF, the equipment cost plays a minor role when checking the overall investment (Figure 13).

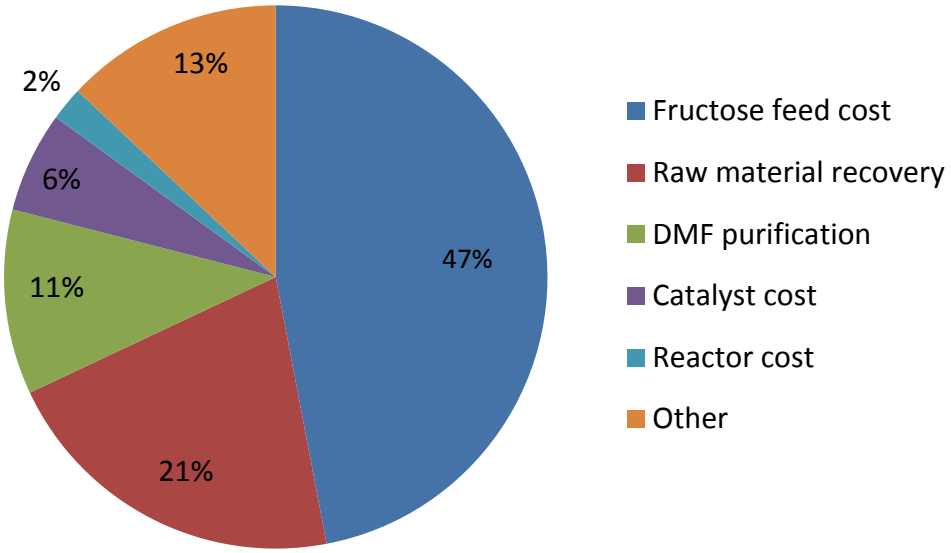

Figure 13: Representation of costs contributing to the production of DMF, using a wet-chemical production process. Adapted from Kazi et. al. [104]

The major contribution, how the final DMF price is related to the single items of the raw materials and the equipment cost is summarized in the figure. In this techno-economic analysis we can mainly differentiated between raw material costs and equipment costs, whereas the raw material indeed contributes the most. Fructose cost and raw material recovery as well as product purification make up almost 80 % of the costs. The continuous production plant and especially the reactor costs are only 2 %. When using a heterogeneous continuous reactor set-up the costs can be kept low. No additional labor, handwork or recycling steps are necessary. That is why a continuous flow concept is so valuable and is worth to be developed.

1.3. Outline of the thesis

To finally make DMF attractive to be produced out of renewables, a compatible process needs to be found to produce this chemical in a continuous approach, with relatively cheap and available catalysts. The aim of this work is the usage of sugars as a basis for the production of DMF and useful side-products, combined with an easy continuous flow set-up as well as solvents like ethanol. The catalyst needs to operate in a stable way as long as possible, to ensure an unobstructed run over a long time period. The products need to be separated and purified in an easy way, also in terms of reusing the solvent.

By using a two-step flow approach, it is possible to lift the processes from the lab scale to a scale, interesting as a pilot plant application. Besides using the process in a big and scaled industrial application, whereas the energy balances and therefore the overall efficiencies can be controlled and engineered in a more efficient way, it is also thinkable to develop a smaller system applicable in decentralized fashion, say in a small farm.

In chapter two the development of a solid acid catalyst is enforced. Different solid acid catalysts are synthesized by carbonization and further sulfonation. These catalysts are compared to commercial species and set in context by calculating the specific productivity. Heterogeneous solid acid material is important to dehydrate the fructose in order to produce 5-hydroxymethylfurfural and ethyllevulinate for mainly biofuel applications and blends, but also for chemicals.

In the third chapter the consecutive hydrogenations of the resulting reaction products from chapter two are developed. In terms of reactivity as well as stability, a stable catalyst support is necessary for a successful integration in a continuous flow process. Therefore tungsten carbide, an often discussed alternative for platinum is investigated. Additionally different noble metals are deposited on top of this ceramic metal in order to research a synergistic effect for the upgrade of HMF to DMF.

Finally, all findings are combined in one continuous flow system, and the thesis closes with a fourth chapter, dealing with engineering and equipment development. Dehydration as well as hydrodeoxygenation are working independently, but need to be combined in a two-column system. In order to simplify towards a one-column approach, an outlook will be

given towards the upgrade of fructose immediately to DMF. A further scale up is done, opening the way for an industrial application.

2. Acid catalysis: Sulfonated carbon derived from biomass

2.1. Introduction

Regarding abundant biomass sources, carbohydrates like monosaccharides as well as their polymers, such as oligosaccharides like starch constitute most of the biomass on earth and are therefore logical to take into account for using as raw material for fuel and chemical production as well as catalyst synthesis. Starch[105] is a chain of glucose units connected via α(1-4)-glycosidic linkages in the form of amylose and additionally branched with α(1-6)-glycosidic bonds in the form of amylopectin. Saccharides (e.g. glucose) can be generally described by the molar constitution of $C_nH_{2n}O_n$. As these molecules are rich in carbon, the molecules are suitable as a "green" carbon source. The biggest disadvantage is the high amount of oxygen.[17] Thinking of biofuels and the current engine design, oxygen rich molecules result in a less efficient combustion compared to hydrocarbons like alkanes, when used as fuels. Thinking on the other hand of the synthesis of carbon material as catalysts and catalyst support, the oxygen can be actually beneficial. Especially oxygen containing functional groups in cellulose and hemicellulose are known for releasing mainly water, some carbon dioxide and carbon monoxide when heated. These gases are responsible for the synthesis of pores, whereas the lignin contains a lot of chemically inert aromatic structures, what results in non-porous material due to a limited gas formation.[106] Out of surface area reasons, a porous material is advantageous in catalysis. It offers more surface and therefore more potential spots for active sites. For acid catalysis, it is also not necessary to remove the oxygen completely from the catalytic surface. Oxidic functionalities (e.g. hydroxyl groups) constitute a polar environment and are therefore favorable for dehydration reactions.

However, the acidic character of most obtained carbons is limited, but acid groups are necessary for the use as catalyst in dehydration reactions. With the removal of water from a carbohydrate like fructose, the oxygen content in the molecule is decreased and thereby a furan ring structure is synthesized. These furan structures have the potential as substitutes for petroleum-based building blocks, fuels and chemicals.

Acid functionalization of carbons can be realized by treatment with strong acids, having the ability of introducing functional groups.[91] As sulfuric acid is known for its high activity in acidic dehydration, sulfonic acid functionalities are aimed to be linked to the carbon

structure in order to make the carbon material a suitable solid acid catalyst for heterogeneous catalysis.[107] Commercial sulfonated polystyrene (Amberlyst 15 dry hydrogen form) is one of the strongest solid acids and is often used in batch and dehydration reactions, whereas it serves as a model catalyst for comparison with our material. The polystyrene backbone however is only resistant to temperatures not higher than 120 °C, due to imminent degradation of the polymer by heat. For processes that need higher temperatures and harsher conditions, this catalyst is not suitable.[108] Carbon structures on the other hand are known for their resistance towards heat treatment and their stability during reaction. This emphasizes the great promise of carbon-based sulfonated catalysts. The amount of acid groups introduced into the structure is a key aspect of the catalytic performance of the materials.

The conversion of biomass in a flow system reaches out as a promising alternative to the frequently reported batch processes. The focus of this chapter will be first set to the production of sulfonated solid acid catalysts, used in a simple flow application for dehydration of fructose. For further application in a continuous scaled process, the avoidance of back pressure, because of a suitable particle size is aimed. Due to disadvantages, like difficult recyclability or slight corrosion when it comes to conventional acid catalysts in biorefinery (mostly homogeneous, but also heterogeneous), this chapter will focus on the synthesis of heterogeneous carbon catalysts from biomass to target sustainability and green chemistry in dehydration flow conversion.

2.2. Synthesis of solid acid catalysts

Carbonization of glucose and starch

One simple approach for transforming an organic substance into a carbon structure is carbonization.[109] Here, a pyrolytic process in the absence of oxygen takes place. However, the process itself is not simple but shows a complex reaction cascade, which depends on the conditions used. As a result, multifold carbon structures composed in different ways are obtained.

Temperature has a great impact on the carbonization process, because it provides the energy for releasing mainly water and several gases from the molecule´s structure. Therefore glucose and starch were heated at different temperatures, whereas the observation results are summarized in Figure 13.

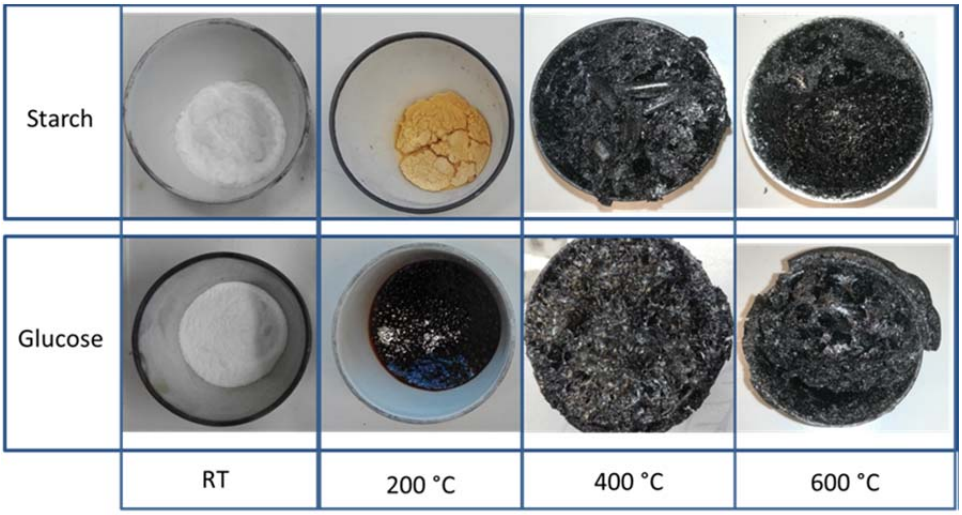

Figure 13: Glucose and starch carbonized at different temperatures. Conditions: Two hours ramping from room temperature towards the final carbonization temperature and 15 hours at the desired temperature (200 °C, 400 °C and 600 °C) in the nitrogen oven.

The parameters and conditions were adapted according to the paper by Toda et al. (Nature Com 2007).[110] The trend of carbonization that can be observed is intuitive and similar to caramelization at lower temperatures, known from the kitchen. Glucose starts to melt (at around 150 °C)[111] and to undergo degradation, forming first a brown glass-like structure at 200 °C [112] [113], whereas the starch is also degraded, forming a yellow, but still fluffy powder. At 400 °C and especially at 600 °C under nitrogen, full carbonization is observed, and porous foam is obtained. The bubbles in glucose are trying to leave the melt, but are trapped and

expand the material. The carbonization process can go faster, as the molecules in the liquid glucose melt are able to move, compared to starch, what stays in solid form. Starch does not have a melting point, but decomposes at higher temperatures. The brownish powder at 200 °C represents this starting degradation, whereas glucose is already melted. If the powder is heated under non inert gas conditions in the presence of oxygen, the sugars are completely converted to carbon dioxide and water.

Synthesis of activated carbon material

Additionally to the glucose and starch carbon materials, a third activated carbon was produced. Using a salt / biomass-carbon mixture enables to synthesize a porous material with tunable pore size. The salt occupies specific space within the structure and undergoes a conversion during the heating, resulting in a dehydration process of the carbonaceous material, also known as activation. Only few is known about the exact mechanism, but the catalyzed carbon consumption in combination with the release of gaseous species under alkaline conditions is a commonly accepted fact. The resulting porous structures are washed with solvent, in order to remove the remaining salt components. The used precursor carbon was provided by the company Micromidas and represents an alternative to the carbohydrate derived catalysts. The precursor carbon was grinded together with urea and calcium hydroxide (mass ratio precursor carbon: urea: $Ca(OH)_2$ = 2 : 1 : 2). The mixture was placed in a ceramic crucible and is then heated to 850 °C under nitrogen flow with a heating rate of 6.5 K min^{-1} and held at the elevated temperature for 2 hours. Finally, the crude product was washed with 2 M hydrochloric acid and water. The material was dried afterwards overnight under vacuum at 40 °C.

Sulfonation of the obtained carbon material

The resulted sugar-carbon foams made of glucose and starch were grinded to powder before used for sulfonation. The activated carbon was already a fine powder. Carbon black was chosen as a reference carbon, on which the sulfonation was tested and the biomass derived carbons were compared to. For 1 gram of material, 20 ml of excess fuming sulfuric acid was applied. The dispersion was placed into a 100 ml round bottom flask and stirred over night at 80 °C in an oil bath. During this process the sulfonic acid groups are slowly incorporated into the carbon structure. This slurry is intensively stirred to assure a properly mixed solution. The following day the fuming sulfuric acid was quenched with ice water. The slurry was

slowly added to the cold water and afterwards filtered with a non-cellulosic polypropylene filter, applying vacuum over a vacuum bottle. After filtration and washing with distilled water, the powders were dried overnight with 60 °C. During the filter process the filtrate was constantly checked by litmus paper to make sure all the soluble acidic compounds are fully removed.

Before the application in a stainless steel flow system, all catalysts were carefully checked using different techniques giving insights, how the material is composed and structured. Because the materials need to be set into context to already existing catalysts, commercial Amberlyst 15 was characterized in a similar fashion.

Several techniques for characterization are meaningful when working with carbon materials. In order to determine the morphology and overall structure of the prepared materials, scanning electron microscopy (SEM) and transmission electron microscopy (TEM) were conducted. The surface area was examined by nitrogen sorption (BET). Elemental analysis (EA) gives insight into the atomic composition. The quantity of incorporated sulfonic acid groups was investigated by titration. The differentiation between different acidic moieties and their acidic strength present in the material was not considered.

2.3. Characterization of solid acid catalysts

2.3.1. Optical characterization

The overall morphology gives a first hint towards how the material is structured macroscopically and if anomalies are present in the material. The obtained pictures of the materials are shown in the single sections. The SEM pictures were taken using 10 kV and 10 µA. The TEM device was a Zeiss EM 912Ω microscope operating at 120 kV. The non-sulfonated as well as sulfonated materials are compared to each other.

Carbon Black

Carbon black[114] is a commercial product synthesized by an incomplete combustion of mostly heavy petroleum products. It has a high surface to volume ratio and would therefore be a good candidate for application as catalyst precursor. The resulting SEM pictures are shown in figure 14.

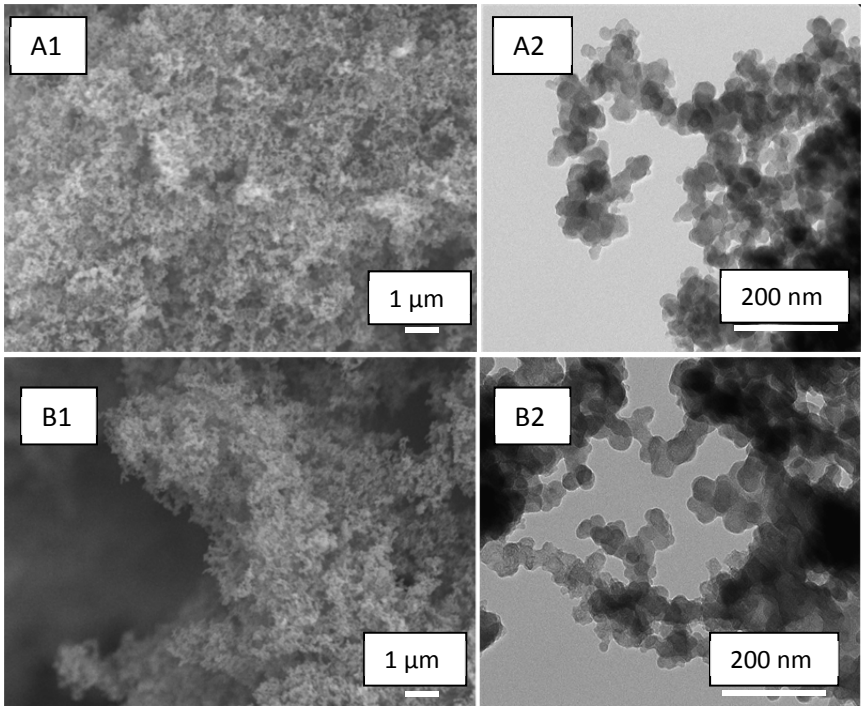

Figure 14: Carbon black material before and after the treatment with an excess of fuming sulfuric acid overnight in a round bottom flask, using 80 °C with intense stirring. A) represents the non-sulfonated material, whereas B) stands for the material treated with acid. 1) stands for the SEM recording, 2) for the TEM pictures.

Comparing the non-treated material A) and the treated material B), there is no big difference at first sight. The SEM still shows a very porous material, which is obviously not much affected by the treatment. The interstitial space is still clearly visible, and the whole structure forms a material with a lot of interconnected pores. The TEM investigation with a higher magnification reveals carbon particles interconnected in agglomerates of high porosity.

Glucose catalyst

After carbonization with 600 °C, the obtained structure in the crucible looks like a foam (figure 13). The gases internally released during the carbonization process blow the whole structure, whereas the bubbles were backed into the carbon resulting in interconnected pores in the micrometer range. By grinding the material, these holes are destroyed, but can still be seen at the rounded edges of the big blocks obtained. This structure does also not change after the sulfonation procedure. Big micrometer particles are good in terms of not blocking the filter or resulting in a high back pressure in a continuous application, as it would be the case for nanometer material. The TEM pictures support the already drawn conclusions of the structure and morphology. All pictures of glucose are summarizes in figure 15.

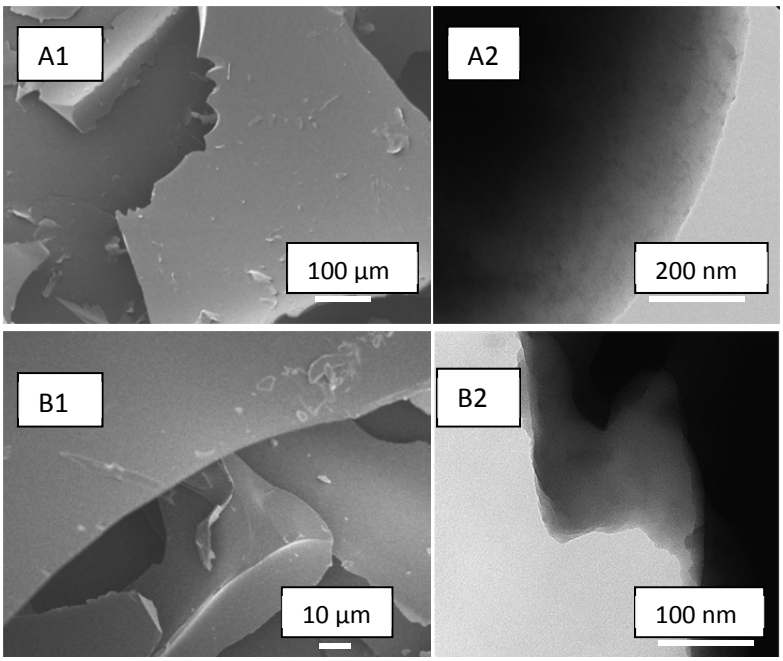

Figure 15: Glucose carbon before and after the treatment with an excess of fuming sulfuric acid in a round bottom flask, using 80 °C with intense stirring overnight. A) represents the non-sulfonated material, whereas B) stands for the material treated with acid. 1) stands for the SEM recording, 2) for the TEM pictures.

Starch catalyst

The overall morphology of starch carbon is similar to glucose and follows the principle process already described. The gases which blow up the material are responsible for the rounded particles, which can be seen in figure 16. The particles are relatively bulky, but also show more thin parts compared to the carbon from glucose. These thin structures remain during the sulfonation process. The transmittance electron microscopy shows a similar structure before and after acid treatment and exposes a smooth regular shaped carbon.

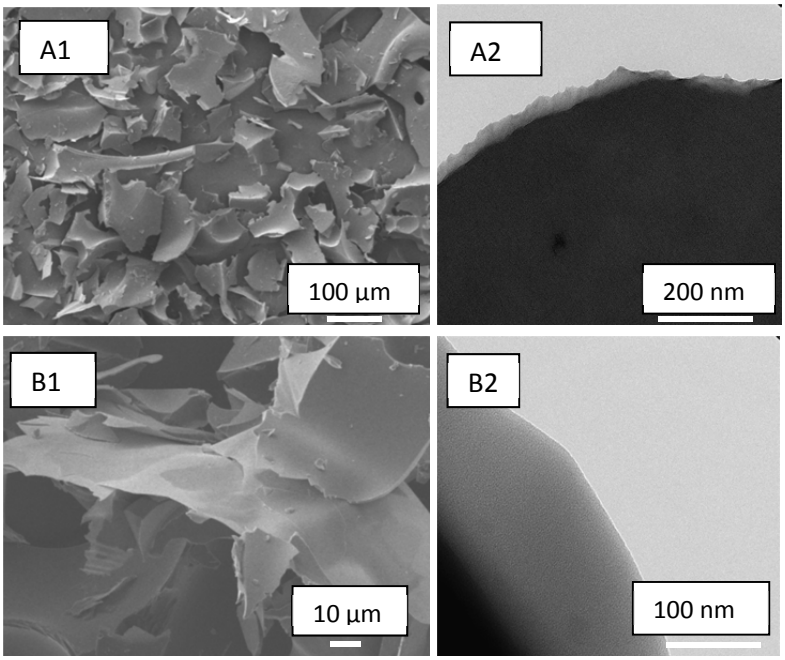

Figure 16: Starch Carbon material before and after the treatment with an excess of fuming sulfuric acid overnight in a round bottom flask using 80 °C with intense stirring. A) represents the non-sulfonated material, whereas B) stand for the material treated with acid. 1) stands for the SEM recording, 2) for the TEM pictures.

Activated carbon catalyst

Active sites are indispensable for an application in catalysis. Surface area should be high while simultaneously micrometer particles should be preserved. In this sense, agglomerated nanostructures could be favorable, which are interconnected but leave enough space in between resulting in pores. Such a material is obtained by an activated carbon method. These structures are depicted in the figure 17.

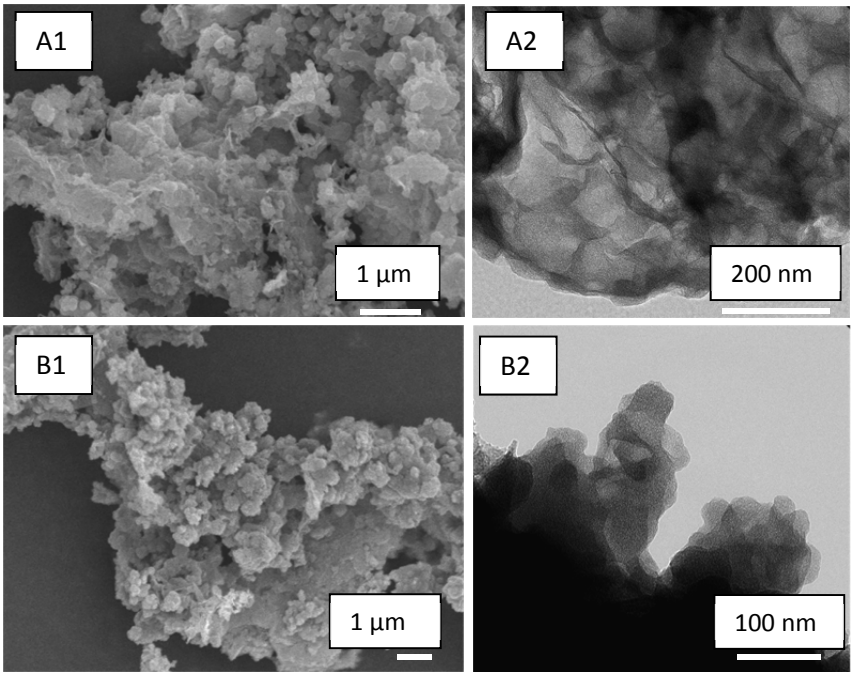

Figure 17: Activated carbon before and after the treatment with an excess of fuming sulfuric acid overnight in a round bottom flask, using 80 °C with intense stirring. A) represents the non-sulfonated material, whereas B) stands for the material treated with acid. 1) stands for the SEM recording, 2) for the TEM pictures.

While A1 represents the SEM results before the acid treatment, B1 is showing the material after the fuming sulfuric acid treatment. The material after the carbonization and the catalyst after the acid have a similar morphology. It preserves the overall desired structure and is believed to show good activity as well as the avoidance of a big pressure drop over the column, due to micrometer particles with porosity. The carbon before the acid treatment (A1) shows a cobweb structure, what might result from a partial graphitization. These sheets are also seen in the TEM. The carbon forms graphitic layers, which are deposited over each other. Such crystalline graphene sheets are also able to carry functional groups or contain oxygen or nitrogen, also present in the biomass precursor. This overall structure is as well preserved after the acid treatment, also when these sheets are less frequent. The XRD investigation did not show metal residues in the activated carbon and confirmed crystal structures at 25° and 45 ° (SI-F1).[115]

2.3.2. Surface area and porosity

The Brunauer-Emmett-Teller-Analysis (BET) gives insights into the overall surface area, as well as the pore size distribution. Nitrogen is adsorbed on the surface and the area is calculated according to the amount. As already mentioned before, the carbon structures are compared to the commercial Amberlyst 15 catalyst. The results are shown in table 1.

Table 1: Comparison of surface areas, obtained by different carbon structures and Amberlyst 15. It is differentiated between the area before and after the fuming sulfuric acid treatment.

	Surface area $_{\text{before sulfonation}}$ [m^2 g^{-1}]	Surface area $_{\text{after sulfonation}}$ [m^2 g^{-1}]
Carbon Black	220	164
Glucose Carbon	0	6.9
Starch Carbon	0	7.4
Activated Carbon	726	144
Amberlyst 15	-	62

In agreement with the SEM pictures, carbon black shows a higher surface area compared to all sugar derived carbons. The 220 m^2 g^{-1} however decreased with the addition of acidic groups and resulted in 164 m^2 g^{-1}. This trend is not only seen with the carbon black, but also with activated carbon. The acid seems to reduce the area by interconnecting the particles and filling as well as changing the pores, what results in a loss of micropores and therefore surface. (SI-F2)

Glucose and starch carbon have a very small and therefore not detectable surface area. Also after sulfonation the area is still low (around 7 m^2 g^{-1}) for both materials. With such low surface areas, the interpretation is difficult, and the results need to be interpreted with care. The activated carbon shows the biggest surface area of 726 m^2 g^{-1}, which is decreased to 144 m^2 g^{-1} for the solid acid catalyst. This decrease of surface can be a result of sulfuric acid staying in the pores and blocking them. Additionally a pore closure can occur whereas polymeric molecules are forming and tar is deposited in the pores. Sulfuric acid is also known as a solvent, able to dissolve higher mass molecules. This results in a partial closure of pores, as the carbon may not be interconnected very well. “Graphenoidic structures”, as observed by Ana Primo et al. are forming during biomass carbonization, known as “graphitization”.[115] These graphene layers can capture liquid and therefore being blocked for an active

observation of surface area, even after washing and drying. Amberlyst 15 gives a nitrogen sorption result of 62 m^2 g^{-1} and is therefore in good agreement with values reported in the literature (52 m^2 g^{-1}).[108] The surface area is bigger than the one of glucose and starch. Because Amberlyst 15 is a macroreticular polymeric resin based on crosslinked styrene divinylbenzene copolymers, the elemental analysis will give more detailed information on the composition in the following.

2.3.3. Elemental analysis

The insertion of sulfur is directly connected to the active sites in the solid acid catalyst. Comparison of sulfonic acid groups in all four cases proves the integration, as can be seen in table 2. While the carbon black, glucose and activated carbon samples exhibit a low increase of 0.5 to 0.7 wt% of the total catalyst weight, the starch catalyst could be enriched in sulfur by a value of 1.5 wt%.

Table 2: Sulfur content of carbon samples after sulfonation, according to elemental analysis. The difference to the unsulfonated material is expressed in $\Delta_{unsulfonated}$. All values are mean values of 2 - 4 measurements.

Sulfur Content / wt%	Sulfonation Degree	$\Delta_{unsulfonated}$
Carbon Black	2.1	+ 0.7
Glucose Carbon	1.1	+ 0.5
Starch Carbon	2.1	+ 1.5
Activated Carbon	1.4	+ 0.6
Amberlyst 15	14.5	-

In comparison with the sulfonated carbon samples, the sulfur content of Amberlyst 15 (14.5 wt%) is seven to thirteen times higher. The implementation of sulfonic acid groups into carbon is therefore possible, but the final value is not as high as it can be found in Amberlyst 15. The sulfonation degree is very similar in all carbon materials. 14.5 wt% is in satisfying accordance to the literature value of the manufacturer and reported values, speaking of 4.7

mol equivalent SO_3H (14.7 wt%) per gram of catalyst for Amberlyst 15 and 0.9 mol equivalent SO_3H (2.8 wt%) per gram of activated carbon.[116]

2.3.4. Titration

In order to accurately determine and compare the numbers of acid functional groups per weight of the respective catalysts, titration has been conducted on all synthesized materials. Samples of carbon black, Amberlyst 15, starch carbon, glucose carbon, as well as activated carbon have been examined by titration.

Each of the alkaline analytes has been prepared by first mixing the respective materials with 0.05 M NaOH in H_2O solution (25 / 5 mg of catalyst per ml of NaOH solution). After stirring for 45 minutes and ultrasonic bath treatment for 30 minutes, the solid constituents were filtered off the respective dispersion and an aliquot of 9 ml was used as analyte for the titration. A 0.05 M HCL in H_2O solution was used as the acid titrant solution in all cases.

The titration curve of a sulfonated material has its equivalence point at a lower volume of titrant added (e.g. carbon black 8.65 ml of 0.05 M HCL solution added), compared with the unsulfonated one (8.84 ml), as can be seen in table 3. This fact, as well as the slightly higher initial pH of the analyte, confirms the successful integration of sulfonic acid groups into the carbon structure, albeit to a low extent. The total density of acidic functional groups accessible on the surface of the sulfonated starch sample can be calculated accordingly to SI-F3.

Table 3: Conditions and results of the titration of several solid acid materials and their precursors. All measurements are executed at 24 °C. This titration determines all acid groups present in the material.

		Carbon Black		Amberlyst 15	Starch Carbon		Glucose Carbon		Activated Carbon	
		unsulf.	sulf.		unsulf.	sulf.	unsulf.	sulf.	unsulf.	sulf.
Concentration of catalyst in dispersion	[mg ml^{-1}]	5,00	5,00	5,00	25,00	25,00	25,00	5,00	5,00	5,00
Volume of titrant at equivalence point	[ml]	8,84	8,65	5,01	8,82	8,30	9,15	8,75	8,35	8,00
Density of acidic sites	[meq g^{-1}]	0,16	0,39	4,43	0,04	0,16	0,00	0,28	0,72	1,11

Despite the lower mass concentration of Amberlyst 15 in the prepared dispersions, the Amberlyst 15 analyte exhibits a considerably lower basicity compared with the other samples (SI-F4), hence considerably higher density of accessible acid functional groups (4.43 meq g^{-1}) in the dispersion.

2.4. Catalytic activity for carbohydrate upgrade

2.4.1. Conversion of fructose in packed columns

As all catalysts were characterized, sulfonated carbon black, Amberlyst 15, sulfonated glucose and starch carbon as well as the activated carbon catalyst were applied in a test set-up, using a simple stainless steel column. The set-up is schematically illustrated in figure 18. It consisted of a stainless steel column, what was able to be sealed with a filter plate on both ends. The columns used are 150 to 250 mm in length and have a diameter of 4.6 mm. Therefore, an empty volume of 4.2 ml and 2.5 ml was calculated respectively. The column can be heated up to 250 °C, using an external heating band and the residence time in the column is controlled by the flow rate applied. The flux is adjusted by using a piston pump. The resulting pressure of the system mainly originates from the back pressure of the filled powder.

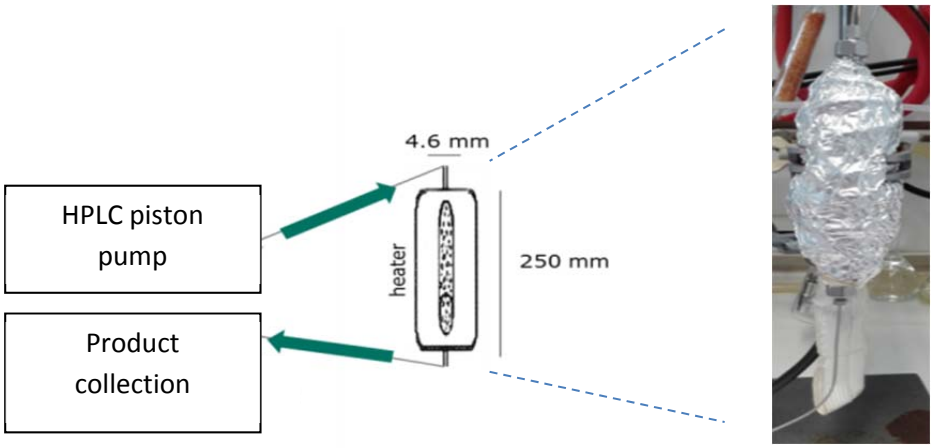

Figure 18: Schematic illustration of the reaction set-up (Supelco Blank Kit, 250 mm x 4.6 mm ID ¼" OD) used for the dehydration reaction of fructose. The left part represents the schematic sketch whereas the real set-up is shown on the right side.

The reaction medium consists of a 0.05 M fructose solution in an ethanol / 0.5 M formic acid mixture. The resulting dispersion is stirred intensively until all solid reactants are dissolved and the solution has a clear appearance. The solubility of fructose in alcohol is limited and acid addition is therefore necessary in order to keep the fructose in solution as well as to avoid recrystallization during the continuous process. The formic acid concentration was selected to have a ten times excess compared to fructose. During the hydration process over

solid acid catalysts, forming levulinc acid and furthermore ethyllevulinate, formic acid is released and is therefore anyhow present in the solution (Figure 19). The influence of formic acid as homogeneous catalyst plays a minor role, as could have been shown by Jiang et al.[117] They investigated the influence of formic acid concentration in water / n-butanol solution, residence time and temperature and showed, that after about 20 minutes, using a concentration of 2.5 M formic acid at 170 °C, the maximum yield is under 4 %. Therefore the influence of formic acid on the conversion can be neglected in the here introduced system.

The reaction cascade is shown in figure 19. The fructose is first dehydrated to 5-hydroxymethylfurfural, whereas three water molecules are released. Because there is ethanol as well as formic acid present in the solution, the HMF is further etherified to HMF derivatives (Figure 19, 1 and 2). The main product is 5-ethoxymethylfurfural (EMF) (1), proved by mass spectrometry (GC)-MS (SI-F5). A further consecutive reaction leading to ethyllevulinate is occurring, using the released water from the dehydration in a further hydration to levulinic acid.

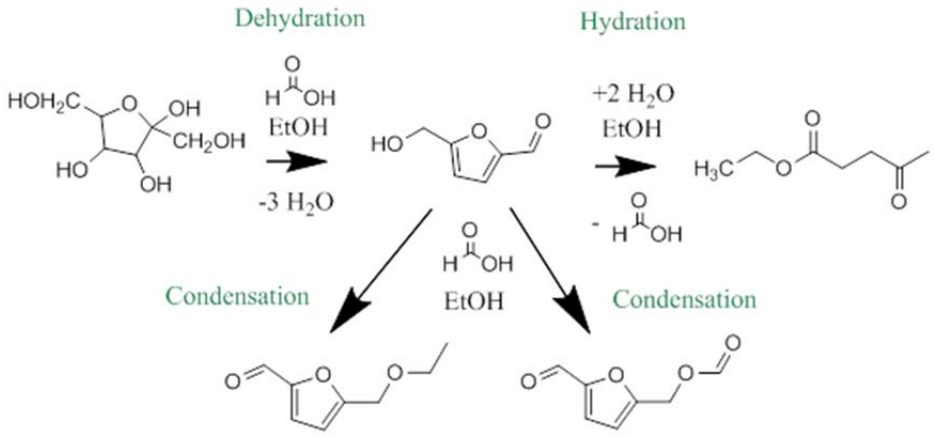

Figure 19: Illustration of the reaction cascade during the reaction from fructose to HMF derivatives. The main reaction product is 5-ethoxymethylfurfural. 5-(hydroxymethyl)furan-2-yl)methyl-formate and ethyllevulinate are consecutive products.

The results of the catalytic reactions were monitored employing a GC-MS system in combination with calibration curves to calculate the yield of the products.

2.4.1.1. Carbon Black

Carbon black has a large specific surface area (220 m^2 g^{-1}) and can be sulfonated from the edge terminations. After filling 0.7 gram of this sulfonated catalyst powder into the stainless steel column, the liquid substrate flow is immediately giving a high back pressure at small flow rates (>100 bar). This circumstance even intensified during the test run, and it was never possible to flow through the fixed catalyst bed. This result shows the importance in combination of a carefully selected particle size with particle porosity, to enable the flow of the liquid stream through a catalytic bed. High surface area is not enough, like it is always pursued in batch reactions to increase the number of active sites. When it comes to continuous systems, high surface area in combination with adequate particle / grain sizes is necessary, in order to not block the used filter at the ends of the stainless steel column. Pressure drops over a catalytic bed always need to be avoided, because the amount of energy going into the system is increased by the pressure build-up, as well as by safety concerns.

2.4.1.2. Amberlyst 15

Another commercial resin, which is already used for years and is therefore well characterized, is Amberlyst 15, a polymerized ethenylbenzenesulfonic acid, used for cation exchange or as solid acid. 2.4 gram of this 300 µm in diameter material was filled in the 250 mm stainless steel column and first flushed with pure ethanol to equilibrate the whole system at the according temperature and to check the back pressure. The particles of this catalyst are in a sub-millimeter range and back-pressure was never higher than 3 bar, which can be considered rather low when compared to the previous case. Amberlyst 15 (1.7 g cm^{-3}) was used at the maximum applicable temperature of 110 °C. The flow rate was adjusted in order to achieve residence times between around 2 and 30 minutes. These conditions were selected to analyze the connection between contact time with the catalyst and selectivity towards HMF derivatives. It is known, that the contact time to active sites play a crucial role in terms of the selectivity, as the reaction to the less wanted ethyllevulinate is a consecutive one. The results of this study are shown in figure 20.

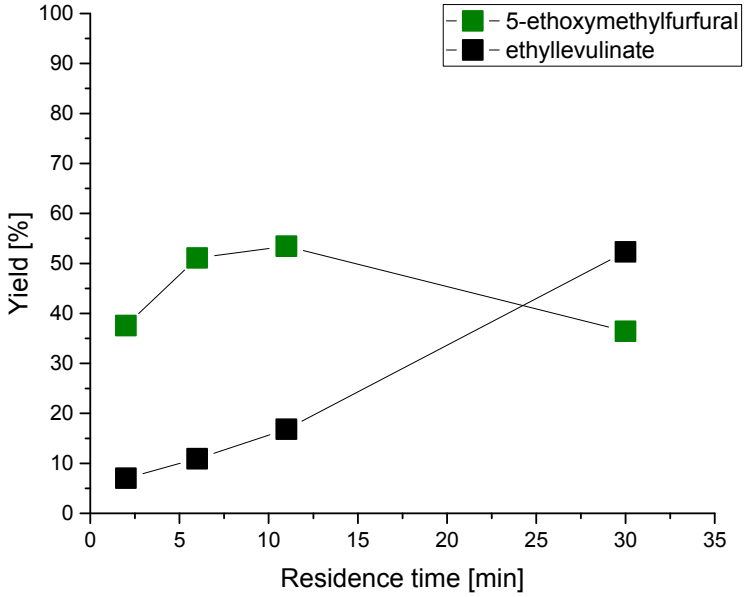

Figure 20: Resulting yield of HMF derivative and ethyllevulinate over different residence times in the Amberlyst 15 column, applying a temperature of 110 °C. The conditions are: 0.05 M fructose with 0.5 M formic acid in ethanol solution. Adapted from reference 139.

Residence time is of great importance when it comes to desirable products. The longer the solution and therefore the molecules are in contact with the solid acid catalyst, the more of the consecutive reaction towards ethyllevulinate takes place. The highest reactivity to the desired product is obtained using a flow rate of 0.25 mL min^{-1}, translated to a residence time in the column of about 11 minutes. With this residence time a yield of 53 % is achieved in addition to about 17 % ethyllevulinate. The EMF production seems to run through a linear initial phase, where the reactivity can be raised until 51 % yield at about 6 minutes. After this point the curve starts to flatten and the yield decreases, what goes inversely to the fact that the consecutive reaction sets in. Again, a linear yield increase of the ethyllevulinate can be seen until about 53 %Y after 30 minutes residence time. This result is already very promising, as the system does not need to be heated to more than 110°C.

2.4.1.3. Carbohydrate based material

For a possible increase of temperature and an as well more green approach in terms of catalyst production, the glucose / starch carbon based materials were tested with the same set-up.

Glucose carbon catalyst

1.73 gram of sulfonated glucose carbon material was filled into the 250 mm stainless steel column and screened in a temperature variation. The results are shown in figure 21. The yield of HMF derivatives as well as ethyllevulinate are outlined.

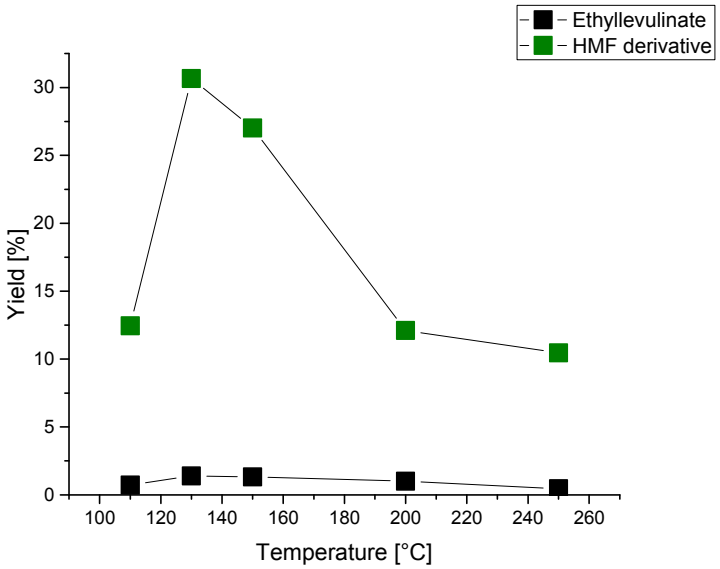

Figure 21: Resulting yield of HMF derivative (mainly EMF) and ethyllevulinate over different temperatures in the sulfonated glucose carbon filled column. The conditions are: 0.25 mL min^{-1}, 0.05 M fructose with 0.5 M formic acid in ethanol solution.

The results at 110 °C differ significantly from the results of Amberlyst 15 in terms of yield of HMF derivative and EL. 12 %Y of HMF derivative was achieved, whereas EL was just present in traces. As the main goal is to increase the selectivity to HMF (further production to DMF), this is already a promising result, even if the yields are low. The highest yield (32 %) was achieved with 130 °C and is hence the maximum of the curve. With higher temperature, the reactivity dropped again to values of around 10 %. This increase of heat favors consecutive reactions, different from levulinic acid and ethyllevulinate. With the Amberlyst 15, this

behavior was not observed before in a continuous run. The ethyllevulinate yield was however never higher than 1.5 %. The relatively low yields in general are believed to result from the very low surface area (6.9 $m^2 g^{-1}$) and the bulky particles. The acidic site density was only 0.28 meq g^{-1}, compared to 4.43 meq g^{-1} for Amberlyst 15. Nevertheless the 31 %Y of HMF derivative of sulfonated glucose carbon is quite promising in combination with such an easy catalyst and system.

Starch carbon catalyst

Starch was showing a similar surface area (7.4 $m^2 g^{-1}$) as glucose and 0.8 gram were filled into a 150 mm stainless steel column. The results are shown in figure 22.

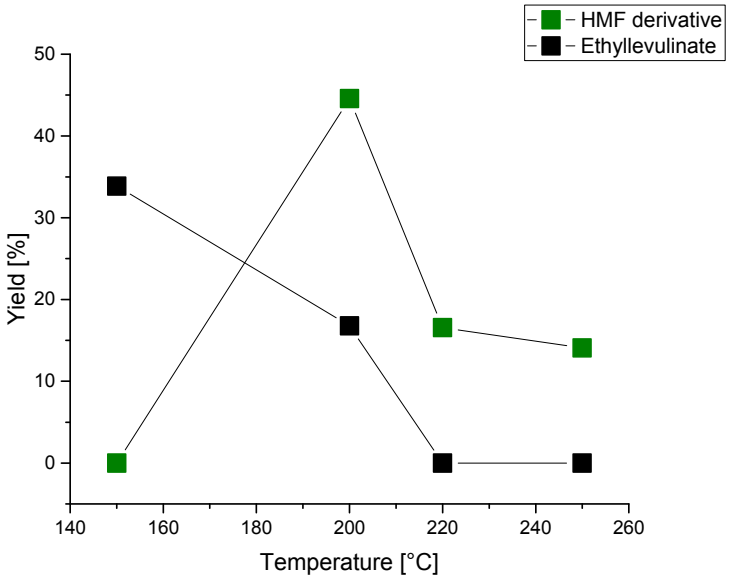

Figure 22: Resulting yield of HMF derivative (mainly EMF) and ethyllevulinate over different temperatures in the sulfonated starch carbon column. The conditions are: 0.25 mL min^{-1}, 0.05 M fructose with 0.5 M formic acid in ethanol solution.

The results shown in this chart are different of what we have seen with glucose. The HMF derivative also reaches a maximum (44 %Y), but it occurs at 200 °C, instead of 130 °C. At lower temperatures, the ethyllevulinate yield reaches its maximum with 34 %, but drops to 0 % with increasing temperature. In general the selectivity towards the favored products is relatively low, as also unknown reaction products (higher mass molecules, humin fragments)

occur in the GC-MS. But overall the more sheet like structure seems to prefer a different selectivity, but also gives better yields for HMF compared to glucose carbon. This fact can be explained by a high sulfonation degree (-SO_3H groups), as measured with elemental analysis. Whereas sulfonated glucose had a degree of 1.1 wt% sulfur, the sulfonated starch gave a result of 2.1 wt%. The higher temperature needed to achieve a 44 %Y can be a drawback in terms of a higher energy input necessary compared to glucose carbon. Results like shown with Amberlyst 15 could have not been achieved, as this commercial catalyst just needs 110 °C to show high dehydration activity. But thinking of a mixed column approach (combining catalysts), wide temperature stability is beneficial.

2.4.1.4. Activated carbon

To complete the study with a sample showing a high surface area (144 $m^2\ g^{-1}$), the activated carbon was used in the 250 mm stainless steel column. In this study however the selectivity differs from all the catalysts tested before. For instance, no HMF derivative was observed, but a further reaction product called 5-methylfurfural, which represents a structure with one less alcohol group (Figure 23, 2). This molecule is a consecutive reaction product with an already occurring hydrodeoxygenation reaction (HDO) / transferhydrogenation. This fact is also supported by the occurrence of 2,5-dimethylfuran (Figure 23, 3), which is an even further HDO product, where also the aldehyde group of the 5-methylfurfural is cut additionally. With these results, it is speculated, that the formic acid can be activated by the carbon structure to act as a hydrogen donor for a transferhydrogenation.[118] As catalysts used for reduction, including hydrogenations are typically noble-metals, hydrogenation by carbons is a young field of research. Not much is known about “carbocatalysts”[119], especially for reduction reactions. The observed transferhydrogenation is therefore promising, as until now, only standard reactions like nitrobenzene or 4-nitrophenol conversions were really tested. It is mainly reported, that the reactivity is a result of graphene structures, oxide functionalities and doped graphene materials. As reported by Primo et al, it is possible to convert biomass into graphene-like structures, what is also the case with our activated carbon from biomass precursors. As biomass possesses a lot of oxygen, the possibility of forming graphene oxide is given as well. In general this activated

carbon material seems to have functional groups, able to activate hydrogen, which are not present in the other carbons. Also ethyllevulinate is produced with a yield of 26 % at 150 °C (SI-F6). All qualitative and quantitative reaction results are shown in figure 23.

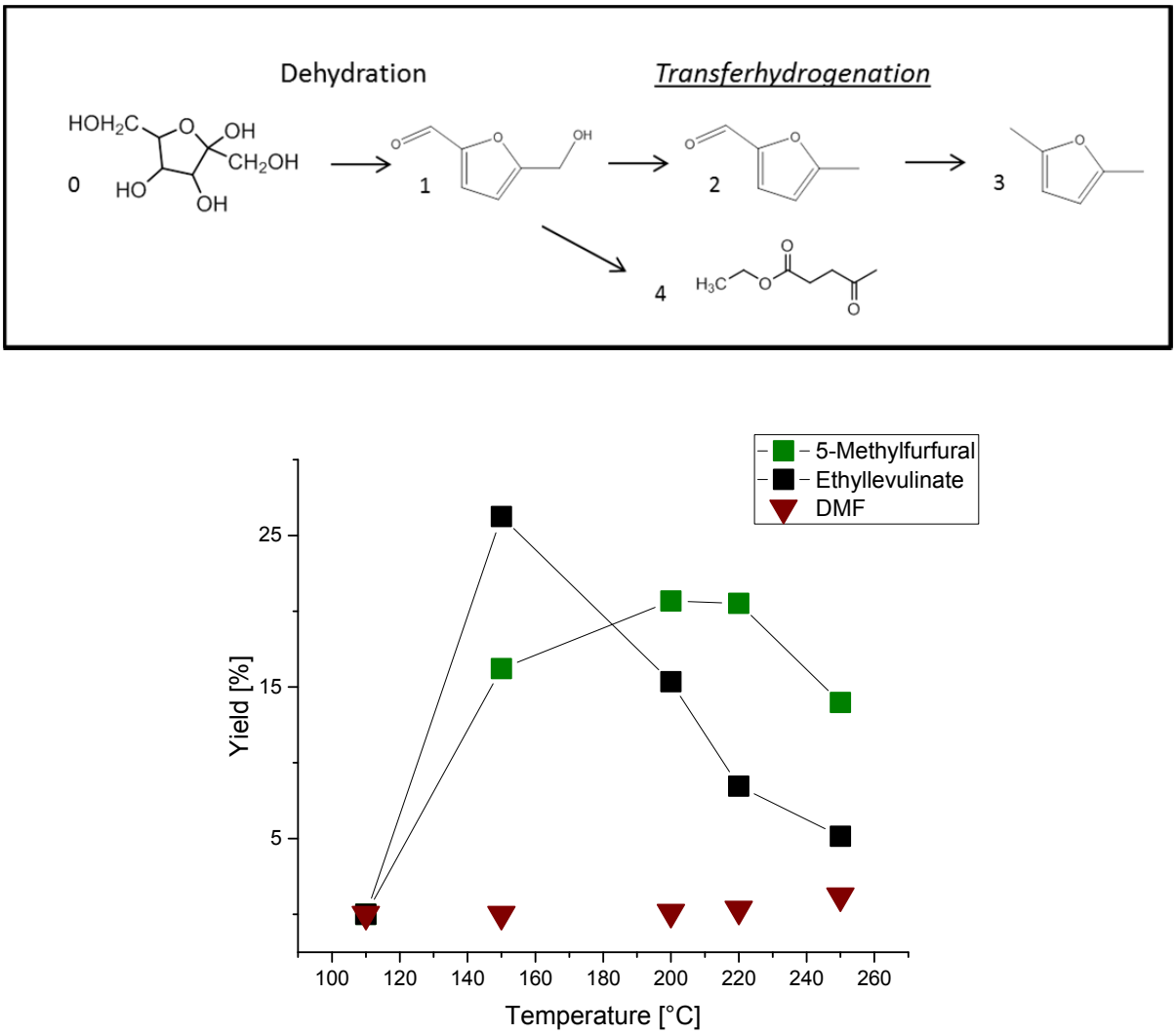

Figure 23: Reaction scheme of the dehydration of fructose using activated carbon material. Besides the qualitative results, the quantitative results are shown. The yields of 5-methylfurfural (2), 2,5-dimethylfuran (DMF) (3) and ethyllevulinate (4) over different temperatures in the sulfonated activated carbon column are plotted. Conditions: 0.25 mL min^{-1}, 0.05 M fructose with 0.5 M formic acid in ethanol solution.

This multi-reactivity of carbon is also mirrored in the quantitative results. Synthesizing DMF out of a fructose solution using a "carbocatalyst" in combination with a transferhydrogenation is already remarkable, because it was not observed before. The maximum yield of the obtained DMF is about 1.5 % at 250 °C. Whereas the 5-methylfurfural

and the ethyllevulinate have their maxima at 200 °C and 150 °C. The maximum of yield is lower, even if the sulfonation degree is similar to the other sulfonated carbons. The surface area is high, but where the titration results hint towards a higher amount of acidic groups (1.1 meq g^{-1}), the reactivity does not follow this trend. The dehydration of fructose and the further hydrodeoxygenation is anyway present, but follows a different reaction path, compared to the other carbon catalysts. As a final goal, full hydrodeoxygenation is desirable and DMF is therefore a promising product in which the before mentioned stored energy of the sun is almost fully preserved in the molecule. A "carbocatalyst" would avoid the need to use metal and opens up possibilities, which are cheaper, as the material is abundant. It needs to be understood how the catalyst is working and how to synthesize and optimize it in an easy way, to make it usable for industrial applications.

2.4.1.5. Comparison and concluding remarks using productivity

Every catalyst system has different behavior and activity towards different products. We can conclude with a graphical presentation, whereas the reactivity towards HMF derivatives and follow up products (e.g. 5-methylfurfural for activated carbon) is referred to the time in contact, as well as the catalyst weight. These results are shown in figure 24. The data were calculated using the HMF derivatives, including all the products which are resulting out of HMF. All reactivity strongly depends on the temperature, as this parameter is here considered as one of the most important and therefore used as X-axis. Because of the dependency on the temperature, all catalysts also expose an optimum, on which the highest yields of products are obtained. For glucose carbon, this optimum, which can be seen as the best temperature to operate the catalyst, is reached at 130 °C. Micrometer particles show the lowest activity. The second best reactivity is shown by the activated carbon material. Here the optimum is reached at around 200 °C, almost the same temperature also the starch carbon catalyst shows its best results. The starch carbon material has a lower surface area compared to the activated carbon, but nevertheless shows a better performance at 200 °C. This fact can be explained by the higher sulfonation degree of starch in comparisons to the activated carbon. The broader peak of the activated carbon, what means a broader range of temperature commitment and stable performance, is also significant.

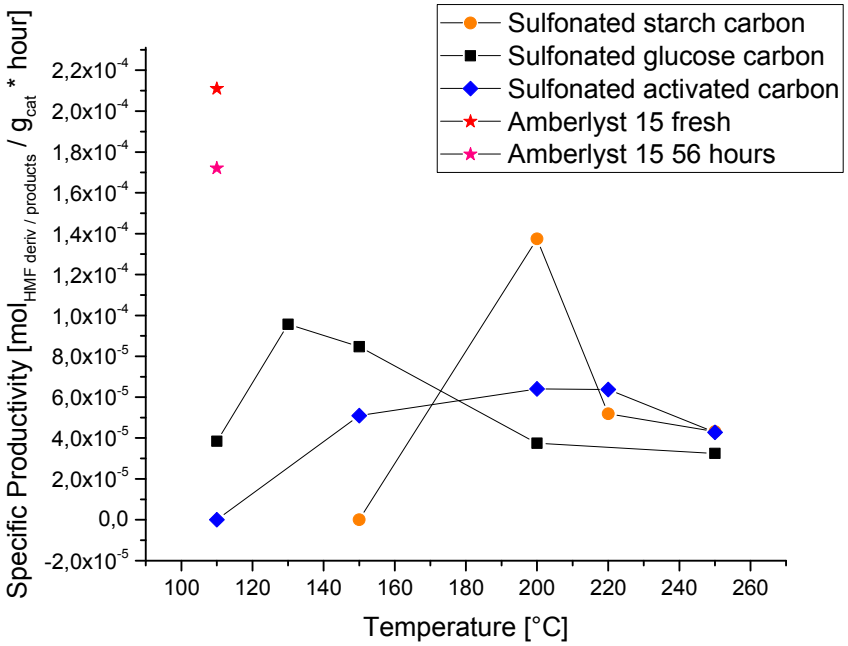

Figure 24: Specific productivity of HMF derivatives plotted against temperature in all columns for comparison. For the activated carbon material, the concentration of 5-methylfurfural as well as DMF was used.

As Amberlyst 15 was tested with 110 °C (limit for application) at the beginning and after a long time run of 56 hours, these results are presented as points. Nevertheless, Amberlyst 15 shows the best reactivity compared to the other materials in a flow system with a residence time of about 11 minutes. Even after 56 hours of continuous run, the catalyst shows high activity and loses only 10 % of its primary reactivity. The catalyst shows by far the highest sulfonic acid loading with having a relatively limited surface area of 62 m^2 g^{-1}. As all carbon catalysts have their optima at higher temperatures compared to Amberlyst 15, this catalyst is further used for studies extending the flow system with consecutive reaction columns for further hydrogenations. A two column system first converts the fructose in a dehydration reaction, before the second column converts the products further. Because the carbon materials show good reactivity at higher temperatures, as well as especially the activated carbon revealed its superiority in terms of directly synthesizing DMF, it will be used in a mixed column approach in further studies in chapter 4.

2.5. Summary

The characterization of the examined catalysts included investigations on the morphology by SEM and TEM, BET surface area by nitrogen adsorption, elemental composition by elemental analysis and the density of accessible acid sites by titration. The reactivity of the catalytic material is analyzed in the light of the relation to their structural properties and chemical identity. The glucose and starch derived carbons were identified as large, non-porous particle blocks in the optical measurements, which is in agreement to the measured BET surface area of ca. 6 $m^2 g^{-1}$. By using an activation method, the surface area of carbon could be increased drastically to 144 $m^2 g^{-1}$. Amberlyst 15 exhibited a low surface area of about 62 $m^2 g^{-1}$, which is in accordance with values reported in literature. As Amberlyst 15 is a well-established and well-known catalyst, it serves as a model material to compare with the prepared sulfonated carbons in terms of catalytic reactivity. The overall activity for the fructose dehydration over Amberlyst 15 was selective for 5-ethoxymethylfurfural (EMF), whereas ethyllevulinate (EL) was the major byproduct. The conversion took already place at 110 °C with high yields of 53 % for EMF and 17 % for EL, at residence times of about 11 minutes. Among the prepared sulfonated catalysts, a similar level of activity (44 %Y) was only reached by the sulfonated starch catalyst, but at a temperature of 200 °C. All catalysts exhibited selectivities on a similar level, with the exception of the activated carbon material, which promoted further hydrodeoxygenation / transferhydrogenation of the furanic aldehyde without metals present. This qualitative analysis was showing 5-methlyfurfural as intermediate, as well as 2,5-Dimethylfuran (DMF) as final product. HMF derivatives like 5-ethoxymethylfurfural or 5-(hydroxymethyl)furan-2-yl)methyl-formate were not observed, but the direct hydrodeoxygenation resulted in a maximum yield of 1.5 % DMF directly. All prepared carbon catalysts did not reach a level of catalytic reactivity at 110 °C, which can compete with the commercial Amberlyst 15. Nevertheless, they are active at temperatures, the Amberlyst 15 material is not usable anymore, due to stability. Further investigation on the integration of sugar dehydration with further hydrogenation of HMF to 2.5-dimethylfuran needs to be done, whereas the “carbocatalyst” offers the most promising way of metal free hydrogenation reactions.

3. Tungsten carbide based hydrogenation catalysts: Active support for transition metals

3.1. Introduction

The upgrade of dehydrated products from fructose (chapter 2), such as the HMF derivatives like 5-(ethoxymethyl)-2-furaldehyde and 5-(hydroxymethyl)furan-2-yl)methyl-formate, or ethyllevulinate is desirable for preparing molecules with higher heat of combustion values for fuel applications. The usage of hydrogen in combination with a suitable catalyst offers herein a promising route, also known as hydrodeoxygenation. Transition metal carbide materials are not only known for their particular physical properties[120], like melting points above 1500 °C or extraordinary hardness and also density (16 g cm^{-3})[121], but also attract recently attention by using them for the hydrogen evolution reactions[122], as well as heterogeneous catalysis[123]. As Levy and Boudart elucidated the similarity in the electronic structure of tungsten carbide to platinum already in 1973, scientific research focused onto using this material increasingly in catalysis. Especially in recent years this material was explored, due to its relatively low price and stability compared to noble metals, which goes along with its resistance towards poisons like H_2S or CO, and the possibility to use it in high temperature applications. Transition metal carbides based on tungsten, molybdenum, chromium or titanium show promising results in different catalytic reactions like desulfurization or hydrogenation.[124] The before mentioned “carbocatalysts” are another family of new catalytic material, whereas the following chapter will focus on transition metal carbides.

As catalytic reactions are strongly dependent on active sites accessible on the surface of a material, the crystalline structure plays a crucial role. Pure metals show different lattice structures compared to metal carbides. The additional carbon in tungsten carbide broadens the crystal unit of the pure metal and therefore the d-band structure of the respective metal by interaction with the s-and p-orbitals of the carbon atom. By doing so, the lattice changes and hence becomes similar to the d-orbital in platinum. This decrease of the d-band in relation to the Fermi level results in a different activity and reactivity, more similar to the highly active sites of the rare and expensive platinum and its catalytic behavior in general.[125]

Tungsten itself is cheaper and more abundant then platinum, which is shown in figure 25, in the so called Goldschmidt classification.

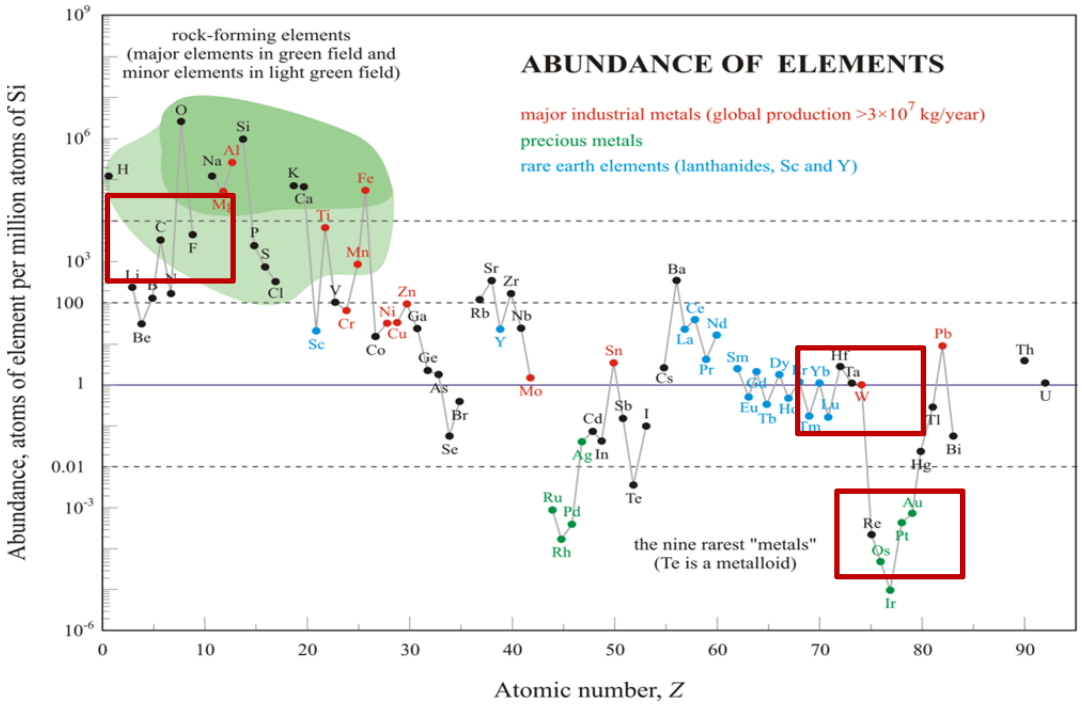

Figure 25: Goldschmidt classification of abundant atoms in the earth's crust. Platinum (Pt), tungsten (W) and carbon (C) are highlighted. (Adapted from Generalic, Eni. "Rare Earth Elements (REE)." EniG. Periodic Table of the Elements. KTF-Split, 29 May 2017. Web. 9 Aug. 2017. <http://www.periodni.com/rare_earth_elements.html>)

This plot relates the abundance of atoms to ubiquitous silicium and is hence an illustration of how much of these particular atoms can be found in the earth´s crust. Considering rare metals and compounds are generally more difficult to extract from a specific volume of stones and rocks, the materials which are scarce are also more expensive. Unfortunately the rarest metals like platinum, palladium, ruthenium, and rhodium or also gold are known for the highest activity in hydrogenation reactions, due to their high affinity and ability to dissociate hydrogen on their surface. The property of a partially filled d-sub shell and the variable oxidation number of transition metals makes them active as catalysts, being able to "store" electrons temporarily. Alternatives in terms of same reactivity but less cost are rare, whereas research recently focuses in a more intense way towards nickel catalysis. One promising approach aims to increase the number of active sites by creating a higher surface

area. To scale down the particles from bulk to micrometer or even nanometer size brings not only higher surface area, but also different activity in terms of selectivity towards other products, as the electronic surface properties are changing with size and shape.[126] [127] The effect of adsorbing and spill over hydrogen on different sites next to other adsorbed intermediates brings molecules close for reaction.[128]

Tungsten carbides are already know and used since decades. They are appreciated for the already mentioned physical properties and are hence used for drilling, ammunition, sports, surgery or even jewelry, considering a hardness of around 9 on Mohs scale (diamond being 10) or around 2600 on Viker´s scale.[120] Tungsten carbide has a strong internal bonding and a typical hexagonal crystal structure, whereas other forms of crystals structures exist under specific conditions.[129] The manufacturing of WC nanomaterial is normally done using high temperatures and harsh conditions. As noble prize winner Richard Feynman gave his famous lecture “There is plenty of room at the bottom” in 1959 it was discovered that in fact nano-scaled materials offer catalytic properties, their bulk structures are not known for. This is true for metals like gold[130], as it is for tungsten carbide. Especially the possible adsorption of hydrogen and its diffusion and spill over on massively increased surface areas, makes it interesting especially in nanometer size.[131]

In this chapter the influence for reactivity by decreasing the particle size of tungsten carbide as a possible alternative to platinum will be discussed. Additionally the tungsten carbide particles are also discussed in the context as an active support for bimetallic catalysis. By decreasing the particle size of tungsten mono carbide, the reactivity for hydrogenation was investigated. Furthermore the deposition of transition metals like copper, palladium and nickel was realized to study the synergistic effects of these materials in reaction. In view of the substrates chosen, the focus was on the investigation of selectivity of tungsten carbide of different particle sizes towards functional groups under mild conditions. The overall and final approach is to use one synergistic material as catalyst for carbohydrate upgrade.

3.2. Synthesis of nanoscaled tungsten carbide via urea route

The existence and industrial production of tungsten carbide is known since the 1920´s. Nevertheless the production of nanometer particles is a big challenge under relatively mild conditions. The hardness of the material as well as the internal bonding makes it difficult to grind it, when thinking of physical "top-down" methods (laser ablation or pulsed-deposition). Chemical approaches like the so called "bottom up" methods are more promising, as also recently an easy approach using the so called "urea glass route" was investigated. The procedure was adapted from Giordano et al.[132], who studied the "easy method" for the production of nano-scaled tungsten carbide, using a simple and inexpensive as well as mild approach, what is summarized in figure 26.

$$R_1 = \frac{g_{urea}\, M_{metal\ precursor}}{g_{metal\ precursor}\, M_{urea}}$$

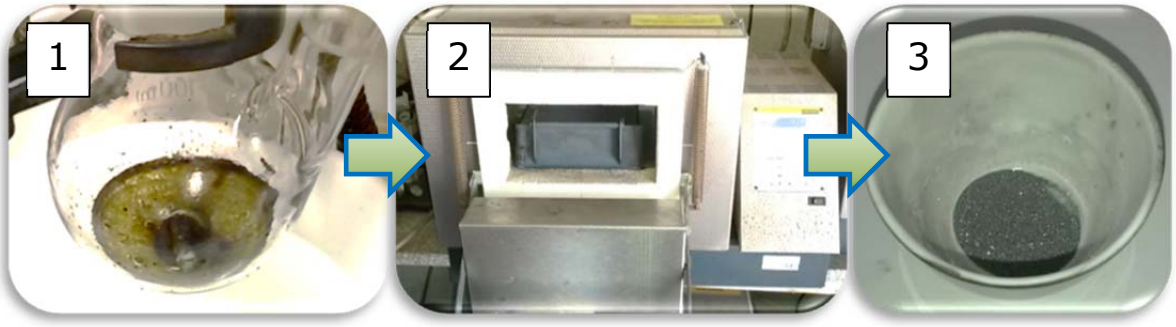

$$R_2 = \frac{g_{EtOH}}{g_{metal\ precursor}}$$

Figure 26: Simplified scheme for calcination of a tungsten urea gel using a nitrogen oven with 800 °C.

The nano-scaled tungsten mono carbide was obtained by carbothermal treatment of a tungsten (IV) chloride / urea mixture in ethanol. Depending on the ratio of metal precursor as well as urea, the results range from tungsten mono carbide WC, over tungsten semi carbide W_2C to tungsten nitrides WN, or even pure tungsten metal W. In our study a molar ratio of $R_1 = 7$ was preferred, because of the interest in a pure tungsten mono carbide phase. The mass ratio for the solvent to metal precursor was $R_2 = 2$. The tungsten (IV) chloride was first weighted in a glovebox, because of a high sensitivity to water. The metal precursor

reacts vigorously with the alcohol solution but less intensive as it would do with water. The hydrolysis reaction releases HCL what goes along with an intense heat production. After handling the solution under stirring and adding the ethanol carefully, the urea was added in a typical ratio of R_1 = 7. The mixture was stirred as long as visible urea crystals disappeared. The solution was exposing a brownish-black slurry, which was transferred to a ceramic crucible after waiting for about 2 hours. During the mixing and with time the solution started to form a gel like structure. After the metal-orthoesters were forming with the ethanol, the urea starts coordinating around these molecules forming a kind of hydrogen bond stabilized structure. Urea is known as a chelating agent and acts in this case as stabilizing agent as well as a source for carbon and nitrogen. During the carbonization at 800 °C for 3 h (4 h ramping to reach 800 °C) the W-gel is converted into WC, whereas urea plays an important role as reducing agent. As it was reported by Giordano et al, the ratio R_1 has the greatest impact on what metal carbide / nitride is obtained. The mechanism of forming the mono carbide was reported previously.[62] The production of the material depends strongly on the conditions and especially on the temperature used. A typical order of formation is reported as follows: $WO_3 \rightarrow WO_xC_y \rightarrow W_nC_m \rightarrow W_2C+WC+W \rightarrow WC+W \rightarrow WC$.[133] WO_3 is least stable and the hexagonal crystal form is converted to the orthorhombic at 600 °C. After 800 °C it is reported to start forming a first oxy-carbide form WO_xC_y. The temperature rise results in W_xC_y, which is then converted to W_2C, WC or pure W. The tungsten mono carbide is the most stable form under high temperatures and is also the main product in our case. With the urea gel route the tungsten oxide was never observed at 800 °C. Nevertheless the samples were only just observed after full carbothermal treatment. The conditions were already optimized, and the method was used to focus on the production of WC as catalyst for hydrogenation reactions.

3.3. Characterization of tungsten (nano) particles

However the material and its "urea glass route" production was already known since 2008, no detailed studies were done taking different particle sizes of WC into account, when it comes to conversion and selectivity using hydrogen in heterogeneous catalysis. Hence the reactivity strongly depends on the properties and surface quality of the catalyst, different sizes of commercial tungsten mono carbides were compared to the urea-route produced material (commercial product one: WC_{com}: -100+270 mesh, 99% metal basis, Alfa Aesar; commercial product two: $WC_{com\ nano}$ 150-200 nm, 99% trace metal basis, Sigma Aldrich). To first get an overview of the macroscopic nature of the material, SEM was performed, shown in figure 27. In all measurements it was thought to compare all used material. To give already a first overall impression, figure 27 also shows the main corresponding sorption and XRD results, what will be discussed in more detail in the following section.

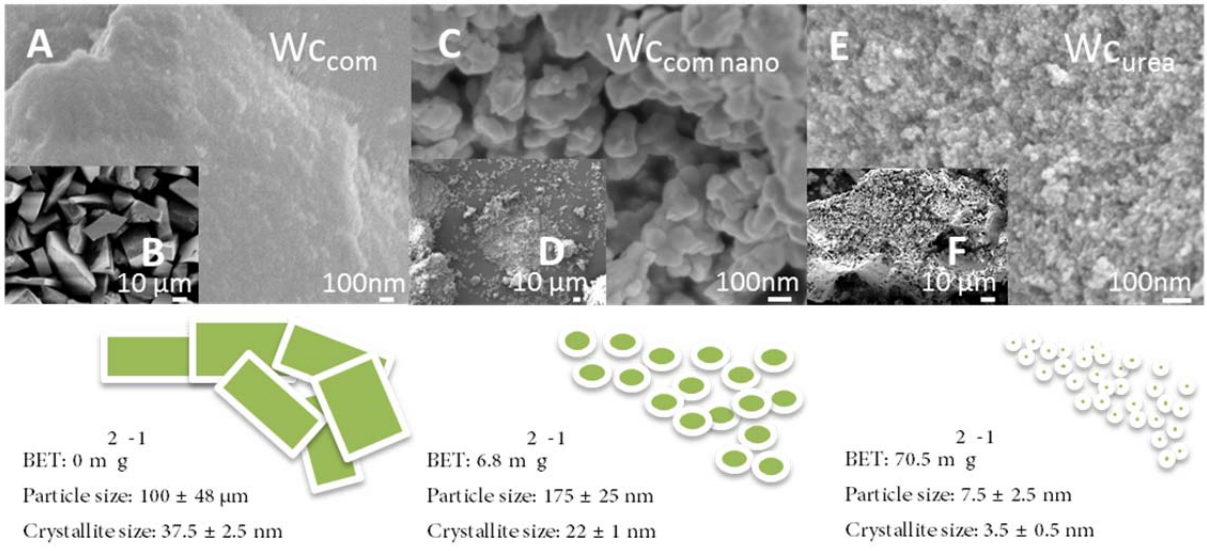

Figure 27: Scanning electron microscopy (SEM) results for commercial WC_{com}, nano-scaled commercial tungsten carbide $WC_{com\ nano}$ and tungsten carbide obtained from urea route WC_{urea}. Additionally the nitrogen sorption, as well as the crystallite sizes, calculated using the method of Scherrer are shown. The particle sizes were determined using TEM pictures. This figure was adapted from reference 135.

The SEM pictures of the different materials with the same scale already show the main differences to what the active sites, and therefore the reactivity can be connected to. The size of the particles is directly connected to the surface area, and TEM pictures of WC_{urea} are shown in figure 28.

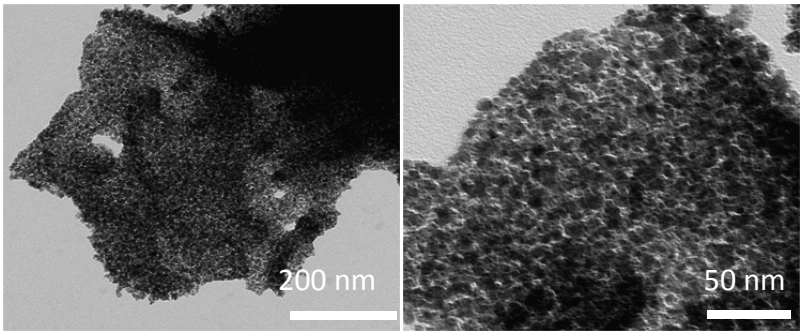

Figure 28: Transmission electron microscopy (TEM) of WC_{urea}. The measurement reveals the average particle size of the material to about 7.5 nm and shows a relatively homogeneous distribution.

The bulky commercial tungsten carbide WC_{com} in figure 27, A, B shows more edgy and rock-like particles of about 100 ± 48 µm in size. Higher magnification discloses the non-porous structure and relatively smooth surface. In contrast to the particles shown in figure 27, C, D, whereas the $WC_{com\ nano}$ particles are about five hundred times smaller with an average dimension of 175 ± 25 nm particle size. The overall appearance of this material is an agglomerated nanoparticle matter. The nanoparticles are loosely attached. The primary crystallite size of $WC_{com\ nano}$ is 22 ± 1 nm, what can be calculated from the XRD diffractogram in figure 29. The crystallite size is hence about 15 nm smaller than the bigger sized WC_{com}. The crystallite size of WC_{urea} is even nine times smaller than the one of WC_{com}, whereas the particle size is 7.5 ± 2.5 nm. With the "urea glass route", it is therefore possible to establish the smallest particle sizes.

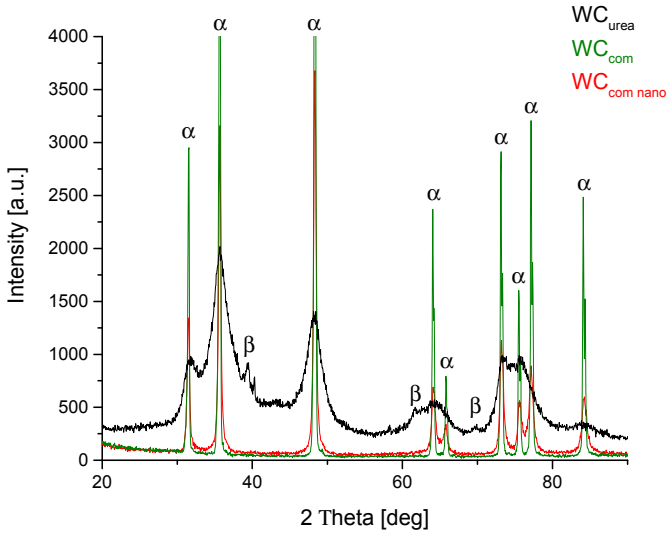

Figure 29: X-Ray powder diffraction of diverse tungsten carbides. WC_{urea}, WC_{com} as well as $WC_{com\ nano}$ are compared, whereas α represents the tungsten mono carbide (WC) peaks and β the tungsten semi carbide (W_2C) peaks. This figure was adapted from reference 135.

Because the crystallite size affects the reactivity, this XRD investigation already hints towards the possible difference in activity. The unit cells of the tungsten carbide crystals are the same in all samples, as the diffraction peaks of the materials are all at the same 2-Theta position (the three main peaks are at 31.7° (001), 35.7° (100) and 48.2° (101)). The unit cell of WC is usually hexagonal, primitive body centered. Due to the preparation method, using the R_1 ratio of seven, mainly tungsten mono carbide is synthesized. But due to slightly inhomogeneous regions in the W-orthoester-urea material, also tungsten semi carbide (W_2C) forms in very small amounts. The commercial WCs are highly crystalline, compared to WC_{urea}, what results in much broader peaks and therefore indicate a more amorphous structure.

A chemisorption using hydrogen would give more reliable results, considering not all the surface bears active sites. The main results of the surface area determination of the nitrogen sorption are as well summarized in figure 27. Like it is already seen from the SEM pictures, the surface area of WC_{com} is very low and is therefore considered as not detectable. 6.8 $m^2 g^{-1}$ for $WC_{com\ nano}$ are a result of the smaller particle size and therefore an increase of area. Nevertheless the area to mass ratio is still very small. Keeping the density of 16 g cm^{-3} of tungsten carbide in mind, the ratio of surface area to volume of material is much higher (e.g. 109 m^2 cm^{-3} for $WC_{com\ nano}$). Due to reasons of simplicity, the common unit (m^2 g^{-1}) will be used throughout the thesis. By using the “urea glass route”, surface areas of 70 m^2 g^{-1} are reached. This finding agrees well with the reported surface area in the paper of Giordano et al.

In terms of checking for the different composition of the different materials, a CHN combustion analysis was performed on all three carbides. The overall results of these experiments revealed a similar composition with the exception of the nitrogen content for the WC_{urea}. Like shown in table 4, the value of nitrogen is slightly higher than the nitrogen content of the commercial material.

Table 4: CHN combustion analysis for checking the composition of WC_{urea}, WC_{com} and $WC_{com\ nano}$.

	N[%]	C [%]	H [%]	C / N
WC_{urea}	0.9	5.0	0.8	5.6
WC_{com}	0.2	6.3	0.9	37.8
$WC_{com\ nano}$	0.2	6.2	0.62	40.5

The 4.5 times higher nitrogen content of WC_{urea} is believed to be a result of the way of synthesis. Urea itself can provide carbon and nitrogen, and a little amount of carbon nitride or tungsten nitride left in the sample cannot be excluded. The commercial tungsten carbides on the other hand are very similar in composition.

3.4. The smaller the better?

3.4.1. Tungsten carbide as active catalyst

In order to proof the activity for hydrogenation reactions and to show the relationship between particle size and reactivity, all three materials (WC_{com}, $WC_{com\ nano}$ and WC_{urea}) were tested in a commercial continuous fixed-bed reactor set-up, called H CUBE Pro ™ (first mentioned by Jones et al.)[134] This set-up is operated under relatively mild reaction conditions, reaching maximum temperatures of 150 °C and pressures up to 100 bar. The flow rates can be adjusted between 0.1 mL min^{-1} (~ 7.5 min) and 3 mL min^{-1} (several seconds). The cartridge itself, which holds the catalytic material, is 60 mm in height, whereas the inner diameter is 4 mm. The capacity is hence 753 µL. This set-up is therefore as well limited when it comes to residence times and it is also restricted at the temperature conditions, as tungsten carbide is known to exhibit good activity for hydrogenation between 150 °C to 400 °C. A schematic drawing of the set-up can be found in the supporting information of this thesis under figure SI-F7, as well as in chapter 4, where the settings and continuous flow reactors are described in more detail.

When speaking of similar catalytic behavior to platinum, WC should react similar in terms of dissociative chemisorption, uptake capacity and also mobility of the H atoms on the surface. The chemisorption itself occurs between the lowest unoccupied molecular orbital (LUMO) of H_2 and the highest occupied molecular orbital (HOMO) of the tungsten mono carbide. The hydrogen diffusion is anyhow significantly lower than on Ni (0.19 eV), Pd (0.11 eV) or Pt (0.23 eV), because the barrier to overcome is about 0.73 eV, as stated by DFT calculations.[131]

First attention was on understanding how reactive the synthesized tungsten carbide nanomaterial can be towards different functional groups in comparison to more bulky material. By understanding the connection between the activity for specific groups in a molecule and the conditions used, the overall conversion and above all the selectivity can roughly be estimated. For this first study, the bulky tungsten carbide WC_{com} with its very limited surface area was compared to the nanostructured material $WC_{com\ nano}$, as well as the synthesized WC_{urea}. As the fine nano-scaled tungsten carbide $WC_{com\ nano}$ was observed to

create huge back pressure during the flow process and reaction, an inert material (Al_2O_3) was used to disperse the fine powder on top of this micrometer scaled support. Pressure drops and back pressures over a fine-powder catalytic bed always lead to problems arising from the filter cake formation and blockage on a filter in a continuous reactor, when run in dead-end mode. Bulky material in a micrometer range can be applied in the 60 mm x 4 mm test cartridge without any problem, considering the mobile liquid phase has enough space to pass through the particles. The WC_{urea} showed an overall agglomerated structure of fine material (Figure 27, picture F) so that it was no problem to apply this catalyst directly for reaction.

The alumina powder (Al_2O_3) itself did not show any reactivity in the reactions and was therefore considered as a not active component in the hydrogenation under the applied conditions. In order to be able to compare the catalyst, a mass specific reaction rate R was calculated (SI-F8). This calculation correlates the product obtained to the residence time, as well as the gram of actual catalyst used and dispersed. In this way, the inert material, what does not have any influence on the hydrogenation can be excluded. The summarized results can be seen in table 5.

Table 5: Summarized results for the reactivity of WC_{urea}, WC_{com} and $WC_{com\ nano}$ towards different functional groups. Conditions: 10 bar H_2; 100 °C; 0.1 M; ethanol; [a] WC_{urea}; [b] 20 wt% WC_{urea} on Al_2O_3; [c] 20 wt% $WC_{com\ nano}$ on Al_2O_3; [d] WC_{com}; [e] Al_2O_3; [f] Conversion is calculated using GC-FID / MS data; [g] R (see SI-F8). This table is adapted from the reference 135. [135]

Entry	Substrate	Flow Rate [ml min^{-1}]	Conversion[f] [%]	Mass Specific Reaction Rate R[g] [s^{-1}]
1[a]	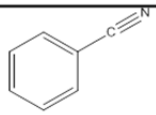	0.6	0	-
2[a]	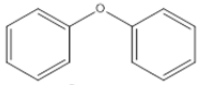	0.6	0	-
3[a]	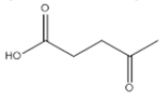	0.6	0	-
4[a]	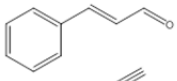	0.6	0	-
5[a]	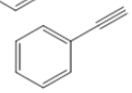	0.6	33	-
6[a]	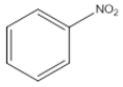	0.6	>99	-
7[a]	"	1.1	30	-
8[b]	"	0.6	>99	66.4 10^{-5}
9[b]	"	0.85	27	44.0 10^{-5}
10[c]	"	0.6	27	5.2 10^{-5}
11[d]	"	0.6	0	-
12[e]	"	0.6	0	-

At first, different functional groups like nitrils, aryl ethers, carbonyl compounds and multiple bonds were tested with pure WC_{urea} catalyst, as it is considered the most active, due to the smallest particle size. Our aim was to work under mild conditions in the range of 10 bar and 100 °C as well as 0.6 mL min^{-1} (~ 1 min residence time). The hydrogenation of none of these

functional groups was possible under these settings (also not at maximum equipment temperature of 150 °C), except for multiple bonds (entry 5) and nitrobenzene reduction to aniline (entry 6). With the mentioned mild conditions, a 33 % conversion of the terminal triple bond in phenylacetylene was observed. The resulting products are styrene, as well as ethylbenzene in different ratios, depending on the conditions used. These results are summarized in more detail in figure 30.

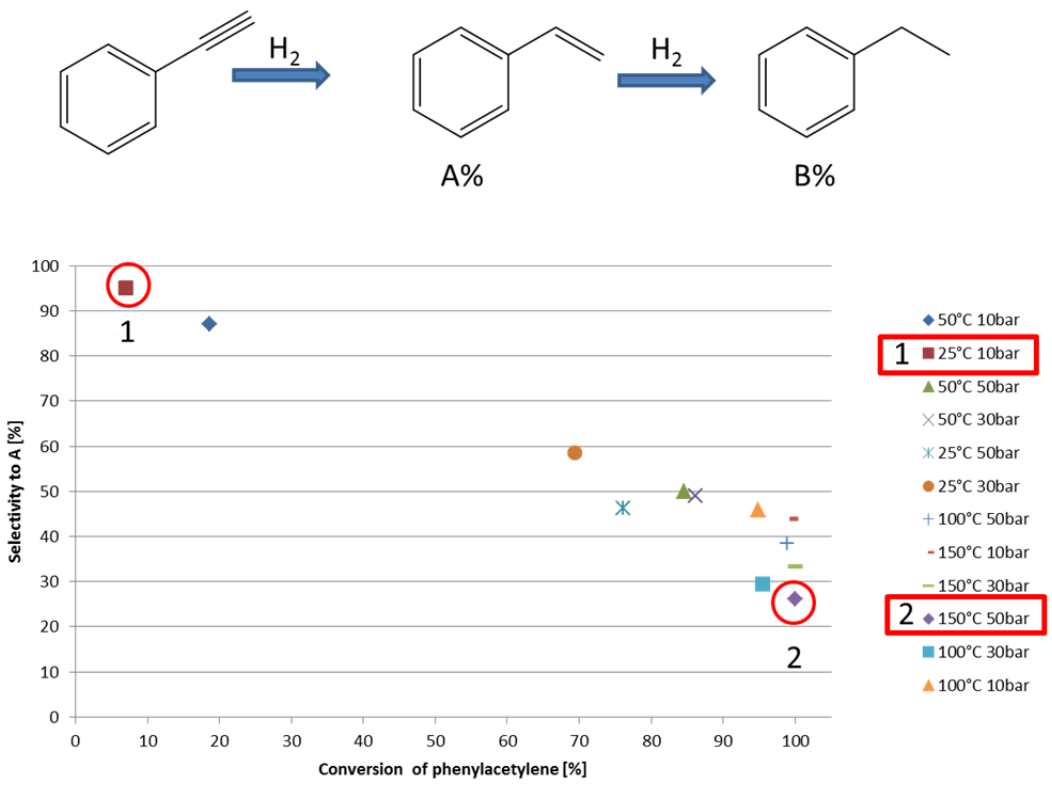

Figure 30: Summarized results for the reactivity of pure WC_{urea} towards phenylacetylene. The selectivity can be tuned by temperature and pressure adjustment. Conditions: 0.6 mL min^{-1} (~ 1 min residence time), temperature range: 25 °C to 150 °C, pressure range: 10 bar to 50 bar.

For the upgrade of phenylacetylene, and the production of styrene, industry is using a very selective catalyst called “Lindlar catalyst”.[136] This active heterogeneous calcium carbonate based material, with the addition of palladium, is deactivated with sulfur or lead as well as quinoline. By deactivation of some active sites of the catalyst, the reaction does not proceed to the alkane and can therefore be very selective for the alkene. Our nano-scaled tungsten carbide does not need to be deactivated and acts as a selective material by simply adjusting the conditions. Mild conditions like 25 °C and 10 bar result in a high selectivity of about 95 %,

but a poor conversion of about 10 %. By adjusting harsher conditions resulting in maximum 150 °C and 50 bar, the reaction can be performed quantitatively but with a poor selectivity of 25 % towards styrene. In summary a temperature and pressure depended reactivity can be concluded, which makes it possible to adjust selectivity towards the alkene or the alkane.

All reactions were done in ethanol solution as a “green solvent”, what can theoretically be obtained out of cellulosic biomass. Other than the mentioned functional groups examined, a full hydrogenation of nitrobenzene was possible and aniline was obtained with about 100 % conversion as well as selectivity, using WC_{urea} (entry 6). The bulkier particles were as well tested but did not show any reactivity like in the case of WC_{com} (entry 11), or limited conversion in the case of $WC_{com\ nano}$ (entry 10). The conversions of WC_{urea} as well as the $WC_{com\ nano}$ were compared, as both catalysts were dispensed over the aluminium oxide by simple mixing. The distribution was achieved by a wet-mixing-method using vigorous stirring for several minutes. Both WC_{urea} and $WC_{com\ nano}$ were therefore similar in distribution (20 wt %) on the aluminum oxide, and can consequently be compared with the mass specific reaction rate R (SI-F8). With WC_{urea}, an 8.5 times higher reactivity (R values) was observed compared to $WC_{com\ nano}$. The comparison was done under the same conversion of 27 % and 44 x 10^{-5} s^{-1} was obtained for WC_{urea} and only 5.2 x 10^{-5} s^{-1} for $WC_{com\ nano}$. With its about 23 times smaller particles, the reactivity is also expected to be higher as the particles also represent a ten times higher surface area.

In a first conclusion it can be stated, that tungsten carbide (in its nanostructured form $WC_{com\ nano}$, as well as WC_{urea}) was more active than its micrometer form. The material can directly be applied or distributed over an inert support. The activity in hydrogenation reactions under mild conditions (150 °C, 30 bar) is however limited and the catalyst was not showing high conversion rates for most of the examined functional groups. Nevertheless it showed a very high selectivity for nitrobenzene functionalities as well as a limited activity for multiple bonds and was further applied in reactions, which carry more functional groups possible to be hydrogenated (SI-F9). Also in here the high selectivity could have been preserved and the nitro moieties were converted exclusively without touching any other functional group. This high activity as well as selectivity can open up application possibilities in flow chemistry, whereas only specific side groups are needed to be converted. These results additionally proof the fact, that nano-structured tungsten carbide can be used in hydrogenation

reactions under mild conditions with high selectivity and conversion, what was in this form not observed before.

The overall stability of tungsten carbide catalysts is extraordinary high. It did not show any deactivation during the reaction of nitrobenzene hydrogenation over 50 hours of continuous run (Figure 31).

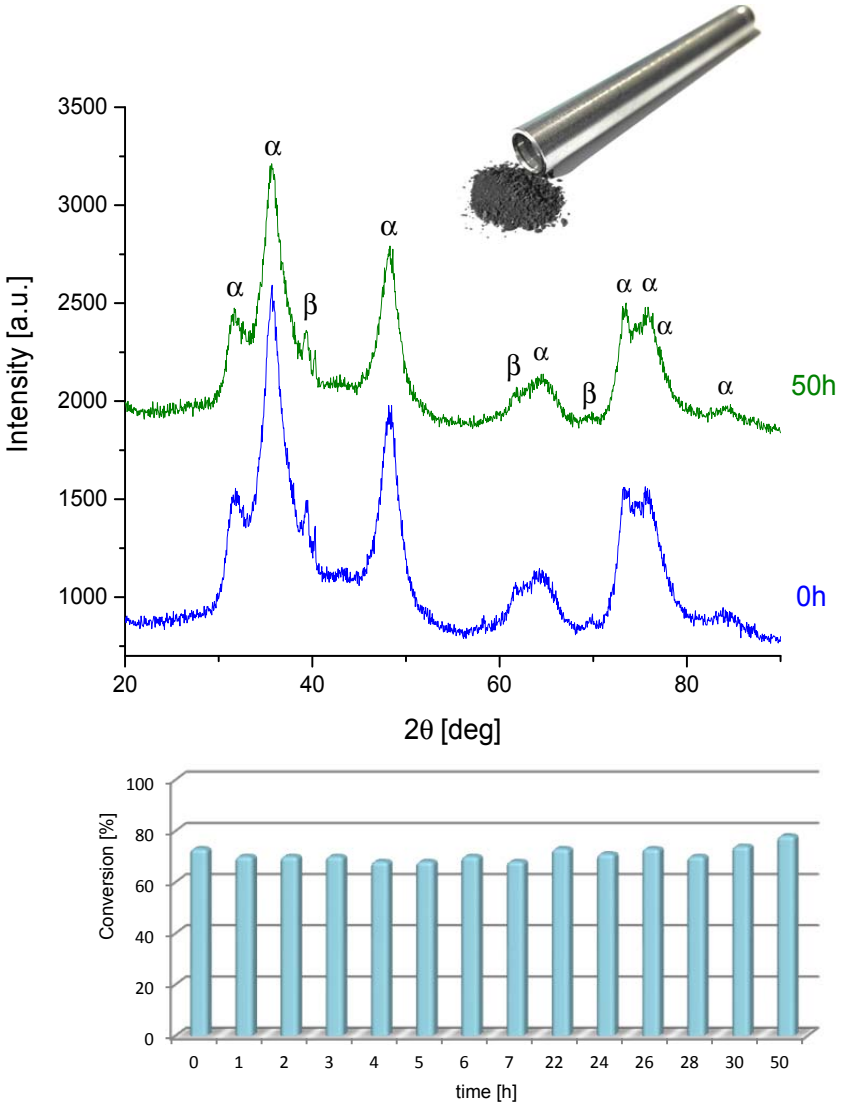

Figure 31: Comparison of XRD results after a continuous run of 50 hours of WC_{urea}. α represents the tungsten mono carbide WC, β the tungsten semi carbide W_2C. The results of the nitrobenzene hydrogenation are shown in the lower part. Conditions used: 1.6 g WC_{urea}, 10 bar with H_2, 60 °C, 0.6 mL min^{-1} (~ 1 min), in a 0.1 M nitrobenzene solution.

The longer a catalytic bed operates under the desired conditions, the less it needs to be restored, changed or renewed. The stability test for the simple nitrobenzene reaction hints towards an unusually high stability. With tungsten carbide WC_{urea}, the 50 hours reaction did not show any deactivation process. The XRD before and after reaction showed almost no alteration or change. The tungsten semi carbide phase β is still present as well as the main phase of WC. The crystallite size of the tungsten carbide particles changed just slightly from 3.73 nm to 3.62 nm, according to Scherrer calculations. The conversion of nitrobenzene to aniline under described conditions was monitored every hour and plotted cumulatively over time. The time differences between the measurements in figure 31 increase, as the reactivity did not change much over the observation period. The whole reaction was done at 70 % conversion, because full conversion experiments cannot tell about deactivation. In this case it is not sure to use the complete catalyst in the cartridge or just the first volume filled. The material is hence very stable and did not show any significant changes during this reaction.

Overall it was shown that the nanostructured material shows a better performance than the bulk material in terms of hydrogenation. The WC_{urea} is easy to synthesize using urea under mild conditions, and the applicability in a flow reactor system was proven. The platinum like electronic structure makes tungsten carbide interesting as an alternative to this expensive noble metal. The selectivity to nitro-moieties under mild reaction conditions is indeed high, as well as an activity saturating multiple bonds could have been shown. Unfortunately the reactivity is not high enough for upgrading biomass derived molecules under these conditions. Two possibilities are therefore feasible when we want to apply the tungsten carbide catalysts in biorefinery: A “chemical extension” or a “reactor (conditions) extension”. Physical extension is possible by expanding the reactor set-up, so harsher conditions in terms of temperature, pressure and residence time are applicable. This extended set-up will be discussed in chapter 4. First, the chemical prospects will be exploited, meaning the deposition of further transition metals onto the WC and the change of reactivity therefore using the synergistic effect of a bimetallic catalyst.

3.5. Tungsten carbide as support for transition metals

Three bifunctional catalysts were synthesized and compared in the following. The synergistic effect of tungsten mono carbide with copper, palladium and nickel was examined. The expensive palladium was chosen in order to compare a known and highly active hydrogenation catalyst to the other metals, as well as to explore the activity for using tungsten mono carbide as active synergistic support. Additionally copper is a relatively cheap material, which is also known to be active for some hydrogenations. For the same reason of availability and reactivity under mild conditions, the use of nickel deposited on tungsten carbide was investigated. Transition metal nanoparticles do not only offer a high activity, they also can become more selective by interacting with the support. By bringing a metal and a metallic ceramic (WC) close, the materials interact on an atomic level, sharing electrons.

Such interactions were recently discussed in the sense of an electron donating material and an electron accepting material. Tungsten carbide is therein an electron donor in the case of palladium.[62] The palladium is getting more electrons donated and is hence more electron rich at the surface. This results in a repelling effect, whereas oxygen containing species are harder to be adsorbed, but adsorption is easier for electron poor species. By coming close, a bifunctional mechanism can be imagined, whereas hydrogen spill over can occur at the interface. With nickel, similar effects are conceivable, whereas in our case the development of such a catalyst needs to be done first. By sharing an interface, it is possible for electrons to be exchanged.

Before exploring the reactions possible with the synergistic materials, it is important to understand the morphology and structure, what is discussed in the following paragraphs.

3.5.1. Synthesis and characterization of copper -, palladium- and nickel@WC

As nanoparticles of tungsten mono carbide were already showing selective activity connected to the small particle size, this material was chosen as a support material for copper, palladium and nickel nanoparticles. In order to synthesize the nano-material in a reproducible way, an oven using 5 % hydrogen in argon as reducing agent was utilized. A wet impregnation process was applied, whereas the metal salt was solubilized or dispersed in the solvent ethanol. $WC_{com\ nano}$ was chosen in order to have a pure, highly crystalline tungsten mono carbide phase without any impurities. The avoidance of tungsten semi carbide as well as an amorphous structure is important in order to exclude all possible catalytically active sites. The $WC_{com\ nano}$ powder was intensively mixed with the metal salt. After stirring the dispersion for several hours, until the salt was homogeneously distributed, a rotary evaporator was used to remove the solvent in order to obtain a dry metal salt @ WC-powder. This powder was collected and placed into the hydrogen oven under 400 °C for 3 hours with a ramping of 5 K min^{-1}.

Cu@WC

Copper is a cheap and abundant material, also known for its catalytic activity.[137] By using copper chloride (Cu(I)Cl) together with $WC_{com\ nano}$, the dispersion was stirred in ethanol for several hours. The vigorous stirring enabled a homogeneous distribution of the salt over the tungsten carbide template material. By evaporating the alcohol, the grey powder consisted of 10 wt% copper deposited on WC. Copper needs to be reduced from Cu^{+} to Cu(0). By using 400 °C, the hydrogen can act as an electron donor and undergoes further reaction to gaseous HCL, which is finally flushed out with the excess gas stream. The resulting material was first characterized using optical measurements like SEM, as presented in figure 32.

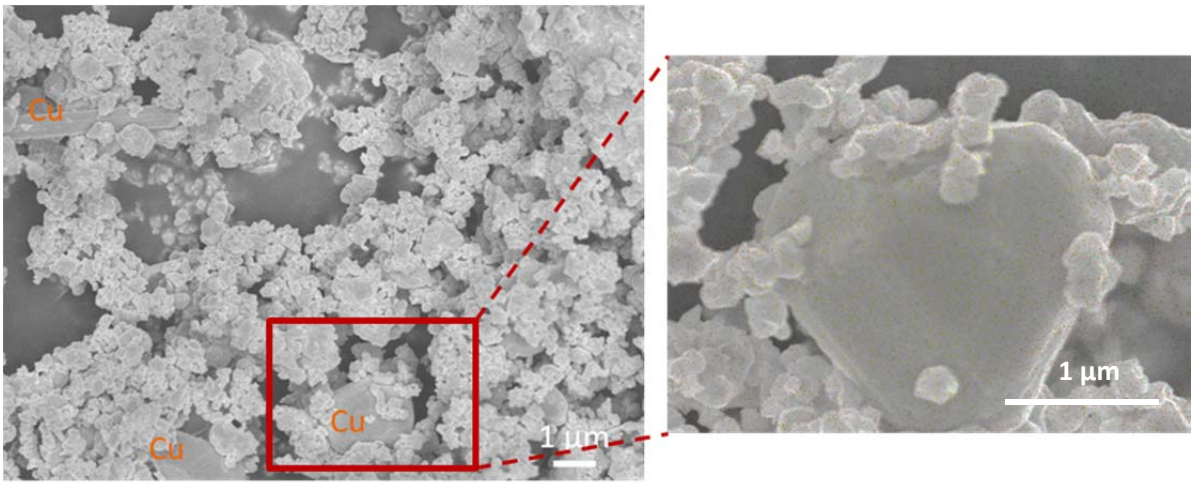

Figure 32: Scanning electron microscopy picture of 10 wt% Cu@WC manufactured in the hydrogen oven with 400 °C for 3 hours.

The tungsten carbide particles are clearly visible as well as the copper particles. The used tungsten carbide is 175 ± 25 nm in particle size and the same as already shown in figure 27 C, D. The copper forms blocks and rods in a rage of 1-2 µm in diameter or length. EDX analysis confirmed the existence of copper. Additionally the map sum spectrum of the EDX analysis is given (SI-F10). Also the XRD results clearly show WC as well as copper (SI-F11). The nitrogen sorption resulted in an area of 6.2 m^2 g^{-1} (~ 100 m^2 cm^{-3}) and is therefore in the same range as it was without copper, indicating no sintering of tungsten carbide.

Pd@WC

The noble metal palladium is known for long to operate as an excellent hydrogenation catalyst. Therefore it was also used in this chapter to show the synergistic effect rising between the metal and the metallic ceramic WC. Palladium acetate (Pd (II) acetate) was mixed with the dispersion of tungsten carbide $WC_{com\ nano}$ and ethanol and it was stirred for several hours before the powder was dried with a rotary evaporator. The resulting SEM pictures of 10 wt% Pd@WC can be seen in figure 33.

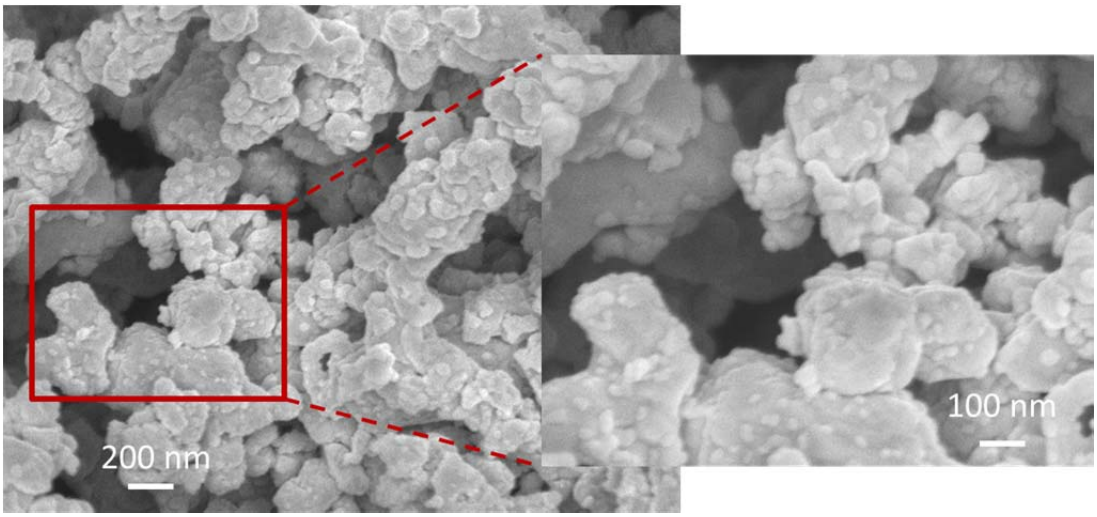

Figure 33: Scanning electron microscopy picture of 10 wt% Pd@WC manufactured in the hydrogen oven using 400 °C for 3 hours.

Copper was showing relatively big particles in the micrometer range, whereas palladium is known for forming smaller particle sizes. The SEM picture shows the $WC_{com\ nano}$ particles of 175 ± 25 nm with the deposition of palladium with particle sizes of 60 ± 40 nanometers. The XRD measurement (SI-F12) allows to clearly see the palladium on WC. The map sum spectrum of the EDX analysis differentiates between the tungsten as well as the palladium (SI-F13). The surface area doubles during the Pd (0) deposition to 14 $m^2\ g^{-1}$ (~ 224 $m^2\ cm^{-3}$).

Ni@WC

As nickel catalysts are one of the most promising "green" alternatives for hydrogenation reactions, the synergistic effects of nickel with tungsten carbide will also be examined in this chapter. There are already strong interactions of these materials known, and an advantageous catalytic behavior was as well mentioned in papers. Depending on the morphology and the structure of the nickel nanoparticles on the support, different behaviors can be observed. The SEM picture in figure 34 reveals the deposition and distribution of nickel. The synthesis of the material was realized by using $Ni(II)Cl_2$ in ethanol, together with $WC_{com\ nano}$. After stirring and evaporation of the solvent the powder was as well placed in the oven and reduced by hydrogen at 400 °C for 3 h.

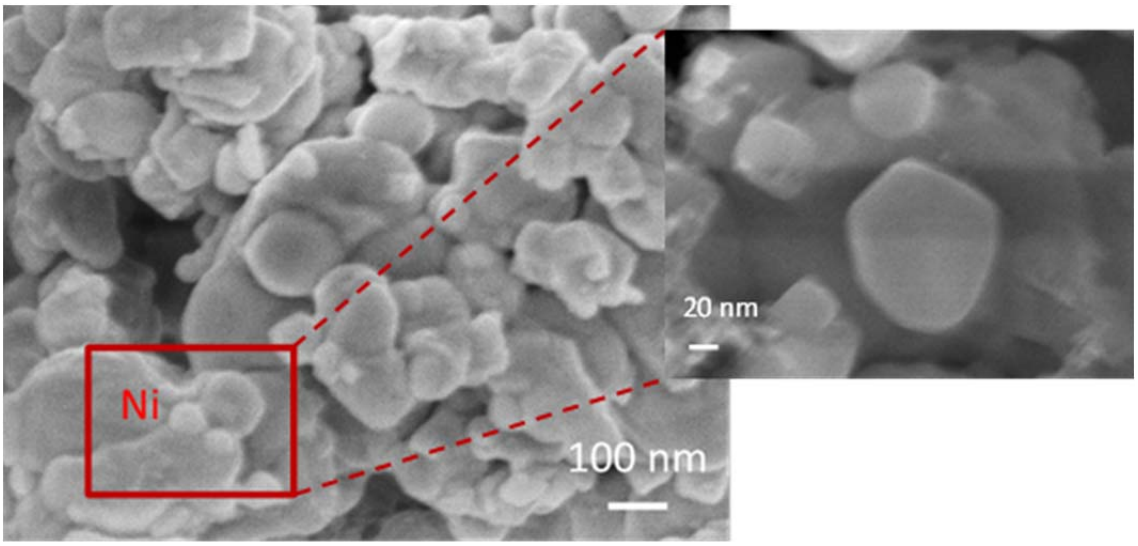

Figure 34: SEM results of 10 wt% Ni@WC reduced by hydrogen in the oven with 400 °C for 3 hours.

The nickel nanoparticles are deposited like droplets on top of tungsten carbide. The XRD measurement clearly show the accordance with the reference (SI-F14). The nitrogen sorption result of 9 m^2 g^{-1} (~ 144 m^2 cm^{-3}) is again in the same range of pure tungsten carbide $WC_{com\ nano}$. The 8 wt% ICP-OES results agree nicely with the calculated value of 10 wt% nickel, whereas the difference can be assigned to experimental errors of the ICP-OES. The EDX map sum spectrum confirmed nickel on tungsten carbide (SI-F15).

The crystallite size and the comparison between the catalysts is important, because the activity of a catalyst strongly depends on the surface properties. The results of the Scherrer calculation as well as the different grain sizes are summarized in figure 35.

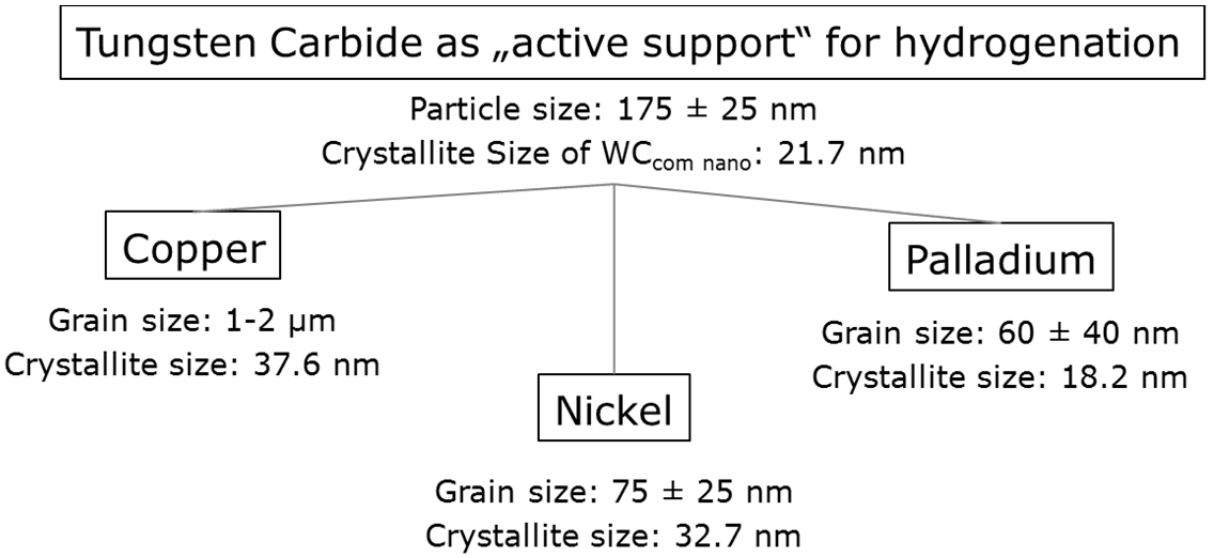

Figure 35: Summary of crystallite and grain sizes from tungsten carbide as well as copper, palladium and nickel, calculated from the XRD results of the freshly prepared catalysts. The grain sizes were determined by SEM pictures.

As shown before, tungsten mono carbide can act as an active catalyst with limited activity under mild conditions. This material is therefore believed to be a valuable support for the deposition of metal nanoparticles to extend its reactivity. Herein, the tungsten carbide crystallite size did not significantly change during the synthesis and remained the same at around 21.5 nm for $WC_{com\ nano}$. On the other hand the deposited metals show very different crystallite and grain sizes, whereas copper was giving the biggest structures with 37.6 nm and 1-2 µm. Nickel itself was calculated to 32.7 nm and 75 ± 25 nm ,whereas palladium was the smallest with 18.2 nm and 60 ± 40 µm.

3.5.2. Catalytic activity of M@WC for chemical upgrade using hydrogen

A catalyst is mainly evaluated based on its conversion and selectivity towards a desired reaction. Therefore all three materials (Cu-, Pd- and Ni@WC) were tested for the reactivity of upgrading furanic components. These building blocks are obtained from the previous acidic dehydrogenation, employing solid acid catalysts for the continuous conversion of fructose into HMF. The dehydration was giving high yields of hydroxymethylfurfural derivatives like 5-(ethoxymethyl)-2-furaldehyde and 5-(hydroxymethyl)furan-2-yl)methyl-formate, as well as levulinic acid / ethyllevulinate by a consecutive reaction. HMF, as well as the consecutive molecules (figure 36) still contains three oxygen atoms, which have to be avoided, when using the molecule as a fuel for combustion engines. Combustion heat value and coking in the motor chamber, as well as motor knocking can be the result. Therefore all the present catalysts are tested in the sense of applicability in hydrodeoxygenation. The catalysts are tested first with pure HMF as well as EL with concentrations of 0.05 M. The desired 2,5-dimethylfuran is as well tested in the sense of checking the reactivity for a further hydrogenation. Ethyllevulinate can be used in a fuel blend, but an upgrade towards γ-valerolactone would bring an additional benefit in terms of higher energy content in the molecule, caused by the ring closing and elimination of a further oxygen. The overall reaction mechanism for the upgrade of HMF can be seen in figure 36. The upgrade of ethyllevulinate was recently discussed by our group.[138]

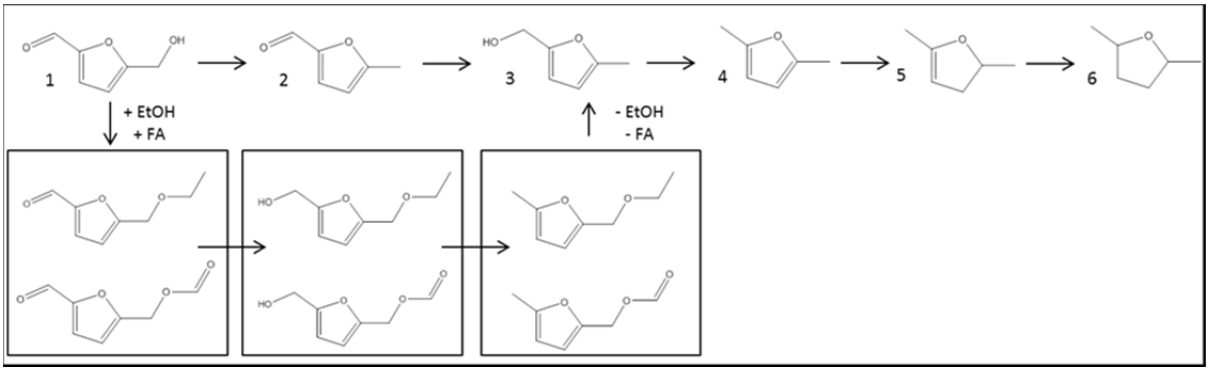

Figure 36: Plausible hydrodeoxygenation reaction mechanism for upgrading HMF over Cu-,Pd- and Ni@WC. The additional etherified products of HMF were as well converted and resulted in DMF as end product, what will be shown in chapter 4 in more detail. This figure represents a general overview.

The hydrodeoxygenation and therefore the removal of two further oxygen atoms within the HMF was described by Saha et al in a review.[22] As HMF possesses an aldehyde and an alcohol group, the first step suggested is the hydration of the aldehyde to alcohol, resulting in 2,5 bis(hydroxymethyl)furan. Elemental hydrogen dissociates on the nickel and offers this proton for the reaction. This intermediate gets hydrogenated and water is released. After repeating this reaction with the second alcohol functionality, DMF is synthesized. The aromatic ring structure does not get hydrogenated and the possible biofuel is left in solution. In the solid acid dehydration from chapter 2, the formation of 5-(ethoxymethyl)-2-furaldehyde and 5-(hydroxymethyl)furan-2-yl)methyl-formate was observed. HMF condensates with ethanol and with formic acid. Nevertheless the hydrodeoxygenation was successful, what will be discussed further on.[139]

3.5.2.1. Cu@WC

Copper on tungsten carbide showed a relatively big grain size (1-2 µm), as well as a relatively small surface area (6.2 m^2 g^{-1}). Nevertheless, the reactivity in terms of the upgrade of pure 0.05 M HMF as well as ethyllevulinate solution was tested. The reaction conditions were set to 10 bar and 30 bar of pressure respectively and 0.25 mL min^{-1} (~ 3 minutes residence time). The temperature was varied from room temperature (25 °C) to 150 °C. The hydrogen, coming from water splitting, was automatically inserted into the system, and the gas-liquid mixture was flown over the catalyst.

Ethyllevulinate did not show any significant conversion using 150 °C and 30 bar with a flow rate of 0.25 mL min^{-1}. The activity for the conversion of HMF is as well not significantly high, as can be seen in figure 37.

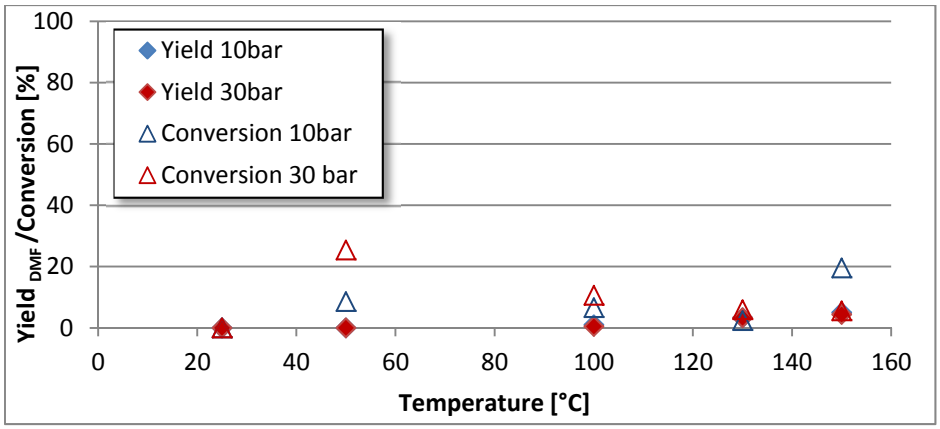

Figure 37: Upgrade of HMF to DMF at different temperatures, with 10 bar and 30 bar of pressure as well as 0.25 mL min^{-1} flow rate (~ 3 minutes residence time). The conversion and yield was obtained using calibration curves of a GC-MS / FID system.

The results are plotted over the temperature from 25 °C to 150 °C. The yield of all reactions was very low and did not exceed 5 %, even at 150 °C. As the temperature and pressure provide the activation energy for the reaction, both parameters were checked. With higher temperature the yield of DMF was increased slightly, but was still very low (maximum 4.4 %). The pressure did not change, and the reactivity and the yield stayed low therefore. The reactivity involved the steps 1 to 4 in figure 36 and did not show a further hydrogenation of DMF (4). In terms of the further upgrade of HMF towards the desired DMF, Cu@WC only offers limited possibilities without further optimization. The low reactivity is mainly connected to the big grain and crystallite size. 10 wt% of active copper nanoparticles, packed in micrometer grains cannot offer much surface area and therefore activity. Tungsten carbide itself does not show any activity for the upgrade of HMF at these mild conditions. Even if copper is showing some reactivity for hydrogenation reactions, it is not known as highly active, even in nanoparticle form.

3.5.2.2. Pd@WC

10 wt% palladium@tungsten carbide was as well checked for its reactivity of ethyllevulinate and the upgrade of HMF. There was no reactivity for ethyllevulinate, whereas the results for HMF are shown in figure 38.

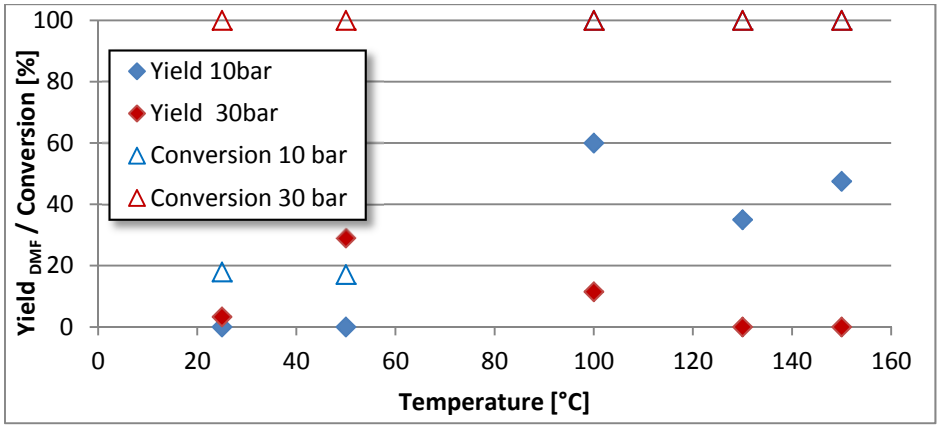

Figure 38: Upgrade of HMF to DMF at different temperatures with 10 bar and 30 bar of pressure as well as 0.25 mL min^{-1} flow rate (~ 3 minutes residence time). The conversion and yield was obtained using calibration curves of a GC-MS / FID system. The conversion for the pressures of 10 bar and 30 bar is 100 % for temperatures of 100 °C, 130 °C and 150 °C.

Palladium on the other hand is known for its excellent hydrogenation activity and can be therefore expected to give good reaction results. Both pressure conditions showed sufficient reactivity at the beginning and obtained yields of 60 % DMF for 100 °C and 10 bar, as well as 29 % yield DMF for 50 °C and 30 bar. Whereas full conversion is obtained using 30 bar already at room temperature, the reduced pressure of 10 bar just results in about 19 % at temperatures of 25 °C and 50 °C. Full conversion is obtained using 100 °C and higher temperatures. Both pressure series show a maximum in their reactivity towards DMF, whereas with 30 bar it is obtained earlier (50 °C) compared to only 10 bar (100 °C). This fact can be explained by a potential “stagnant layer diffusion”. The more overall system pressure, the more partial hydrogen pressure, the more hydrogen molecules can reach the surface of the catalyst where the dissociation takes place. The more dissociated hydrogen is presented on the surface, the more probable it is to react with a reactant and to accelerate the reaction. In terms of selectivity, palladium is not the first choice when trying to avoid the formation of byproducts derived from consecutive reactions of DMF. The reaction does not

stop with the hydrodeoxygenation to DMF (figure 36, 4), but the dissociated hydrogen is also able to attack the double bonds in the furanic ring system. The “over-hydrogenated” product 2,5-dimethyltetrahydrofuran (figure 36, 6) can indeed be used as a solvent and as a fuel. It consumes two further hydrogen from outside sources, and the internal energy as well as the reactive octane number (RON 82) in the molecule is therefore reduced compared to DMF (RON 119), also stated in figure 1.

3.5.2.3. Ni@WC

Nickel was distributed and reduced on tungsten mono carbide as well. The principle of reduction was the same as before using the hydrogen oven and filling the 10 wt% Ni@WC powder into a 60 mm cartridge for testing. The catalytic results using pure HMF are shown in figure 39.

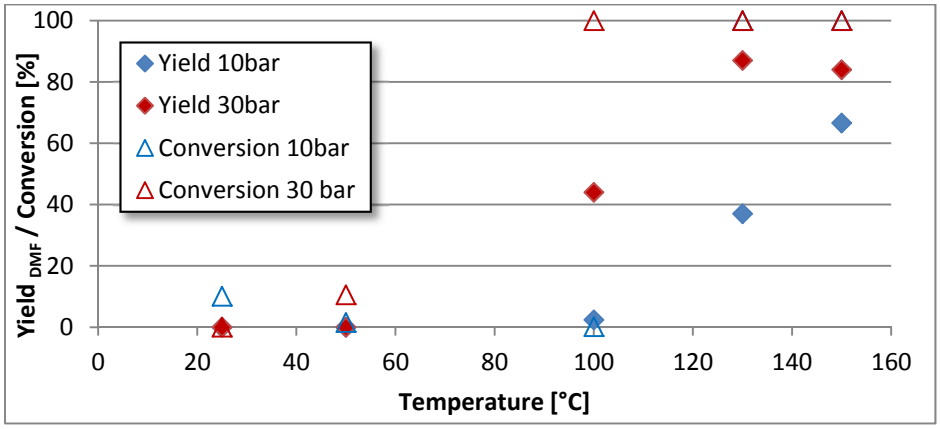

Figure 39: Upgrade of HMF to DMF at different temperatures, using 10 bar and 30 bar of pressure as well as 0.25 mL min^{-1} flow rate (~ 3 minutes residence time), using 10 wt% Ni@WC. The conversion and yield was obtained using calibration curves of a GC-MS / FID system. The conversion for the pressures of 10 bar and 30 bar is 100 % for temperatures of 130 °C and 150 °C.

The reactivity for ethyllevulinate is as well limited with this bimetallic catalyst, whereas the conversion of HMF is showing good results. The catalyst shows less activity at low temperatures and starts getting active at 100 °C and 30 bar. The reactivity increases almost linearly with increasing temperature and can therefore reach a maximum at 150 °C for a pressure of 10 bar with a 66 % yield of DMF. The higher the temperature, the higher the

yield of the reaction. With an increased system pressure from 10 bar to 30 bar the trend towards higher reactivity is continued. Ni@WC has a high selectivity towards DMF and therefore does not catalyze the cracking of the aromatic furan ring system (figure 36, 5, 6 are not found).

Therefore nickel, an abundant and cheap material, turns out to be a superior catalyst in combination with tungsten mono carbide for the purpose of converting the intermediate HMF to DMF in a very selective way. The back pressure of all used 60 mm x 4 mm columns was very low (2-3 bar). The catalysts used are micrometer agglomerates, which allow enough surface for the reaction on the one hand, as well as the liquid to pass without huge resistance on the other hand. The before observed back pressure problems of the pure $WC_{com\ nano}$ powder did not occur after the deposition of metal nanoparticles. The material got slightly sintered, whereas the overall surface area did not decrease.

3.6. Summary

By comparing the limited reactivity of pure tungsten carbide under relatively mild conditions, a size dependence of the used catalysts could have been observed. Urea synthesized nanostructured tungsten carbide showed the highest activity and proved the concept of a change in reactivity with a change in accessible surface area and particle size. The activity of nanocatalysts can be assigned to the increased surface area as well as the change in the surface electronic structure. Catalysis in biorefinery is not trivial, due to the need of activity as well as stability of the catalyst. Noble metals get poisoned easily[140], and cheap alternatives are desirable. Tungsten carbide catalysts in combination with second metals open up a new family of material, whereas activity as well as stability are increased. In addition the catalysts need to be applicable in flow systems without a high back pressure. The upgrade of molecules derived from biomass often have side groups and moieties which need to be selectively converted in order to remove oxygen or for example reduce specific multiple bonds. The selective upgrade of these molecules under relatively mild conditions is one of the main goals and needs to be pushed forward on. WC, with its similar electronic properties like Pt, shows a limited but highly selective activity for nitro-moieties and multiple

bonds, using 150 °C and 30 bar with a residence time of only three minutes. On the other hand the upgrade of biomass derived molecules is necessary, and therefore two strategies for the expansion of reactivity are thinkable. The chemical route is connected to the observation of synergistic effects occurring, when two metals (metallic ceramics) are close enough. Electrons start to interact over valence - as well as conduction band, what leads to different interactions and altered active sites. By the deposition of copper, the reactivity does just slightly change compared to pure tungsten carbide and the activity stays at a very low level. Copper is not known to be a sufficient hydrogenation catalyst, especially in the case of big particle sizes and agglomerates. With palladium the reactivity changes dramatically, and the activity tends to “over-hydrogenate” the product. The catalyst is cracking the DMF ring structure, resulting in 2,5-dimethyltetrahydrofuran. Nickel thereby is abundant and considered to overcome the dependence of noble metals in hydrogenations. The dissociation of hydrogen on the catalyst´s surface is known and it was shown, that in combination with tungsten mono carbide the selectivity can be tuned towards a hydrodeoxygenation. With relatively mild conditions (up to 150 °C and 30 bar) it is hence possible to upgrade HMF to DMF without any further “over-hydrogenation”. The expansion of the reactivity by the deposition of metals on tungsten carbide can be one solution to tune the activity, whereas the application of harsher reaction conditions and an intelligent combination of reaction columns can lead to cascade reactors, making use of the developed and discovered catalysis knowledge. Such a continuous system, mainly combining the dehydration with the hydrodeoxygenation will be presented in the following.

4. An integrated flow reactor system, upgrading fructose into furanic – based chemicals in continuous mode

After investigating the conditions necessary to on the one hand dehydrate fructose over a solid acid catalyst (chapter 2), as well as showing the possibility to further upgrade the resulting furan-ring products into more valuable molecules (chapter 3), the focus in this chapter will be the combination of the successful dehydration as well as the hydrogenation in one flow reactor system in a two-column as well as one-column approach. Whereas the two-column system works with a combination of reactors, the one-column approach aims to bring the catalysts close by using only one mixed-catalyst column.

4.1. Introduction

Physical parameters (mainly heat, pressure and residence time) as well as the set-up itself (material, tubing, and scale) are as important as the chemical properties of the catalyst. These frame conditions provide the activation energy and hence can limit or promote the outcome of the reaction. As about 90 % of the energy harvested during the photosynthesis in fructose indeed end up in the DMF molecule, it is possible building a profitable, continuous and small scaled plant for the direct production of DMF from fructose in a continuous flow reactor. The lack of such a synthesis scheme in the present industry landscape makes it a promising idea and prepares for the future of biorefinery, whereas continuous facilities, making use of biomass are more than necessary, recently also stated in the journal "Nature".[141] DMF with its high heat of combustion value of 32 MJ kg^{-1}[43] enables the realization of a biofuel of a next generation. DMF is a high energy molecule and can be seen as a promising alternative to conventional combustion fuels in terms of similar properties.[142] The side product ethyllevulinate (EL) can be used as fuel blend or can be further upgraded over Raney-nickel catalysts to γ-valerolactone. Further upgrade of DMF and the combination of different continuous reactors in a modular fashion open up possibilities beyond 2,5-dimethylfuran, thinking of p-xylene or further oxidations to terephthalic acid. A modular and continuous reactor set-up offers possibilities for different catalytic reactions in flow.

By using non-hazardous chemicals, sugar and solvents made from wood hydrolysis and saccharification, our proposed upgrade of fructose can be considered as “green”. The details of the combined continuous reaction, as well as the reactor design will be discussed in the following. Most of the biorefinery schemes nowadays are still performed in batch mode, but the upgrade of sugars in a continuous system bears great potential for industry. In order to give an outlook towards an upgrade, using a single column system instead of a two column approach, a direct combination of solid acids as well as Ni@WC is presented. Furthermore a possible scale-up is discussed, coming from milliliter to liter conversions.

4.2. Hydrogenation flow reactor: Set-up for biomass upgrade

4.2.1. State of the art

Set-up requirements and conditions

There are two main ways to transfer energy into a catalytic system: temperature and pressure. Additionally, also residence time is a fact of great importance and can in our approach be adjusted by the flow rate. Hydrogenation, dehydration, retro-aldol condensation as well as decarbonylation are the most important conversions when it comes to the upgrade of biomass.[143] Using renewable hydrogen is one elemental key factor for the reduction, reducing as well as saturating organic compounds. Water splitting by electrolysis can be one alternative to classical hydrogen production like steam reforming. Using for instance excess energy from wind power in combination with water splitting can offer "renewable hydrogen", as recently promoted by the start-up company "Hydrogenious Technologies GmbH".

A typical application for hydrogenations in continuous approach is the saturation of double bonds in fatty acids like oleic or linoleic acid. Here temperatures in the range from 140 °C to 350 °C as well as pressures of 10 bar to 40 bar are applied when using catalysts like nickel.[144] Petrochemical industry is using hydrogen for saturating alkenes or aromatic molecules, offering superior storage properties. Reforming, as well as hydrocracking are two further examples of great importance. Speaking of gaseous reactions using hydrogen, the Sabatier-, Haber-Bosch- and the Fischer-Tropsch-Processes are the most exemplary ones. As hydrogen is such an important reactant all over the chemical industry, the development of catalytic hydrogenations of biomass and biomass derived molecules in continuous fashion fit in the already existing infrastructure and knowledge.

As cellulosic biomass possesses many oxygen atoms, hydrodeoxygenation of the functional groups remove the oxygen. This can be shown when 5-hydroxymethylfurfural undergoes a reduction and functional groups like alcohol and aldehyde are hydrogenated and released as water. Because homogeneous catalysts are in the same phase as the reactants, they are

difficult to remove and reuse. Therefore heterogeneous catalysts are preferred and should be used in continuous approaches, keeping easy recyclability in mind.

The used catalysts and set-up

The aim of this chapter is to show a way to combine the dehydration and the hydrodeoxygenation in one continuous flow system. Both reactions are working in flow, using Amberlyst 15 or other sulfonated carbon catalysts for dehydration, as well as metal nanoparticles@tungsten carbide for hydrogenation. Based on the previous studies, reported in chapter 2 and 3, the use of Amberlyst 15 and 10 wt% Ni@WC is preferred for a two-column approach. Amberlyst 15 shows a high reactivity as well as good flow properties without a high back pressure. The catalyst resin is in the shape of uniform micrometer scaled spheres and is therefore not blocking the liquid from flowing. The sphere diameter (< 300 µm) compared to the column volume (4.2 ml) and length is still beneficial so that only 1-3 bar back pressure are observed. Amberlyst 15 has a limited temperature applicability of 110 °C, but still produced the best results in terms of least energy input (110 °C, atm) with highest productivity of HMF derivatives (11 minutes residence time, chapter 2, figure 20). For single column approaches and the therefore higher temperatures necessary, Amberlyst 15 is not suitable and sulfonated carbon material in combination with Ni@WC is considered. The Ni@WC showed a high selectivity and conversion during the hydrodeoxygenation of HMF and is highly active under relatively mild conditions of 150 °C and 30 bar of pressure.

The scaled system used for the studies, is expanded in several stages. First, the commercial system H CUBE Pro ™ (Figure 40, (I)) is used to run test reactions under hydrogen atmosphere below 1 cm^3 scales. This equipment is further expanded with an additional 250 mm x 4.6 mm column, directly connected the H CUBE Pro ™ (Figure 40, (II)). By having this additional reactor column, a second reaction gets possible, whereas the temperature can be adjusted individually. By choosing the column length, the residence time can be tuned, depending on the flow rate. The external column can be connected before or after the hydrogen inlet and is therefore flexible in terms of using a solid acid or a metal catalyst, depending on the need of hydrogen. The flexibility of the column connection opens up the possibility of using two different catalysts during the same run. By using a solid acid catalyst in a) and a metal-catalyst in b), a continuous run can be realized converting for instance

fructose directly to DMF. All reactions mentioned in the following are based on this extended H CUBE Pro ™ system.

For the construction of this expansion of the H CUBE Pro ™ using a stainless steel column (Supelco Blank Kit, 250 mm x 4.6 mm ID ¼" OD), the temperature of the reactor was controlled using a heating band (Mohr and co, 230 V, 375 A, 450 °C). Reactor column (a) (Figure 40, II) was filled with Amberlyst 15 and heated to 110°C. The free standing system (chapter 2, figure 18) was run by simply pumping the solution at atmospheric pressure. In the combined run, the column was connected after the pressure sensor, but ahead of the hydrogen insertion. Therefore the pressure in the external column is the same as in the H CUBE Pro ™.

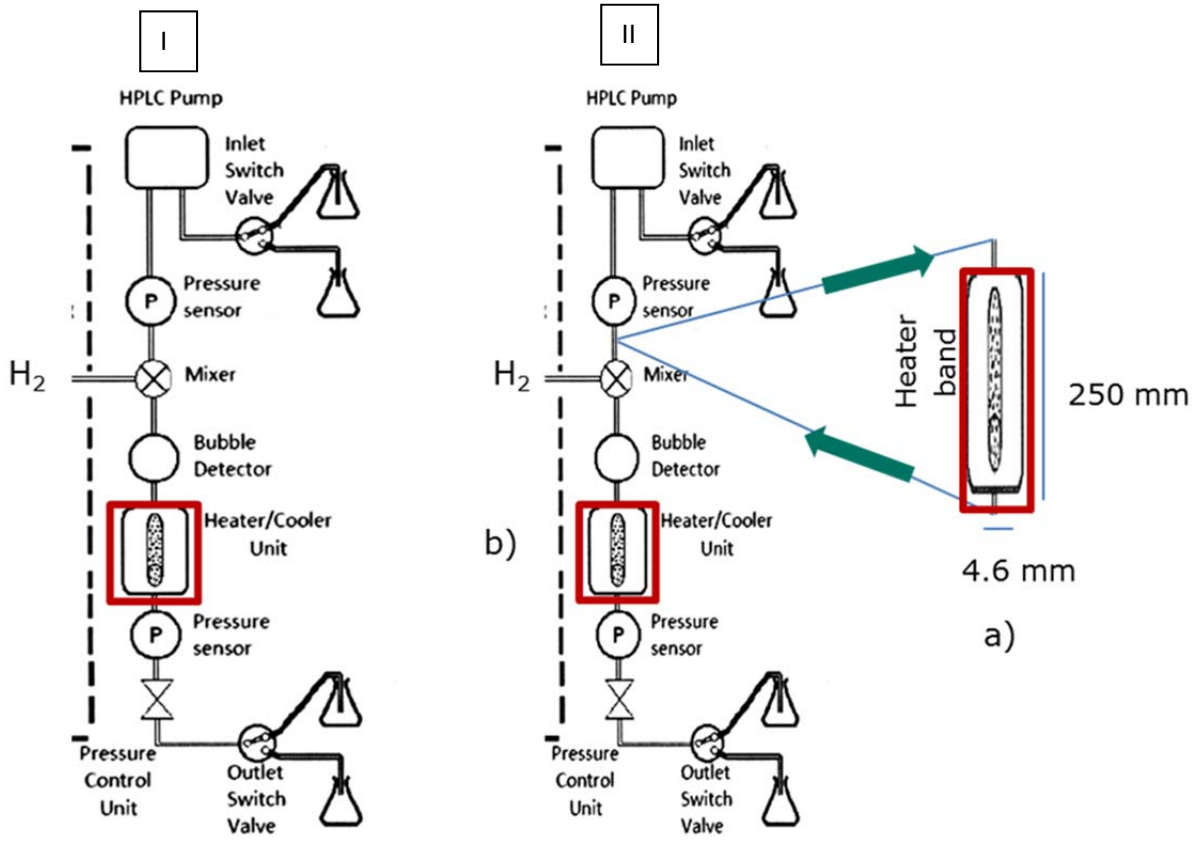

Figure 40: Schematic illustration of the commercial H CUBE Pro ™ system (I) as well as the extension of the system with a stainless steel column for the dehydration of sugar using a solid acid catalyst (II). [Adaption of H CUBE Pro ™ manual, Thales Nano]

When the reactor is connected to the H CUBE Pro ™, the pressure can be adjusted internally, and is regulated by the automated software, which settles down to the adjusted

value by opening or closing a space between a piston and the wall in a chamber. The piston is able to be moved by the system and restricts the flow of the reaction solution. By adjusting the space with a feedback of the pressure sensor, the pressure can be kept constant in the system using a constant flow rate. The extension column did not affect the pressure of the overall system. The hydrogen pressure is provided by the electrolysis cells and is inserted using a gas-liquid mixer. In here the driving force for the flow is a provided pressure difference, adjusted by a mass flow controller (MFC). At a maximum performance of the cells at 100 %, a 60 mL min^{-1} stream of hydrogen can be inserted into the liquid flow.

4.3. Synthesizing 2,5-DMF directly from fructose in a two-step flow approach

4.3.1. Qualitative and quantitative results

Qualitative results – Reaction mechanism

By combining the dehydration as well as the hydrodeoxygenation in one continuous system, a direct production of DMF as well as EL out of a fructose solution is possible. The reactivity as well as the mechanism was investigated in more detail, and the qualitative results are summarized first in figure 41.

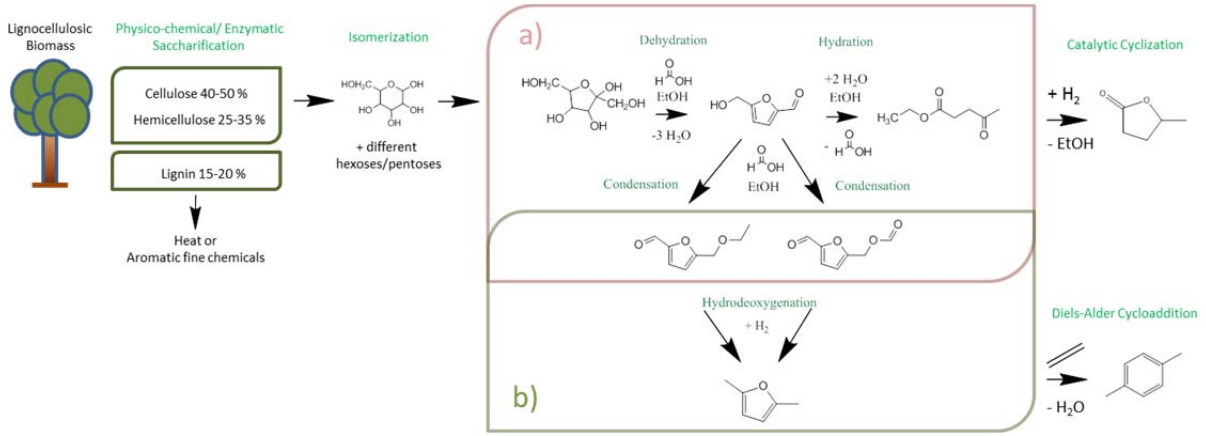

Figure 41: Overview of the applied process, converting fructose into DMF and EL. (a) Amberlyst 15, 110 °C, 30 bar, 0.25 mL min^{-1} (~ 11 min residence time). (b) 10 wt% Ni@WC, 150 °C, 30 bar, 0.25 mL min^{-1} (~ 3 min residence time). The Diels Alder cycloaddition is just exemplarily shown and represent an outlook in terms of future upgrade and alternative applications for DMF. The scheme is adapted from reference 139.

The schematic illustration shows the reaction mechanism, as well as gives an overview of the full cascade from the raw biomass to further realized and possible products. The single reaction pathway in our two-catalyst column approach is highlighted, starting with the dehydration reaction over the Amberlyst 15 (Figure 41, a) and the hydrodeoxygenation of the resulting reaction products (Figure 41, b). Fructose was selected as a starting material,

due to its ability to form fructo-furanose, a five atom furanic ring system, which is optimal for further dehydration forming HMF. The release of three water molecules results in HMF, which is a slightly exothermic and entropically driven process. Acidic conditions result in various follow-up reactions, humins and resin formation amongst others. By adjusting and controlling the residence time, the formation of consecutive reactions can be reduced or avoided and selectivity can be adjusted. The formation of levulinic acid and the condensation with ethanol to ethyllevulinate can be controlled as shown in figure 20. Reaction conditions and optimized reactor regimes can therefore direct the reaction outcome. As HMF also offers reactive site groups, condensation with the ethanol or the formic acid, which are both present in the solution, leading to mainly 5-ethoxymethylfurfural as well as 5-(hydroxymethyl)furan-2-yl)methyl formate are possible.

The mechanism of the reaction is of great interest for understanding the molecular details. On the thermodynamic level the whole process starts with a protonation and a further dehydration of fructose. A positive charge is left behind, what can be stabilized by being shifted in the molecule. The further protonation results in another release of a water molecule and another deprotonation reaction enables to form a double bond within the ring system. By the third protonation and the release of water, the subsequent deprotonation forms the aromatic furan ring structure including two double bonds. The already mentioned 5-ethoxymethylfurfural as well as 5-(hydroxymethyl)furan-2-yl)methyl formate are formed out of a condensation reaction with ethanol and formic acid.[145] The removal of further oxygen atoms from the HMF molecule is done by using the Ni@WC catalyst and a hydrodeoxygenation. By hydrogenation of the aldehyde group, water can be released and a methyl side group is left. The ether functionality of the condensation can as well be hydrogenated and ethanol as well as formic acid can be released again. Additional hydrogen can finally release another water molecule and DMF is the conclusive product. The catalyst did not differentiate between the pure HMF and the condensation products.

Quantitative results using Amberlyst 15 and Ni@WC

The dehydration of fructose using Amberlyst 15 with 110 °C was optimized in chapter 2. The reaction was done at 110 °C, varying the residence time in the column by adjusting the flow rate. The residence time in a 250 mm x 4.6 mm stainless steel column was between 2 and 30 minutes. As levulinic acid and ethyllevulinate are also consecutive products of HMF and its derivatives, it is observed, that the longer the molecules are in contact with the solid acid catalyst, the more secondary products (ethyllevulinate) are produced. In view of realizing a DMF production, the HMF derivative is the desired product of the first dehydration reaction. The optimum of 5-ethoxymethylfurfural with 53 % is reached with a residence time of 11 minutes. This time is realized by adjusting 0.25 mL min^{-1} flow rate in the 250 mm x 4.6 mm column. The ethyllevulinate yield is in average 16 %. With longer time the consecutive reaction takes over and increases the yield of ethyllevulinate significantly. This should be avoided and hence 0.25 mL min^{-1} was selected for the combined run.

In the combined two column system the pressure was raised from atmospheric pressure to 30 bar, due to the direct connection of the 250 mm column to the H CUBE Pro ™ system. The optimum for the hydrodeoxygenation using Ni@WC is 150 °C and 30 bar, and therefore the whole set-up needs to be set under this pressure. By increasing the overall pressure the reaction kinetics of the dehydration gets slightly affected.

In the combined column run, an overall yield of 85 % could have been achieved. DMF was obtained in a yield of 38.5 %, ethyllevulinate in a yield of 47 %, whereas the main remainder is unconverted fructose. With assuming a full conversion of HMF derivative to DMF or ethyllevulinate, and the same conditions as with the single column runs (110 °C, 0.25 mL min^{-1} for Amberlyst 15 dehydration and 150 °C, 30 bar and 0.25 mL min^{-1} for Ni@WC) the additional 30 bar of pressure positively affected the reactivity. The before measured 53 % of ring products (chapter 2, figure 17, 11 min) from the dehydration reaction dropped to 38 %. This loss of furan products is found in the increased yield of 47 % of the consecutive product ethyllevulinate, resulting of the increased pressure and a therefore increased conversion.

In other words: Converting a sugar solution in a continuous two-column reactor set-up in about 14 minutes, using ethanol as solvent, without noble metals and harsh conditions, is promising for scale-up and further study.

4.3.2. Long time run and stability

In order to check the long time applicability and stability of the used two column system, a continuous 7 hour run was performed. The reaction was continuously run for 7 hours using a 0.05 M solution of fructose in ethanol with 0.5 M formic acid. The results of the continuous run are summarized in figure 42.

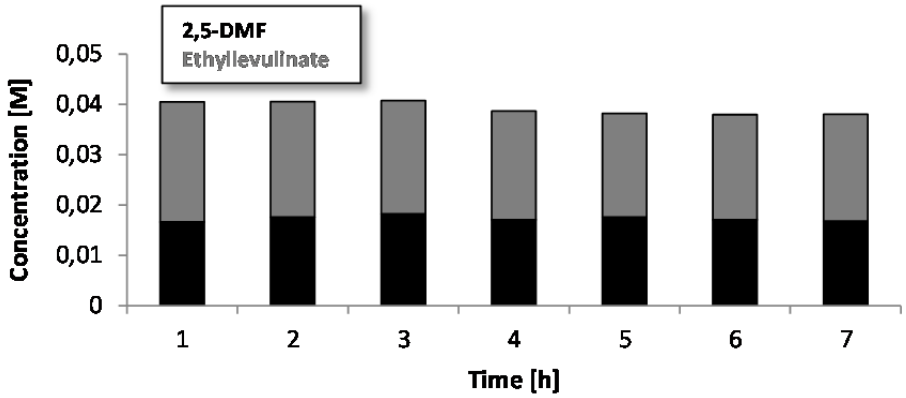

Figure 42: Concentration of DMF and ethyllevulinate over 7 hours of continuous run in a combined system with about 85 % overall yield, converting a 0.05M solution of fructose. Adapted from reference 139.

These data were obtained by GC-MS and quantified using calibration curves. The results of the two products DMF and EL are shown here. At the beginning of the reaction an overall yield of 85 % (38.5 % DMF and 47 % EL) was observed. After 3 hours the yield of EL started to drop slightly but reached a steady state, so that after 7 hours the reactivity was still high. The slight decrease of activity can be explained by the formation of humins starting to block the active sites. This blocking can be directly observed after opening the reaction column after 7 hours. The formation of a black precipitate at the entrance of the solid acid column could have been seen, shown in figure 43.

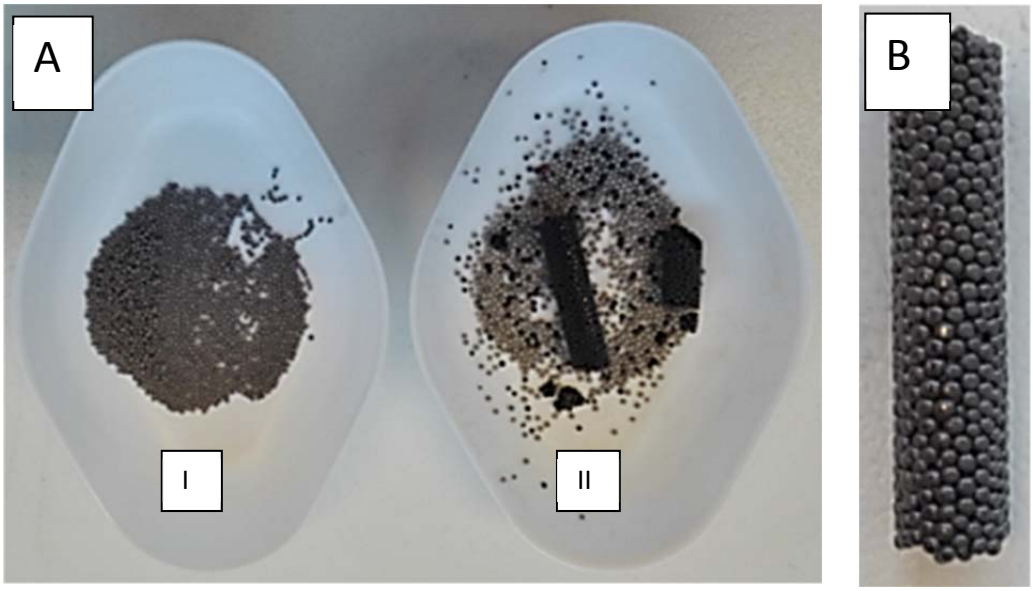

Figure 43: A: Amberlyst 15 catalyst before (I) and after reaction (II) with fructose solution and 110 °C and 0.25 mL min^{-1} in a 250 mm column. B: Enlarged picture of Amberlyst 15 spheres after usage in reaction.

Humins are polymers forming in consecutive condensation reactions, and are higher mass molecules, which deposit on top of the catalysts. By the deposition of these higher mass molecules, the micrometer spheres are glued together, forming agglomerates. Nevertheless, the rest of the catalyst showed no black precipitates, and these catalysts are therefore still active what is also observed by the constantly good performance over 7 hours.

A significant pressure drop was not observed in both cases, neither in the first, nor in the second column. The precipitates and the caking of the particles did not have an effect on the flow behavior through the solid acid column, and the flow was able to pass through with a limited pressure drop of about 1 - 3 bar. This cannot be compared to powder catalysts like carbon black, which are blocking the reactor column completely by forming a layer of fine powder on top of the filter, which causes back pressures of more than 100 bar. A homogeneous mixture of Amberlyst 15 was as well characterized by titration after the 7 hours run, and a loss of acidic sites was traced. A decrease of about 11 % was observed (SI-F16), what was also seen by elemental analysis, wherein the sulfur content was decreased (SI-F17). At the same time, the carbon content increased due to the black precipitate, especially at the beginning of the column. This finding supports the idea of the deposition of high mass molecules with a slight leaching of sulfonic acid functional groups.

The Ni@WC catalyst was characterized after the 7 hour run, and a slight increase of the nickel particle size was observed. The XRD diffractogram in figure 44 illustrates the catalyst before and after the reaction and shows the general stability. The crystalline phases did not change over seven hours.

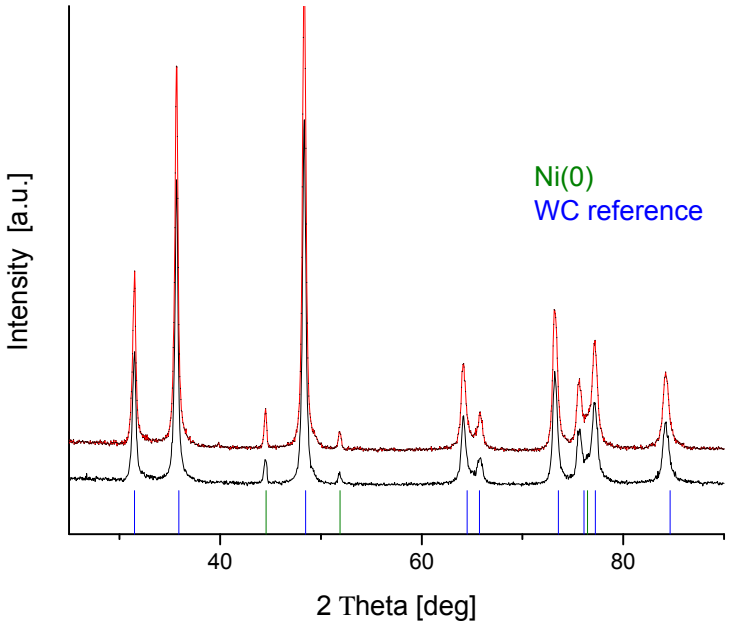

Figure 44: XRD results before (black) and after 7 hours (red) of reaction. The nickel is shown in green, whereas the tungsten carbide peaks are labeled in blue. Black is before the reaction and red is after the 7 hours run with 150 °C, 30 bar and 0.25 mL min^{-1}. (Reference pattern PDF4 database: Ni 00-004-0850; WC 01-077-4389).

Table 6: Additionally the ICP-OES results are shown before and after the 7 hours run. In here no decrease of nickel content can be observed over time.

ICP Analysis	Ni wt %
fresh Ni@WC	8.3
7 h used Ni@WC	8.5

Nickel particles are growing most likely due to Ostwald ripening. In order to prove the fact of not leaching nickel from the catalyst, the nickel content in the sample was checked by inductively coupled plasma optical emission spectroscopy (ICP-OES) (Table 6). In here the about 8 wt % content did not change. The leaching of nickel was therefore not observed, what supports the strong interaction hypothesis from chapter 3. This absence of leaching is

practically very important and supports the catalyst choice. The strong atomic interaction between nickel and tungsten carbide seems to stabilize the whole system and benefits the usage of this catalyst.

4.3.3. Simplicity of purification of product components

As DMF and EL are the main products out of the continuous run, while ethanol / formic acid is used as a solvent, the purification of these products is a question to be answered. The purification costs of chemicals are usually a big part of the production costs (11%, chapter 1, figure 13) and are hence a cost driver when it comes to the production. DMF, a relatively easy to evaporate molecule (bp: 95 °C) has a similar boiling point as the solvent ethanol with 78 °C. Ethyllevulinate is a larger, elongated molecule with three oxygen atoms in the molecule´s structure. Oxygens are able to form hydrogen bonds, and hence the boiling point of ethyllevulinate is located at 205 °C. By using water as a solvent, it would be harder to separate the products afterwards in comparison to ethanol. With a low-boiling-point solvent like ethanol a distillation separates the DMF together with ethanol from the ethyllevulinate and high weight product molecules. Additionally, the evaporation of DMF requires three times less energy compared to the evaporation of ethanol, even if the boiling point of DMF is 14 °C higher.[37] We used therefore a simple rotary evaporator. After collecting about 20 ml of product solution, the evaporator was used with a 55 °C water bath and 150 mbar of reduced pressure. The GC-MS chromatogram of the obtained product solution using 0.25 mL min^{-1} and 30 bar of pressure with 2.4 g of Amberlyst 15 at 110 °C and 1.68 g Ni@WC at 150 °C is shown in figure 45. Additionally the resulting GC-MS chromatograms of the product solutions after the rotation evaporation are shown as well.

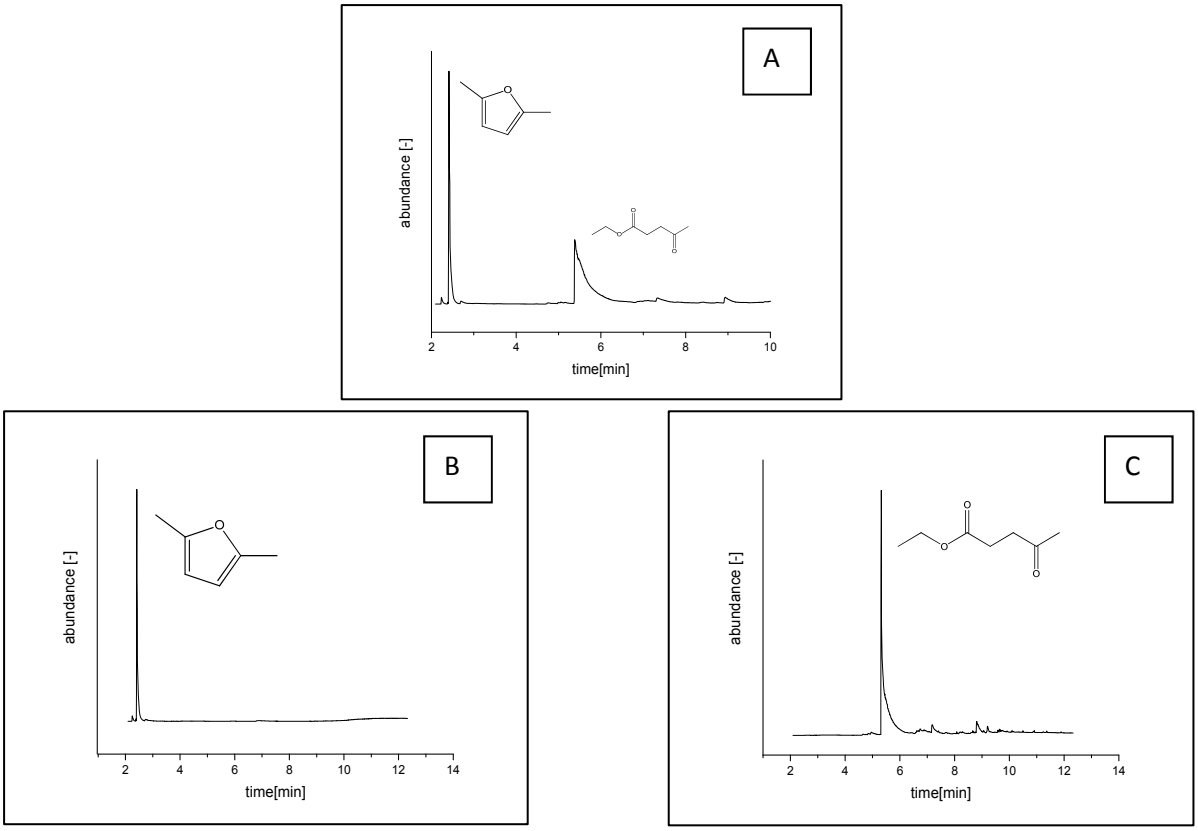

Figure 45: GC-MS chromatograms of product solution after a continuous run in a two-column system (A). (B) and (C) represent the chromatograms after using the rotary evaporator. (B) represents the evaporated fraction, whereas (C) shows the yellow fraction left in the bottom of the flask.

By using a fairly easy technique like a rotary evaporator, it could have been shown, that it is possible to separate the obtained molecules in a practical fashion. The practically pure products are therefore able to be directly further processed in secondary reactions, in order to obtain products like γ-valerolactone or p-xylene.

4.3.4. Profitable efficiency consideration

By showing promising results in terms of an easy set-up as well as an 85 % overall yield towards DMF and EL using ethanol as a solvent, it is also interesting to illuminate the economic side. When speaking of a profitable reaction set-up, converting fructose in a two-column approach, an almost full conversion, with 38.5 % yield of DMF and 47 % yield of EL was measured. As recently stated in a techno-economic analysis[104], improvements in terms of cheap feedstock, high yields and high selling prices are necessary. A continuous reaction process calculated on the basis of a biphasic reactor showed the difficulties when the process needs to compete with already existing fuels from fossil feedstocks. The improved yields and the relatively cheap catalysts used in our approach can hence promote the production of DMF out of fructose, but needs to be further optimized. The resulting yields of DMF and EL, but also of the semi-finished products like HMF, can lead a way towards a commercial production plant. One main disadvantage from an economic point of view is the fructose feed cost (figure 13), what makes up 47 % of the DMF price. Pure fructose cannot compete and alternatives like glucose need to be considered, especially when speaking of the production of biofuels. The direct integration of cellulosic biomass with such optimized yields, as well as the integration of the process into the industrial landscape, can promote the usage of fuel from sugar.[146] As pure compounds are expensive, mixtures of different sugars need to be considered. The sugar industry produces waste streams, like molasse, which is usually used as animal feed, as the contained sugar cannot be crystalized any further. The waste product contains sucrose and raffinose, next to many other products like vitamins, organic acids or diverse salts. Working with such mixtures in catalysis is necessary but challenging, whereas just small residues of salt and metal ions, can already poison the active sites of the catalyst. Inverted sugar syrup is as well a product, what mostly contains glucose and fructose, which is split from sucrose. Sugar made by saccharification of wood contains glucose, fructose, HMF and xylose, representing another example for a mixed product, what need to be considered as reactant. These non-pure chemicals need to be used, when DMF production out of biomass should be possible to compete with fossil feedstocks nowadays. Furthermore, offering the possibility of modularized catalytic columns like in our work, the upgrade of fructose / glucose towards chemicals like p-xylene can make the process profitable even today, as the prices paid for specialty chemicals are much higher.

Considering the partial reaction of HMF to DMF, the alternative upgrade to 2,5-furandicarboxylic acid (FDCA) may be a reaction worth to contemplate.[147] But also in this case, the feedstock cost, which contributes to the final product price (39%)[148] is the bottle neck for commercialization. Considering the usage of non-noble metals and relatively cheap nickel or resin catalysts, ethanol as solvent, as well as the use of a simple, easy and scaled-up wet chemistry flow set-up, brings the current research closer to the realization of a profitable industrial plant.[149] [150] [151]

4.4. Synthesizing 2,5-DMF directly from fructose in an one-step approach

A two – step flow reactor is not the final stage of simplicity. A single column approach would simplify the whole set-up and is easier to scale-up, whereby fewer instruments are required. If the dehydration is uncoupled from the second hydrogenation step, the products are not immediately converted further to DMF, what is a molecule without reactive functional groups, compared to HMF. One way to avoid the reaction of HMF to ethyllevulinate is bringing the reactions and therefore the catalyst´s active sites more close. Meaning, right after the dehydration, when the HMF molecule is present in solution, it needs to be converted to DMF, without giving the chance to react in a consecutive reaction (e.g. levulinic acid).

Ni@WC was selected and showed very good results in terms of selectivity and general activity as well as stability for the HMF to DMF reaction (chapter 3). The optimum conditions were 150 °C with 30 bar pressure. As Amberlyst 15 is resin based and not stable above 120 °C, it is not possible to use this catalyst in a single column approach at 150 °C for a longer time. Out of this reason, a more stable catalyst must be chosen. The carbon based materials discussed in chapter 2 showed promising results, whereas the glucose based material as well as the activated carbon catalyst showed the best performance at 150 °C. The higher surface area of the activated carbon (144 m^2 g^{-1}), with at the same time micrometer agglomerates, enables to use this porous material in flow application. Even with a high surface area, the pressure drop is sufficiently low at around 4 - 5 bar over a catalyst column of 250 mm x 4.6 mm. The activated carbon could even increase its ability in dehydration up to 200 °C. On the other hand this “carbocatalyst” already showed activity for the production of DMF during the reaction without any metal deposition. Out of these reasons, this sulfonated carbon material was selected for further preparation to use it in a one column approach for the upgrade of fructose together with Ni@WC.

During the sulfonation process using fuming sulfuric acid, sulfonic acid groups are inserted into the material. The wet-mixing of Amberlyst 15 together with Ni@WC did not show any activity in terms of hydrogenation, most likely because of a strong poisoning effect. Amberlyst 15 was still active for the dehydration (SI-F18) but did not show a further reactivity with hydrogen. Because sulfur is known for its poisoning of metal catalysts, a dry mixing approach, instead of a wet-impregnation approach was applied for further catalyst production. Therefore, one gram of activated carbon material was mixed with 1.9 g of 10 wt% Ni@WC. The powder was shaken by hand very intense for several minutes, until the material was homogeneously distributed without any color difference in the vial anymore. The grey Ni@WC powder is visible between the black carbon material. After mixing, the powder was filled into a 250 mm x 4.6 mm stainless steel column and tested under 150 °C, 30 bar and 0.25 mL min^{-1}. In this set-up the external column was connected after the hydrogen inlet at the H CUBE Pro ™, whereas the Ni@WC needs hydrogen to directly convert the HMF to DMF. The connection scheme is presented in figure 46.

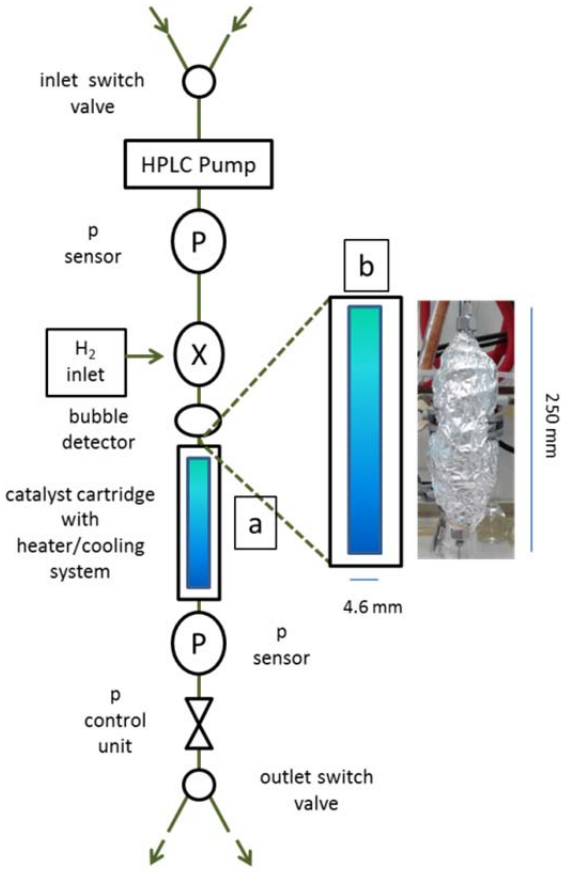

Figure 46: Flow diagram connecting the external column for the one-column approach. The small column 70 mm x 4 mm a) was filled with inert silica material and did not take part in the reaction. The bigger column 250 mm x 4.6 mm b) was filled with a mixture of activated carbon and 10 wt% Ni@WC.

The second 70 mm x 4 mm column (a) was filled with inert material, and therefore did not take part in the reaction. The hydrogen flow was adjusted to 100 %, what means a flow rate of 60 mL min^{-1} controlled by the internal MFC. The results indicated an increase of 10 % yield of DMF, while EL decreased to 0 % (GC-MS, SI-F19). The selectivity therefore was shifted towards the furan ring product DMF and the consecutive reaction was suppressed as intended. The summarized results can be observed in figure 47.

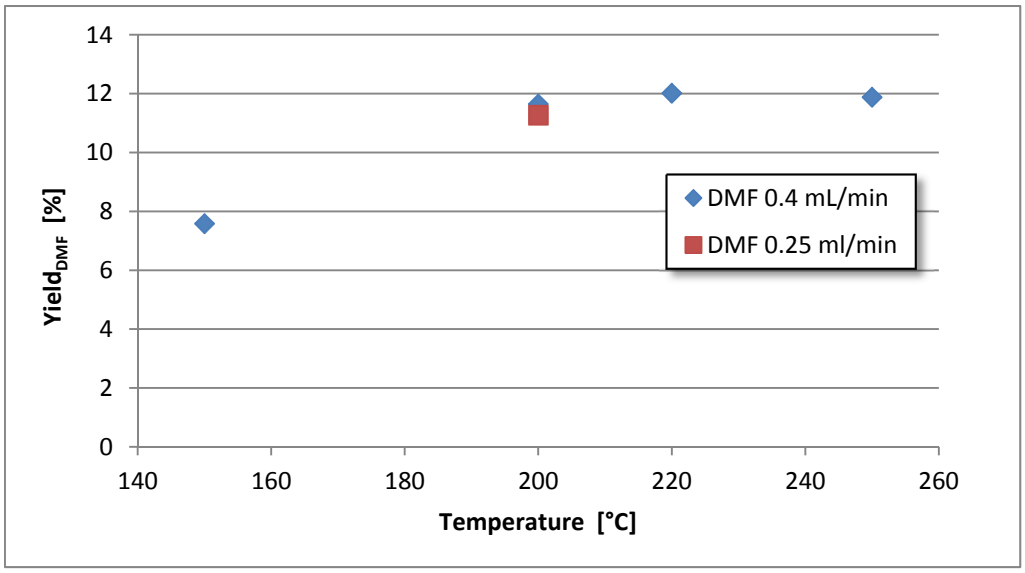

Figure 47: Temperature depended yield of DMF, using a mixture of activated carbon and 10 wt% Ni@WC. The catalyst was filled into a 250 mm x 4.6 mm stainless steel column and connected to the H CUBE Pro ™ for hydrogen supply. Reaction conditions: 0.05M fructose in ethanol, 30 bar with H_2, 0.4 mL min^{-1} (blue) or 0.25 mL min^{-1} (red).

Activated carbon material in combination with Ni@WC is able to withstand temperatures higher than 120 °C and is therefore tested at 30 bar of pressure at temperatures from 150 °C to 250 °C. The column was externally heated. At a flow rate of 0.4 mL min^{-1} (blue spots) the reaction was able to be increased from 7.5 % at 150 °C to a maximum of 12 % at 200 °C. In addition, a further test was using only a 0.25 mL min^{-1} flow rate, whereas the same yield of nearly 12 % was achieved. This hint towards a maximum reactivity, already achieved at 0.4 mL min^{-1}, which cannot be increased further by increasing the contact time between the reactants and the catalyst. The decrease of flow rate resulted in an almost doubled residence time compared to the 0.4 mL min^{-1} run.

By an increased temperature, longer residence times and a higher energy input, consecutive or side reactions are more likely to occur. Whereas the DMF yield is increased from 150 °C to 200 °C, ethanol starts to degrade as well. This degradation is slightly increased at 200 °C and massively increased from 200 °C to 250 °C. Whereas side reactions are not desirable, because it is more difficult to separate the products, conditions at 200 °C are best in our case. Furthermore the catalyst can massively get affected by the deposition of higher mass molecules, namely humins and polymerization products. A so called “coking” can occur, what decreases the accessibility of active sites. The yield of DMF will not increase anymore due to a maximum reactivity and the side reactions are still low. Anyway the analysis showed high mass side products as well, resulting from unwanted reactivity. But as DMF as well as ethanol are easy to evaporate, higher mass products will stay in the bottom of the distillation plant, due to higher boiling points, whereas the separation and purification of the products is possible.

4.5. Design of a scaled-up tube reactor system for continuous approaches

Two-column systems have the disadvantage of uncoupled reaction cascades. As previously shown, fructose needs to be fully dehydrated before the hydrogenation reaction converts the reactive products further. By mixing the catalysts, a one column set-up can be used, bringing the catalysts so close, that products from the first reaction are immediately converted to the final product. The conversion of fructose in such a mixed column system was shown to be possible, but still suffers from milliliter scale conversions. In order to enable a higher reactivity by an expansion of the reactor conditions as well as to run the system in a liter scale, a scale-up was planned and assembled. This set-up can run reactions completely independent from the H CUBE Pro ™. The final goal is to show the feasibility of the continuous reaction process and to demonstrate a directly combined run what can be further scaled up to an industrial approach. The principle study was therefore expanded from an often reported one-pot batch reaction to a one-flow concept, what is considered the most important step in the current landscape of knowledge for industrialization.

The conditions possible with the H CUBE Pro ™ are limited to maximum 150 °C, 100 bar and 3 mL min^{-1}. Depending on the catalyst, these conditions may not be suitable for hydrogenation reactions, which need higher temperatures and residence times, using less effective, but cheaper catalysts. The usage of tungsten carbide under mild conditions did not lead to sufficient conversion results in diverse hydrogenation reactions. Literature reports the usage of conditions up to 400 °C, which is simply not possible with the H CUBE Pro ™.

Therefore the next step of the scale-up was to plan and assemble a completely free-standing system, presented in figure 48. Additional photos and description of the set-up can be found under figure 49.

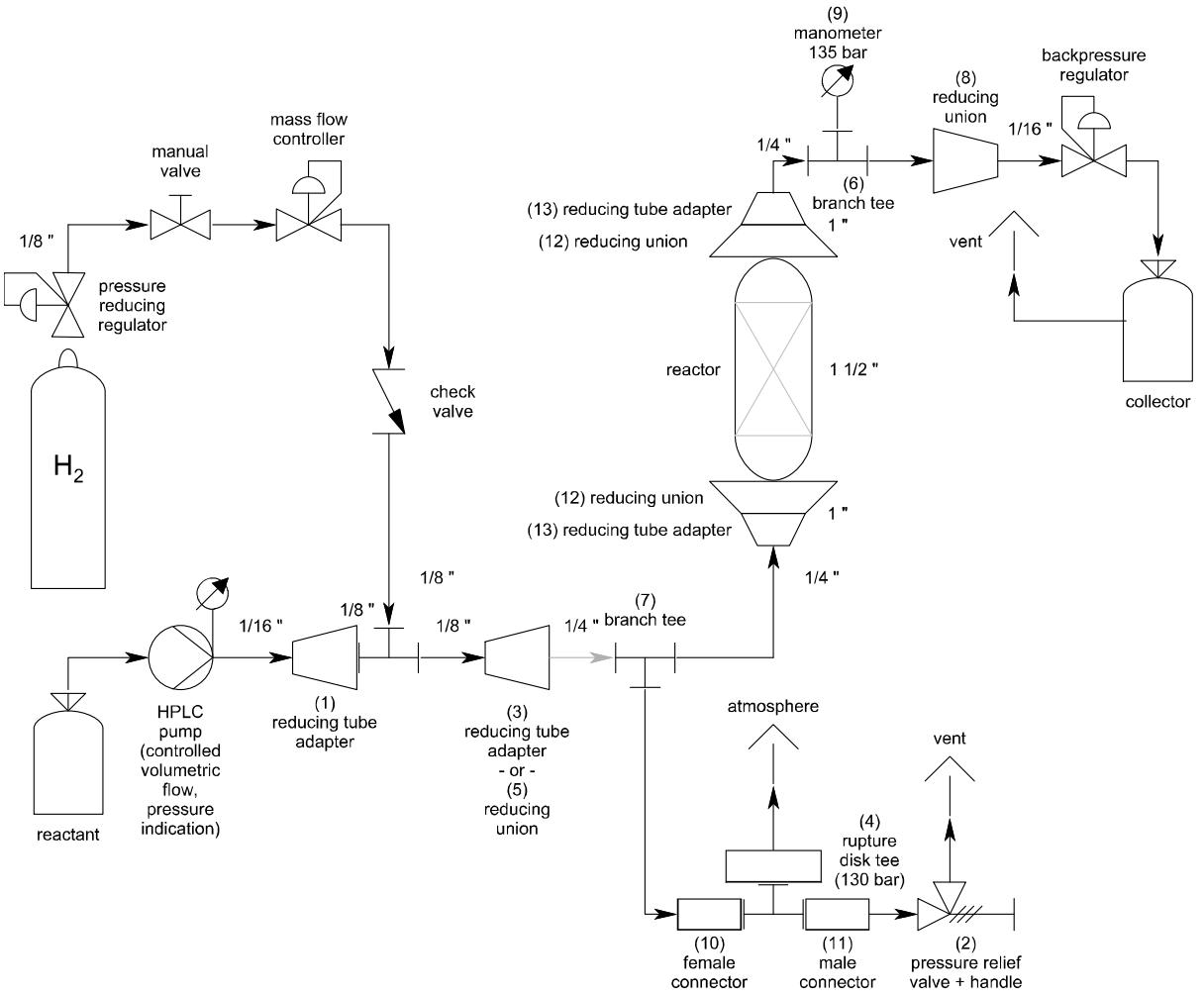

Figure 48: Schematic illustration of the self-constructed scaled reactor system, showing all tubing, connections, devices and the 1 ½ “ reactor.

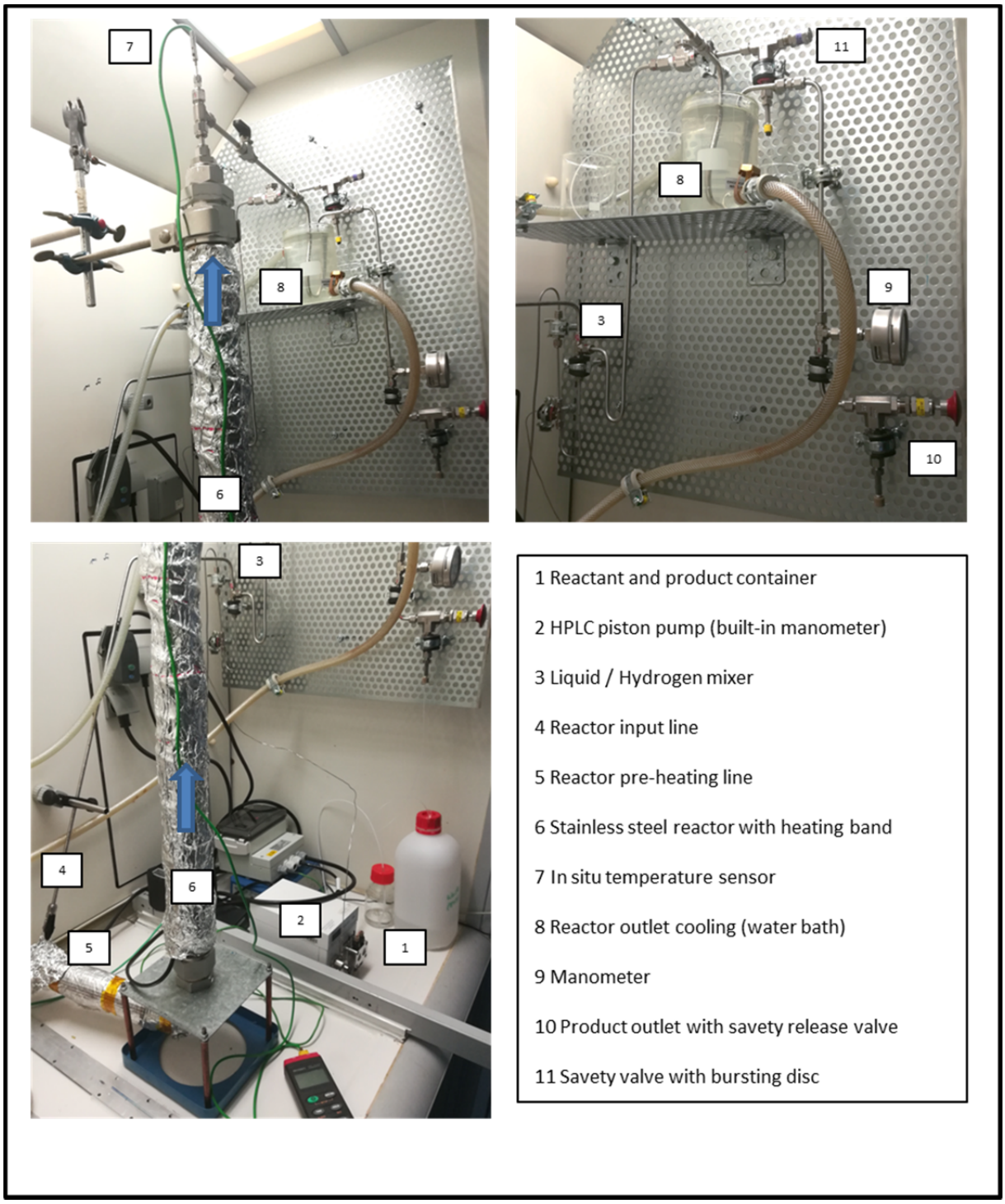

Figure 49: Photos of the reactor set-up after assembling. All important parts are numbered and respectively explained. The hydrogen bottle is stored in a safety cabinet and the gas is transported by an installed high pressure tube. The mass flow regulator, controlling the gas inlet is not shown.

The flow rate can be adjusted by a piston pump (Knauer, Azura P4.1 S, maximum 50 mL min^{-1}, ceramic head). It needs to withstand a certain pressure and be able to also work against it. The adjustable ranges are between 0.01 mL min^{-1} and 50 mL min^{-1} at a pressure of maximum 150 bar. This pressure will be controlled by using a back pressure regulator at the end of the

tubing system. The regulators are available in 10 bar to 30 bar (VICI Jour, JR-BPR1) and 30 bar to 100 bar (VICI Jour, JR-BPR2) and are freely adjustable. The tubing system itself needs to withstand maximum 100 bar and needs to confine the liquid reactant mixture through the reactor column (stainless steel, 800 mm length, 28.5 mm inner diameter, 4.8 mm wall thickness). Stainless steel was chosen for this purpose, in order to ensure safety. Additionally the system needs to be heated by a heating band (Mohr and co, 230 V, 375 A, 450 °C) or an oven (MTI corporation, GSL 1600x). The tubing itself will not see the heat, but the reactor can be pushed up to 500 °C, depending on the reaction temperature needed.

The reactor itself needs to be able to keep the catalyst inside and will not take part in the reaction itself. For that reason stainless steel filter plates were chosen (5 µm mean opening width) offering enough space for the liquid and solubilized reactants to pass, but holding back the catalytic bed. For the scaled-up version of the system, a higher amount of reactant pumped through the catalyst bed needs to be considered, connected to a bigger diameter, with the possibility of sufficient residence times. The reactor length should be planned according to its diameter, meaning the ratio of the particle size to reactor diameter of at least a number of 10, whereas the length of the reactor should be at least 25 times the diameter of the tube. (*EUROKIN_fixed-bed_html*, EUROKIN spreadsheet on requirements for measurement of intrinsic kinetics in the gas-solid fixed-bed reactor, 2012)

The hydrogen for the reaction using a metal catalyst will be provided by an external hydrogen bottle and a mass flow controller (MFC Brooks, SLA 5800 Series). The maximum hydrogen pressure can be set by the user directly at the gas bottle (maximum 100 bar) in a safety cabinet and the gas is transported through a high pressure stainless steel pipe towards the reactor. The MFC is controlled by a software (Brooks Expert Support Tool 3.2.2.4.) and a computer, whereas the flow can be adjusted. By an internal regulatory mechanism of heat transfer and resistance, the flow is precisely measured and the valve is closed or opened accordingly. The valve motor can deal with pressure differences up to 95 bar.

The overall advantage of this self-constructed system is an extension of the reactor volume (0.753 ml, H CUBE Pro ^{TM} 70 mm x 4 mm cartridge **<** 4.2 ml, 250 mm x 4.6 mm column **<** 510 ml, 800 mm x 28.5 mm) and therefore an enhancement of residence time and output, according to the flow rate adjusted. The system is simple and can be further scaled-up. The

planning was reduced to a minimum of parts and can be seen as a flow system, easy to build. Constructing a simple flow reactor system with a minimum of investment (< 10 000 Euro), ensuring safety and reliability and using elemental hydrogen as gas, can open a way to produce chemicals and fuels also delocalized in continuous fashion.

4.6. Summary

The dehydration of fructose as well as the further hydrogenation, in our case the hydrodeoxygenation, are two important reactions. The combination of these two reactions open up possibilities in the direction of synthesizing DMF out of a fructose / ethanol solution in a continuous process directly from the carbohydrate. The dehydration process, using Amberlyst 15 as the most promising catalyst, as shown in chapter 2, was integrated into a set-up together with the H CUBE Pro ^{TM}. The two column system provided 30 bar of pressure, additionally to the 110 °C and 0.25 mL min^{-1} flow rate, predetermined by the optimum conditions for 10 wt% Ni@WC in the 70 mm cartridge. By pressurizing with 30 bar, the overall yield of the reaction is 85 % (38.5 % DMF and 47 % ethyllevulinate). The increase of reactivity is potentially due to a higher partial pressure as well as a higher concentration in the solution itself. The increase of 30 bar gives an increase of ethyllevulinate of 30 %, whereas the furan ring products are decreasing. The 15 % loss of furan ring products show the enhanced consecutive reaction of HMF derivatives to ethyllevulinate. The consecutive reaction gets more important and is increased with higher pressure. The run was additionally checked for a time period of 7 hours under continuous conversion, and no pressure drop as well as no significant loss of activity was recognized. The Amberlyst 15 however showed a black precipitate at the entrance of the column, what hints towards the formation of humins and polymers on the catalyst. The sulfur to carbon ratio in Amberlyst 15 was decreased of about 7 %, whereas the Ni@WC did not show a significant loss of activity neither in stability or particle size.

To overcome the disadvantages of a two column system, a further aim was to establish a single column approach. The activated carbon material showed already good results in terms of the direct production of DMF and a hydrodeoxygenation activity of the carbon material itself. This carbon was chosen to mix with 10 wt% Ni@WC in order to achieve a combined catalyst, able to directly produce DMF in 12 % yield out of a fructose / ethanol solution in

one shot, using the optimum conditions for Ni@WC of 150 °C, 0.25 mL min^{-1} as well as 30 bar. Consecutive reactions towards ethyllevulinate can be avoided, when every produced HMF derivative molecule will be immediately converted to a DMF and undergoes a hydrodeoxygenation instead of a further dehydration.

After achieving good results with the two column system, as well as showing promising results with the single column approach, a profitable efficiency consideration was contemplated. As it is possible to separate the easy to evaporate molecules like ethanol and DMF from the ethyllevulinate by distillation, this profitable consideration is meaningful. One big cost driver is the purification of products after the reaction (figure 13, 11%), as well as the feedstock cost (figure 13, 47%). The improved yield in a continuous system brings the research closer to an industrial realization, upgrading fructose to DMF. But from an economical point of view, this upgrade is nowadays not profitable as such, when using pure fructose. Feedstocks like molasse or other waste streams, as well as sugar mixtures need to be considered, to make the fuel economical in terms of the current competition on the market. Nevertheless, our modularized column approach, in combination with a possible scale-up shows the possibility of integration of DMF production into the current landscape, also considering the further upgrade to chemicals instead of fuels. Producing bulk or specialty chemicals out of biomass-derived molecules open up possibilities to already integrate the here presented system into the current industrial landscape. A mixed feed stock is the standard situation in fossil oil refinery, so we should not be surprised that similar will hold true for biorefinery.

Additionally a scaled-up reactor was planned and build, possible to operate completely independent from the H CUBE Pro ™. The reactor volume (510 ml, 800 mm x 28.5 mm) was 120 times bigger then the first expansion of the H CUBE Pro ™ system (4.2 ml, 250 mm x 4.6 mm column). The flow rate can be adjusted by a HPLC pump, with a maximum flow of 50 mL min^{-1}. The temperature limit is about 500 °C, what can be achieved by a high temperature oven or a heating band. Pressure regulation was done by back pressure valves, adjustable up to 100 bar. Hydrogen gas is coming from an external hydrogen bottle and is controlled by an installed mass flow controller. This hydrogenation flow reactor system is able to upgrade reactants, using heterogeneous catalysis in the liter scale.

5. Concluding chapter

5.1. General summary

The conversion of carbohydrates is one of the most promising fields in green chemistry, as it enables to produce bulk chemicals and fuels out of renewable and abundant resources, instead of further exploiting fossil feedstocks. The focus in this thesis is set on the conversion of fructose using dehydration and hydrodeoxygenation. The main goal is to find an easy continuous process, including the solubility of the sugar in a green solvent, the conversion over a solid acid catalyst as well as over a metal@tungsten carbide catalyst. Biomass derived and hence carbon-based solid acid catalysts are synthesized for dehydration; micro- and nanoparticle sized tungsten carbide catalysts, using nickel as an alternative to noble metals are used for hydrogenation. The resulting molecules are mainly 2.5-dimethylfuran (DMF) and ethyllevulinate (EL), both valuable as biofuel as well as for fuel blends. The usage of non-noble metal catalysts in the final continuous approach is as important as to keep the whole process as simple as possible, in terms of applicability and implementation in the current bioenergy landscape.

At the beginning of this thesis, the synthesis of solid acid catalysts based on carbohydrates was presented. The acid catalysts were synthesized by using carbohydrate material like glucose and starch at high temperatures (up to 600 °C). Additionally a third carbon was synthesized, using a precursor obtained by the company Micromidas. After carbonization and further sulfonation, using fuming sulfuric acid, the three resulting catalysts were characterized by scanning electron microscopy (SEM), transmission electron microscopy (TEM), nitrogen sorption (BET) and elemental analysis (EA). The introduction of sulfonic acid groups into the structure was additionally checked by a titration method, giving insights into the amount of acid sites. All produced catalysts were compared to sulfonated carbon black as well as Amberlyst 15 as commercial materials. Whereas the catalyst based on sugar and starch carbon showed a limited surface area of around 6 $m^2\ g^{-1}$, the activated carbon material offered 144 $m^2\ g^{-1}$. The implementation of sulfonic acid groups was successful for every produced carbon, but the density of these functional groups was much lower than in the commercial resin Amberlyst 15.

In order to test all solid acid catalysts in reaction, a 250 mm x 4.6 mm stainless steel column was used as continuous reactor, connected to a piston pump. The temperature (110 °C to 250 °C) and flow rate (residence time 2 to 30 minutes) was varied, and a direct relationship between contact time and selectivity was determined. With ethanol as solvent, the reaction mechanism, as well as the product distribution was showing a dehydration step of fructose towards 5-hydroxymethylfurfural (HMF). Consecutive reactions were producing levulinic acid, as well as condensation products with ethanol and formic acid like ethyllevulinate, 5-ethoxymethylfurfural and 5-(hydroxymethyl)furan-2-yl)methyl-formate. The longer the acid catalyst was in contact with the fructose solution, the more consecutive reactions prevailed. The maximum of HMF derivative formation 5-(ethoxymethyl)-2-furaldehyde and 5-(hydroxymethyl)furan-2-yl)methyl-formate was observed at a contact time of 11 minutes with a yield of 53 % using Amberlyst 15. The carbon solid acid catalysts were staying behind this value and achieved a maximum yield of 44 % with sulfonated starch at 200 °C.

The activated carbon was additionally showing a 2 % yield of 2,5-dimethylfuran (DMF) production, pointing towards the extraordinary properties of this catalyst. Without any metal present, what is normally necessary for hydrodeoxygenation reactions, a transferhydrogenation (with formic acid) was observed. The active catalyst was therefore carbon itself, what activated the hydrogen on its surface. This phenomenon was just very rarely observed so far and holds great potential for the further development of catalysts, based on carbon materials, without using rare metals. Graphene, graphene oxides or also doped graphene structures show activity as “carbocatalysts”.

A specific productivity ($M_{HMFderiv}\ g_{cat}^{-1}\ time^{-1}$) was calculated to compare all acid catalysts and set them in context to each other. This specific productivity shows the superiority of Amberlyst 15 catalyst in terms of lowest input temperature (110 °C), but best DMF yield results. The sulfonated carbon catalysts also showed sufficient activity for the conversion of fructose, but reached their maximum of specific productivity at higher temperatures. This result is promising in terms of using the carbon material instead of the resin, due to the limited stability above 120 °C.

In order to upgrade the HMF and its derivatives, a stable and selective hydrogenation catalyst is needed, to directly convert these dehydration reaction products further to DMF. As noble metals are rare and therefore expensive, cheaper alternatives were considered.

After postulating a similar electronic structure of tungsten carbide (WC) to platinum by Lewy and Boudart, research was focusing on the replacement of platinum. The “easy production” of nano-sized tungsten carbide particles (7.5 ± 2.5 nm, 70 m^2 g^{-1}) was enabled by the so called “urea glass route” and was compared in reaction to commercial material in the micrometer range. It was shown, that the activity is strongly dependent on the size of the particles as well as the surface area. The nano-sized WC particles showed a strong selectivity towards the conversion of multiple bonds as well as nitro functionalities under mild conditions at maximum 150 °C and 30 bar. The smallest particles showed full conversion and the best activity, as well as were stable over a run of 50 hours. The upgrade of nitriles, aryl ethers, carbonyl compounds and functionalities is however not possible under these conditions. Tungsten carbide is known to become more active at harsher conditions up to 400 °C or by using co-catalysis with other metals. Nevertheless it was shown, that nano-scaled tungsten mono carbide is active for hydrogenation reactions under mild conditions, having a promising potential to replace platinum.

One of the most promising and abundant metals for hydrogenation is nickel. This material shows excellent hydrogenation as well as hydrodeoxygenation reactivity, which is necessary in terms of cutting the functional groups of HMF in order to synthesize DMF. By using nickel on carbon support, the particles tend to leach and nickel is lost during reaction. To avoid this wash-out, the catalyst needs to be more stabilized on top of an equally stable support. Tungsten carbide offers these properties, additionally to the activity for hydrogenation. Different metal nanoparticles of palladium, copper and nickel were deposited on top of WC. With palladium on top of tungsten carbide, particle sizes of 60 ± 40 nm could have been achieved. Whereas this material resulted in a conversion of the desired DMF to 2,5-dimethyltetrahydrofuran by attacking the furan ring system, copper with particle sizes of 1-2 µm showed almost no activity for DMF production. The nickel nanoparticles are strongly connected to WC and undergo a strong and stable deposition, prohibiting leaching and showing very good hydrodeoxygenation properties with DMF yields up to 90 percent. In general it was shown, that nickel at tungsten carbide offers stable as well as excellent performance in terms of hydrodeoxygenation and the very selective upgrade of HMF to DMF.

In order to enable the upgrade of fructose to DMF in a continuous system, the current H CUBE Pro ™ hydrogenation system was extended with a second reaction column. A 250 mm x 4.6 mm stainless steel reactor column was connected ahead of the hydrogen insertion, enabling the dehydration of fructose before inserting the products directly into the second column for hydrogenation. The external heating enabled to run the reactions independent from the heating of the H CUBE Pro ™ as well as enabled to increase the residence time by selecting a 250 mm column.

The overall residence time of the two column continuous system is 14 minutes (0.25 mL min^{-1}), whereas the reactants stay in contact with the Amberlyst 15 for 11 minutes before inserted into the column filled with Ni@WC, where the solution stayed 3 minutes on average. With conditions of 110 °C and 30 bar for Amberlyst 15, as well as 150 °C and 30 bar for Ni@WC, the overall results were an almost full conversion with a yield of 38.5 % DMF and 47 % yield of EL. The additional adjustment of pressure to 30 bar, in comparison with the Amberlyst 15 used under atmospheric pressure before, enabled a 30 % higher yield, but also shifted the selectivity towards the consecutive reaction product ethyllevulinate. The main disadvantage is the formation of higher mass products, so called humins, which start depositing on top of the catalysts. The solid acid catalyst Amberlyst 15 was covered with carbon at the entrance of the reactor, resulting in a higher carbon value with reduced sulfur content. This fact indicates a loss of sulfuric acid groups, with at the same time a deposition of carbon. The nickel at tungsten carbide showed a slightly increased particle size of nickel, but no nickel leaching, indicating the stability of the nickel on the active support in a 7 hour run. The catalyst did not differentiate between the pure HMF or the derivative forms like 5-ethoxymethylfurfural or 5-(hydroxymethyl)furan-2-yl)methyl-formate. The purification of the products was done by a distillation, separating the DMF / ethanol as low boiling point molecules from the molecules with higher boiling points like ethyllevulinate.

In general it can be stated, that a two column system goes along with a higher investment as well as more maintenance costs, compared to a one column catalytic approach. To develop a catalyst, which is on the one hand able to dehydrate as well as hydrodeoxygenate the reactants, was aimed for at the last part of the thesis. The direct mixing of Amberlyst 15 as well as 10 wt % nickel@tungsten carbide was not showing any hydrogenation activity, due to the fact that sulfur is known for its poisoning of metal catalysts. As the concentration of

sulfur in Amberlyst 15 is very high (4.3 meq g^{-1}), the active sites on the nickel nanoparticles are likely to be poisoned. The activated and sulfonated carbon however showed already activity for hydrodeoxygenation without any metal present and offers itself therefore as an alternative to overcome the temperature instability of Amberlyst 15. Sulfonated activated carbon was therefore mixed in a dry approach with 10 wt% Ni@WC. The activity for the upgrade to DMF was increased from 2 % to 12 % of DMF yield, indicating less or no poisoning effects. The synthesis of ethyllevulinate was suppressed and not present anymore in the product solution. The dehydration and the hydrodeoxygenation were directly running next to each other on neighboring active sites (mixed catalyst), converting products of the solid acid reaction immediately. The chance for a consecutive reaction of HMF to levulinic acid is therefore lowered.

In order to scale up this entire one column approach, an 800 mm x 28.5 mm inner diameter column was planned and manufactured. The system was scaled up, whereas the flow reactor system is able to be run with 50 mL min^{-1} maximum flow rate, to stand a pressure of maximum 100 bar and be heated to around 500 °C. The tubing and connections, as well as the used devices were planned and assembled according to be save and easy in use. This scale-up expanded the possibilities of reaction conditions in terms of temperature (Δ 350 °C), reactor volume (Δ 506 ml) and therefore residence time according to the flow rate.

5.2. Outlook

Because of the promising results in terms of yield and time, using the continuous system, one aspect of future developments is the further optimization of a bi-functional catalyst for extension of the one column approach. The controlled placement of acidic sites next to metal nanoparticles on top of one support will enable a full conversion with high yield towards the desired product DMF. This single column system needs to be scaled up taking care of the pressure drop, which is getting more important using bigger columns and systems together with small particle sizes. A simple and preferably “easy” plant for the production of liter-scaled products should be used, on the basis of the already planned system, to run the reaction independent from commercial approaches.

Furthermore the solubility of the reactant needs to be ensured, when running a continuous system as introduced in these chapters. The solution will be pumped through the reaction plant and not soluble biomass cannot be processed in such a wet-chemistry system respectively. As the solvent has also a big influence on the product conversion and selectivity, different liquids for enhancing the selectivity are promising to address. The main hindrance for using cellulose as raw material is for instance the solubility in most commonly known solvents. Ionic liquids offer opportunities to dissolve the material as well as using the ionic liquid as catalyst at the same time. DMF is a volatile molecule, whereas the separation is therefore simple.

As this thesis is giving insights into the conversion of fructose towards DMF and ethyllevulinate, fructose needs to be produced and purified out of cellulosic biomass before it can be used called a completely “green” approach. To enlarge the vision towards more raw biomass and going the next step using glucose as a more cheap and abundant molecule, the isomerization of glucose to fructose needs to be addressed on the bigger scale. Modular reaction columns open the possibility of combining the catalysts flexible as how it is needed.

Even if HMF as well as DMF are already promising reaction products, a further upgrade to p-xylene, as well as gamma-valerolactone is thinkable. A catalytic column, able to further convert DMF in combination with ethylene makes it a promising approach as an expansion, considering p-xylene is normally produced from fossil resources. The usage of hydrogen over

Raney-nickel to convert ethyllevulinate was already demonstrated and shown. The resulting γ-valerolactone as well as the 2,5-dimethyltetrahydrofuran have a higher energy density within the molecule and are promising “green“ solvents, as well as primary material for more complex reactions.

The usage of formic acid, helping to solubilize the fructose in ethanol can also be changed towards other acids, as it was shown, that acetylated HMF can be obtained in a good yield using acetic acid as solvent. This approach opens therefore the possibility of producing acetylated HMF, what provides throughout its additional side group a protection for the further reactivity towards the side product ethyllevulinate. Acetylated cellulose is furthermore known since decades and may offer an alternative entry into cellulosic biomass upgrade because of its improved solubility, compared to pure cellulose.

Addressing the improvement of catalysts, alternatives to noble metals for hydrogenation reactions are not commonplace yet and need to be addressed by research. Cheap alternatives are not easy to find and the reduction of the amount of these rare and expensive metals is an urgent aim. One alternative material is therefore tungsten carbide, due to its similarity to the electronic structure of platinum. Albeit tungsten is a relatively abundant material compared to platinum, palladium or ruthenium, it is still ranked among the so called conflict minerals and should therefore be used with care. In combination with carbon, the material features stability as well as resistance and can be reused as a catalyst for a long time. It combines these advantageous properties with high reactivity and is therefore a promising candidate for hydrodeoxygenation. In nanoscale, together with nickel it was found as a stable and good alternative, using synergistic effects, bringing high activity and selectivity for DMF. This metal@WC prototype can be a new family of material, which needs to be further optimized in order to tune activity for hydrogenation reactions. Another direction of research focuses on the complete avoidance of metals and proposes pure carbon materials as catalysts. This relatively new research exhibits just some rare examples in literature at the moment, but is believed to have a huge impact on catalysis the next years. Graphene, graphene oxides and doped graphene materials, synthesized out of biomass can help to achieve a more sustainable future in heterogeneous catalysis.

6. Applied methods

X-Ray powder diffraction (XRD)

XRD measurements were performed on a Bruker D8 diffractometer using Cu-Kα radiation (λ = 0.154 nm) and a scintillation counter (Scinti-Detector). All reference patterns are taken from the database ICDD PDF-4+ (2012 and 2013 edition).

The XRD device is able to give information about the crystalline phase, because of an interaction of the crystal structure with the X-ray beam. Planes of different parameters will give different diffraction angles, and thus crystalline phases can be detected by diffraction techniques.

The Bragg law describes the diffraction of a wavelength through different crystalline planes.

$$n\lambda=2dsin\theta$$

θ is the angle that the beam forms with the crystal

d is the distance between the planes

n is a positive integer and represents the order of the diffraction

The result will be a characteristic diffraction pattern; with peaks and relative intensities at specific positions, labeling the crystalline planes accordingly.

We generally measured the diffracted peaks on the range 2 – 90 2Theta.

The crystallite size can be calculated by the Scherrer equation. The crystallite size must not be confused with the particle size, as the latest can be composed by a large number of crystallites.

$$s = (K\lambda)(\beta\cos\theta)^{-1}$$

s is the diameter of the crystallite

K is the shape factor, usually the value of 0.9 is used

B is the broadness at half intensity of a signal in the pattern

Transmission electron microscopy (TEM)

TEM pictures were obtained by a Zeiss EM 912Ω microscope operated at 120 kV as acceleration voltage.

By using a tungsten based filament in the TEM microscope, an electron beam of specific wavelengths in the order of picometers (10^{-12} m) is generated. This very small wavelength enables to measure samples in the nanometer range with sufficient resolution.

After the interaction of the beam with the matter, it is visualized on a fluorescent screen. The electrons pass through the sample and are affected, what enables to draw conclusions about the material.

Scanning electron microscopy (SEM)

SEM pictures were taken using a Jeol JSM-7500F, operating at 5 kV /10 kV and 10 µA field emission scanning electron microscope.

Also the SEM microscopes employ the use of an electron beam for the observation of the samples, similar to TEM. By using the SEM microscope the electrons, which are scattered back are detected in contrast to the TEM microscope in which the electrons that pass through are recorded. The resulting 2 D pictures are similar to camera pictures, suggestive of a 3 D axis effect. The samples get sputtered before they are inserted into the device in order to provide enough conductivity. (i.e. platinum)

Energy dispersive X-ray analysis (EDX)

EDX (attached to the SEM) mapping is recorded on a Jeol JSM-7500F field emission scanning electron microscope. This technique is based on the interaction of the electron beam in the microscope with the sample. The electrons interact with the electrons of the inner shells of the atoms and according to the used energy are kicked out. Electrons from the upper shell refill the created “hole” and therefore emit X-rays, which are detected. These rays are characteristic for each atom.

Nitrogen sorption measurements (BET)

Nitrogen sorption measurements were accomplished using Quantachrome Quadrasorb at the temperature of liquid nitrogen. The samples were previously degassed at 150 °C for 20 hours and analyzed with a QuadraWin software.

Nitrogen sorption experiments involve the adsorption of gaseous nitrogen on the surface of the measured material. The volume of gas adsorbed on the sample is recorded at different pressures. By calculations based on mathematical models (QSDFT, slit / cylindrical pores adsorption; moving point average 5) it is possible to obtain information about the surface area of the sample and its pores.

Combustive elemental analysis (EA)

Combustive elemental analyses were performed using a Vario Micro device.

With this technique, the sample is combusted in oxygen atmosphere, and the decomposition products such as H_2O, CO_2, N_2, NO_x, SO_x are detected. The elements are appropriately quantified.

Gas chromatography-mass spectrometry (GC-MS)

GC-MS of the liquid samples were measured using an Agilent Technologies 5975 gas chromatograph equipped with a MS detector and a capillary column (HP-5MS, 30 m, 0.25 mm, 0.25 micron). The temperature program generally used for all the samples started with an isothermal step at 50 °C for 2 min. In a second step, the temperature was increased to 300 °C (rate of 30 °C min^{-1}) and then kept for 2 minutes. The conversion of the reactions were calculated via the integration of the molecule peaks in the chromatogram and compared to the area of standards or calibration curves.

High-performance liquid chromatography (HPLC)-RID / MS

HPLC chromatography was performed using a HPLC-MS system on the one hand, as well as a HPLC-RID (Refractory Index Detector).

Chromatography was performed using Agilent 1200 series equipped with a Phenomenex Rezex ROA-Organic Acid H+ (8 % cross-linked sulfonated styrene-divinylbenzene; length 300

mm, 7.8 mm i.d., flow 0.4 mL min^{-1}) using isocratic aqueous H_2SO_4 (5 mM) as eluent and UV as detector (wavelength: 210 nm).

Secondly a Thermo Scienctific HPLC Dionex Ultimate 3000 was used in combination with a Thermo Scientific Velos Pro MS system. Isocratic conditions were used.

Nuclear magnetic resonance (NMR)

^{1}H- and ^{13}C-NMR spectra were acquired using a Agilent Varian 400 MHz Spectrometer in deuterated solvents. The Software was a VnmrJ Version 4.2.

NMR can be used to detect nuclei of atoms that possess a magnetic momentum. The sample is subject to a pulsed electromagnetic field. The nuclei, initially oriented in a disordered manner, get oriented in presence of the electromagnetic wave. When this force field is removed, the nuclei "slowly" relaxes and the nucleus is turned back in a disordered equilibrium state. The energy detected is characteristic for every nucleus, and depends not only on the nature of its element (H, C, etc.), but also on its surrounding (vicinity of electronegative atoms for instance).

Inductively coupled plasma optical emission spectrometry (ICP-OES)

ICP-OES is used for the detection of metals in previously decomposed and dissolved samples (e.g. aqua regia). The inductive coupled plasma is induced, using argon heated to 7000 K by a Tesla coil. By decomposition of compounds in this plasma, a specific and particular emission spectrum occurs, what can be detected by a CCD camera and photomultipliers. Every metal ion is giving an electromagnetic radiation, very unique for every metal atom. These atoms get broken down in the plasma and loose electrons. By recombining, electromagnetic waves are emitted, indicating the particular metal. By equilibrating with a database, the respective atoms can be identified. The concentration of the metal in solution is proportional to the intensity of the emission.

7. Experimental part

Synthesis of solid acid catalysts:

Carbonization of glucose and starch

Starch from potatoes (pure) was purchased by Carl Roth (Art-Nr. 9441.1), D-(+)-Glucose – Monohydrate (pure) was purchased by AppliChem.

Four gram each were filled in ceramic crucibles. Both substances were heated in the oven under a constant flow of nitrogen with different temperatures to 200 °C, 400 °C and 600 °C. The oven was flushed with nitrogen for one hour, before a ramping of 2 hours to the final temperature was adjusted. The final temperature was kept for 15 hours, according to the method of Toda et al. (Nature Com 2007). The carbonized product was taken out after the oven was cooled to minimum 60 °C.

Activation of carbon precursor

The carbon precursor material for the activated carbon was purchased by the company Micromidas. Urea and calcium hydroxide were purchased by Sigma Aldrich.

The material was mixed and grinded in a ratio of: mass ratio precursor carbon: urea: Ca(OH)2 = 2 : 1 : 2). After the material was filled into a ceramic crucible, the mixture was placed in an oven flushed with nitrogen. The oven was heated to 850 °C with a heating rate of 6.5 K min^{-1} and held at this temperature for two hours. The obtained product was washed using a 2 M hydrochloric acid water solution and subsequently dried under vacuum at 40 °C.

Sulfonation

The fuming sulfuric acid with approximately 20 % SO_3 (Oleum) was purchased by Sigma Aldrich. Carbon Black was purchased by (Cabot Corporation, Vulcan carbon).

Carbon Black, glucose and starch carbon as well as activated carbon was used for sulfonation. One gram of each material was dispersed into 20 ml of fuming sulfuric acid and mixed overnight at 80 °C. The slurry was quenched with ice water afterwards and finally filtered under vacuum. The used filter was made of hydrophilic polypropylene (0.2 µm) and the obtained powder was flushed with deionized water until the wash was not showing any

acidity anymore. The washed sulfonated carbon was finally dried in the oven overnight with 60 °C.

Dehydration of fructose using solid acid catalysts in a continuous system

The D-fructose and the ethanol (> 99.8%) was purchased from Sigma Aldrich; the formic acid from Alfa Aesar, 97 %. Amberlyst 15 hydrogen form dry was purchased by Sigma Aldrich.

In order to characterize the reactivity of the different solid acid catalysts, the material was filled into an empty stainless steel column. The columns used were 150 mm and 250 mm in length and have a diameter of 4.6 mm. The internal volume is therefore 2.5 ml and 4.2 ml. The columns were purchased from Sigma Aldrich (HPLC Column Blank Kit). The column was heated with a heating band (Mohr and co, 230 V, 375 A, maximum 450 °C), which was wrapped around the column. The flow was adjusted by a HPLC pump (Knauer, Azura P4.1 S, maximum 10 mL min^{-1})

The reactant solution contained 0.05 M fructose and 0.5 M formic acid in typically 200 ml of ethanol. The formic acid was necessary to dissolve the fructose in alcohol and to accelerate the dissolving.

Tungsten carbide preparation using urea

The preparation of tungsten carbide was realized by using tungsten (IV) chloride (Alfa Aesar) in a solution with urea (Sigma Aldrich). The solvent was ethanol. The molar ratio of urea to tungsten (IV) chloride was seven; the ratio of ethanol to metal precursor was typically two. The ethanol and tungsten precursor was mixed in a round bottom flask and cooled along the way. After one hour of stirring, the urea was added into the same flask and the material was stirred until the urea was dissolved.

After transferring the brownish slurry into a ceramic crucible, it was placed into a nitrogen oven. After one hour of nitrogen flushing, the oven was heated to 800 °C. The heating ramp was typically 4 hours to reach 800 °C (3.33 K min^{-1}). The tungsten carbide precursor slurry was kept three hours at 800 °C, before it was removed from the oven after cooling to around maximum 60 °C.

Reactivity of WCs

The tungsten carbide obtained with urea was compared to commercial tungsten carbide with different grain size. WC_{com} (Alfa Aesar, -100+270 mesh, 99 % metal basis) and $WC_{com\ nano}$ (Sigma Aldrich, 150 – 200 nm, >99 % trace metal basis). The material was filled into the cartridge of the H CUBE Pro ™ and sealed. As the solvent and reactants were able to pass through the cartridge, the catalysts were kept back in order to achieve a heterogeneous catalyst fixed-bed system. The H CUBE Pro ™ is able to adjust pressures up to 100 bar, temperatures up to 150 °C and flow rates of 0.1 mL min^{-1} to 3 mL min^{-1}. The internal volume of the empty cartridge is 753 µL.

Typical reaction conditions were 10 bar, 100 °C, 0.6 mL min^{-1} flow rate and 0.1 M reactant solution in ethanol.

Metal@WC preparation

Tungsten carbide material was used as precursor, depositing palladium, copper and nickel on top of its surface. $WC_{com\ nano}$ was used as template, and different metal salts were applied.

Copper chloride (Cu(I)Cl) (Sigma Aldrich, 97 %) was used in terms of depositing copper nanoparticles. Palladium acetate (Pd (II) acetate) (Sigma Aldrich, 98 %) was used in terms of the deposition of palladium nanoparticles. Nickel chloride ($Ni(II)Cl_2$) (Sigma Aldrich, 98 %) was used in terms of depositing nickel nanoparticles on tungsten carbide. The salts were mixed with the ethanol / $WC_{com\ nano}$ dispersion in order to result in 10 wt% metal nanoparticles on WC. After removing the solvent by evaporation, the resulting powder was placed into a ceramic crucible and heated to 400 °C in a hydrogen oven. The used gas contained 5 % hydrogen in argon. The heating ramp was typically 5 K min^{-1} and the material was kept three hours at 400 °C.

Reactivity of M@WC

The reactivity tests of M@WC were as well conducted in the H CUBE Pro ™ and were similar to the experiments described in the section “Reactivity of WCs”.

Typical conditions were 10 bar or 30 bar with flow rates of 0.25 mL min^{-1}. The conversion of 5-Hydroxymethylfurfural (Toronto Research Chemicals, Canada; Sigma Aldrich, 99 %) was done with a 0.05 M solution in ethanol.

8. Supplementary information

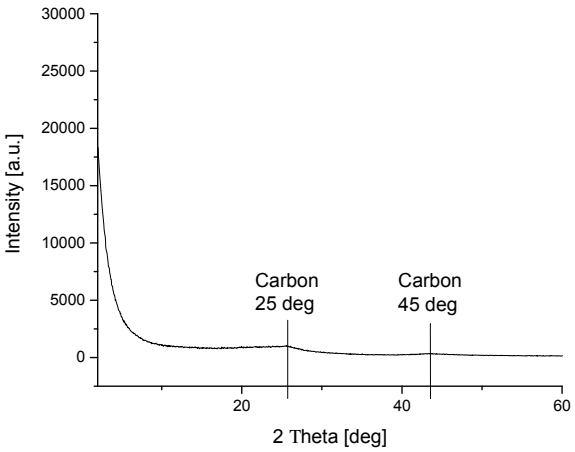

SI-F1: XRD diffractogram of activated carbon material after carbonization at 850 °C. The resulting powder was washed with acid solution to leach out all metal (salts). No metal residues are found here.

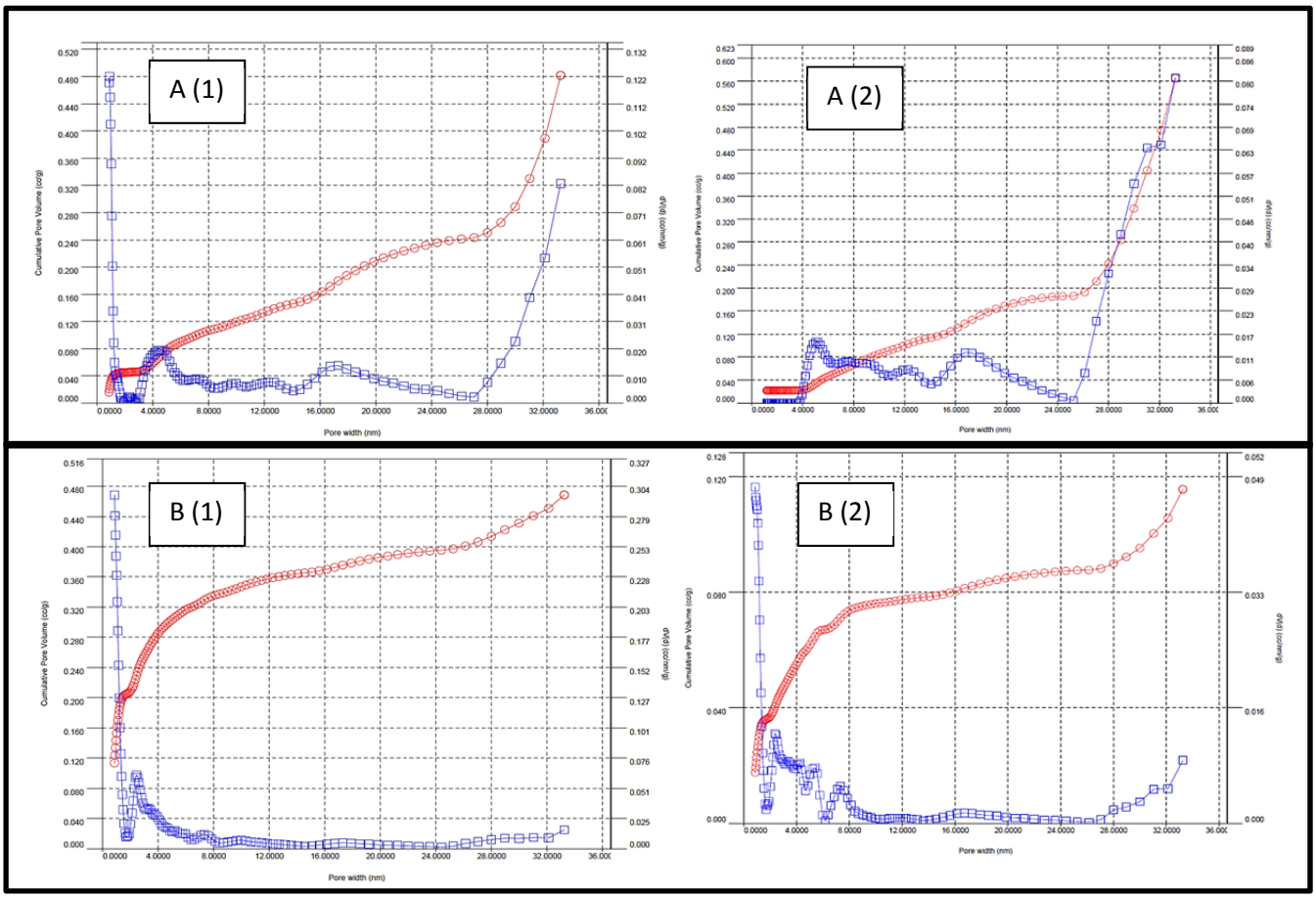

SI-F2: Pore size distribution of carbon black before (A (1)) and after (A (2)) sulfonation with fuming sulfuric acid. Additionally the pore size distribution of activated carbon is shown, before (B(1)) and after (B(2)) the acid treatment. In both cases, a loss of micropores can be observed.

HCL as well NaOH were used as titrants. The solid acid catalyst was mixed with sodium hydroxide solution and subsequently titrated with hydrochloric acid solution. Considering HCL and NaOH as strong acids and strong base, the usage of such titrants determine all acidic sites, weak, as well as strong acidic functional groups.

$$c_{sites} = \frac{n_{acid\ sites}}{m_{catalyst}} \approx \frac{n^0_{NaOH} - n^{eq}_{HCl}}{m_{catalyst}}$$

$$= \frac{[NaOH]^0\, V_{analyte} - [HCl]\, V^{eq}_{titrant}}{c_{mass_{catalyst}} V_{analyte}} = \frac{[NaOH]^0 - [HCl]\left(\frac{V^{eq}_{titrant}}{V_{analyte}}\right)}{c_{mass_{catalyst}}}$$

SI-F3: Calculation of acid sites in sulfonated material.

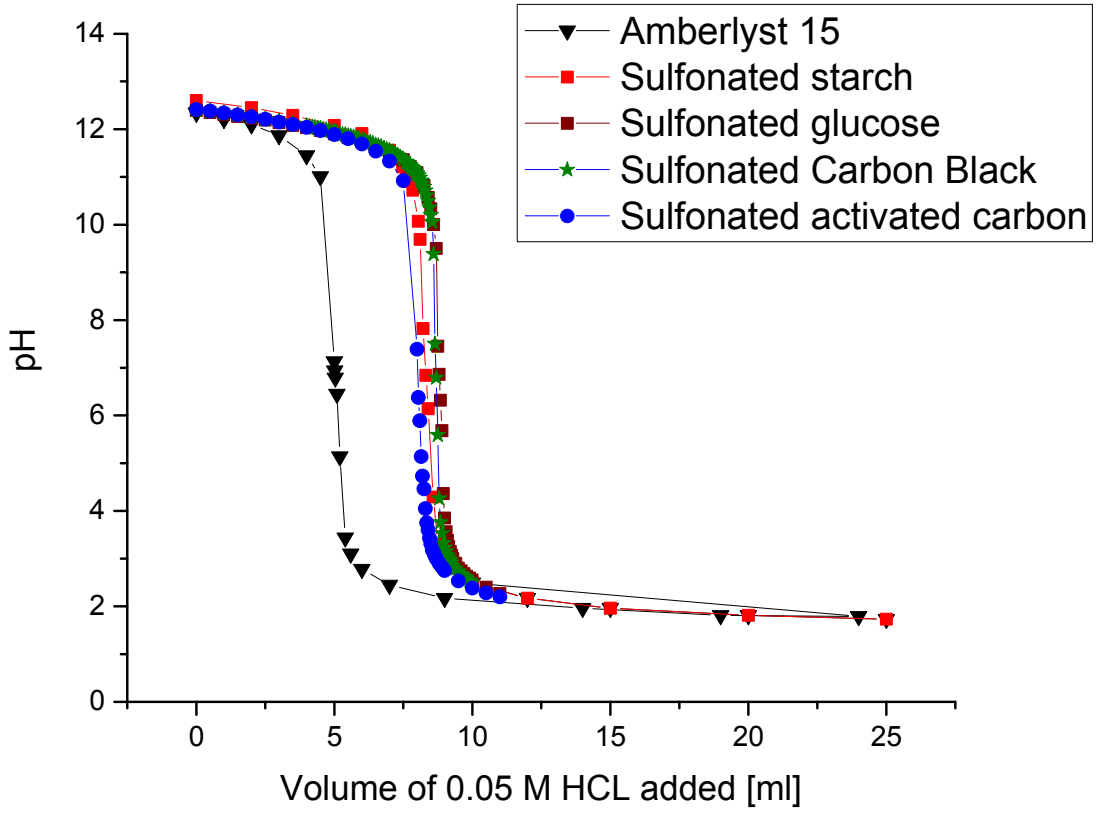

SI-F4: Titration curves of synthesized solid acid catalysts.

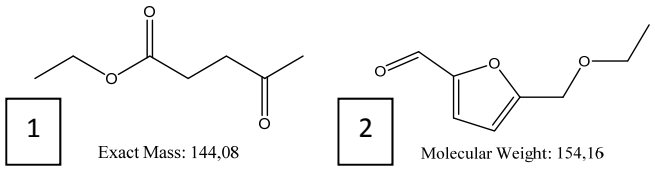

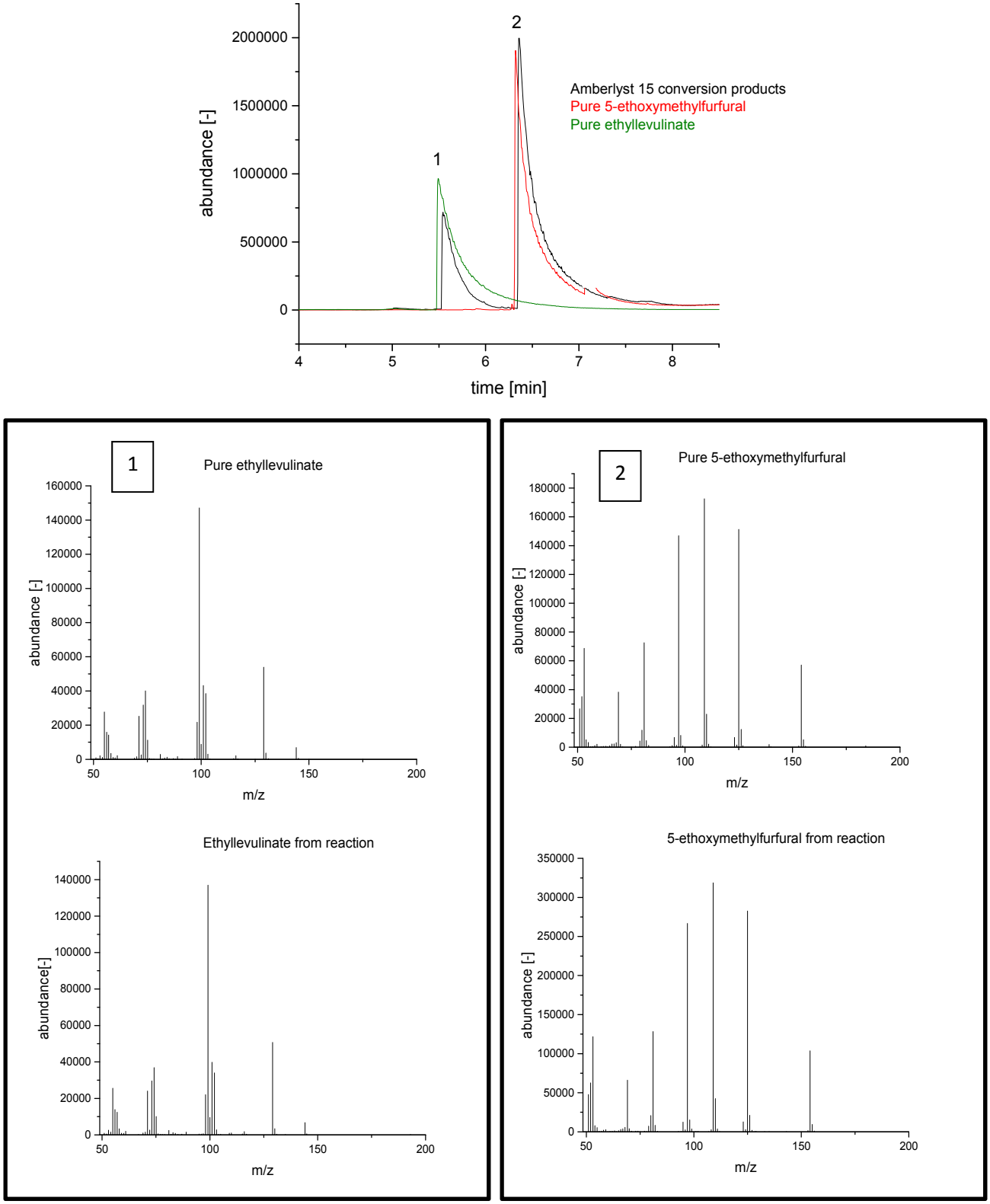

SI-F5: (GC)-MS results for the conversion of Amberlyst 15 to mainly 5-ethoxymethylfurfural (EMF) (2) and ethyllevulinate (1). The results were checked with the gas chromatograph, using pure compounds, as well as with the mass spectrometer.

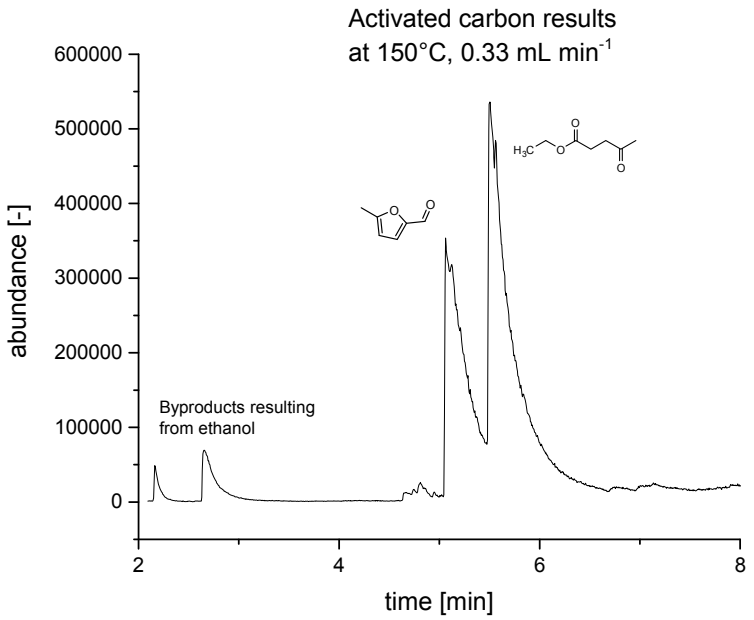

SI-F6: GC-MS results of the activated carbon material, showing 5-methylfurfural and ethyllevulinate as main results at 150 °C and 0.33 mL min^{-1}.

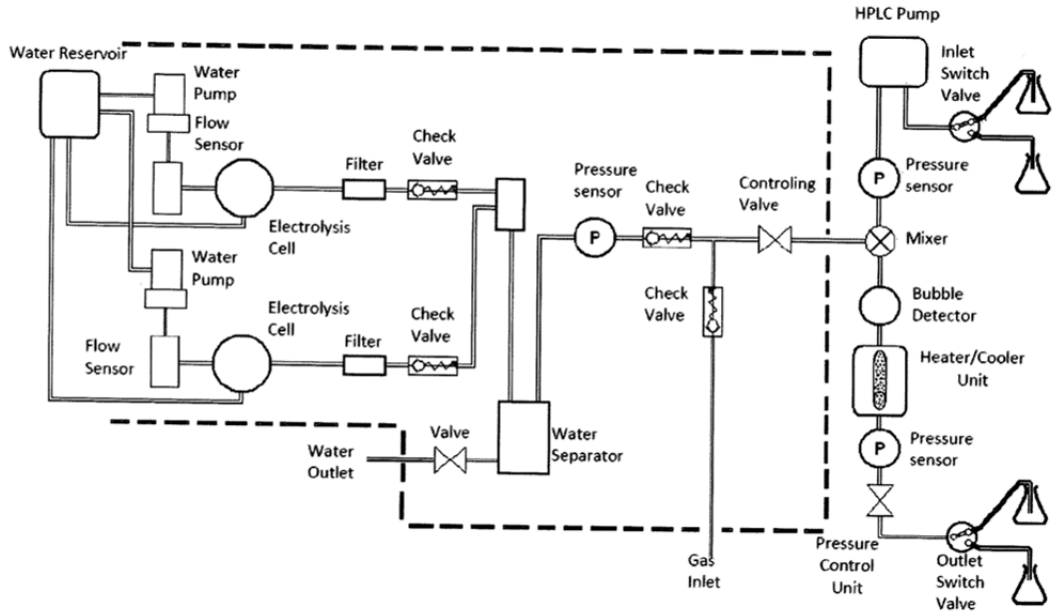

SI-F7: Schematic drawing of the H CUBE Pro ™. Adapted from the Thales Nano, H CUBE Pro ™ manual.

The mass specific reaction rate was calculated according to the following equation:

$$R_{mass} = \frac{g_{product}}{time\ g_{catalyst}} = [s^{-1}]$$

Where $g_{product}$ was obtained by calculation out of GC-FID / MS results and the adjusted flow rate.

SI-F8: Formula for the mass specific reaction rate R.

Entry	Substrates	Products[a]	Concentration [M]	Conversion (Selectivity)[b] [%]
1	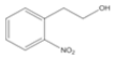	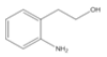	0.005	99 (100)
2	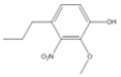	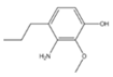	0.05	100 (100)
3			0.1	100 (100)
4	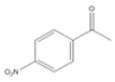	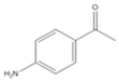	0.05	99 (100)
5	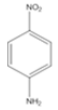	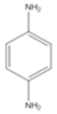	0.05	98 (73)
6	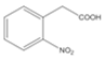	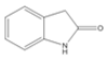	0.05	100 (80)
7	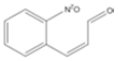		0.05	100 (100)
8			0.1	39 (75)
9			0.05	100 (87)
10	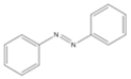		0.05	82 (100)

SI-F9: Summary of nitro moiety selectivity for diverse molecules using WC_{urea}. Conditions: 1.6 g catalyst, 0.6 mL min^{-1} (~ 1 minute residence time), 100 °C, 10 bar with H_2. [a] Reactions were monitored using GC-MS. [b] Conversion and selectivity were calculated by using GC-FID with cyclohexane as standard. Adapted from reference 135.

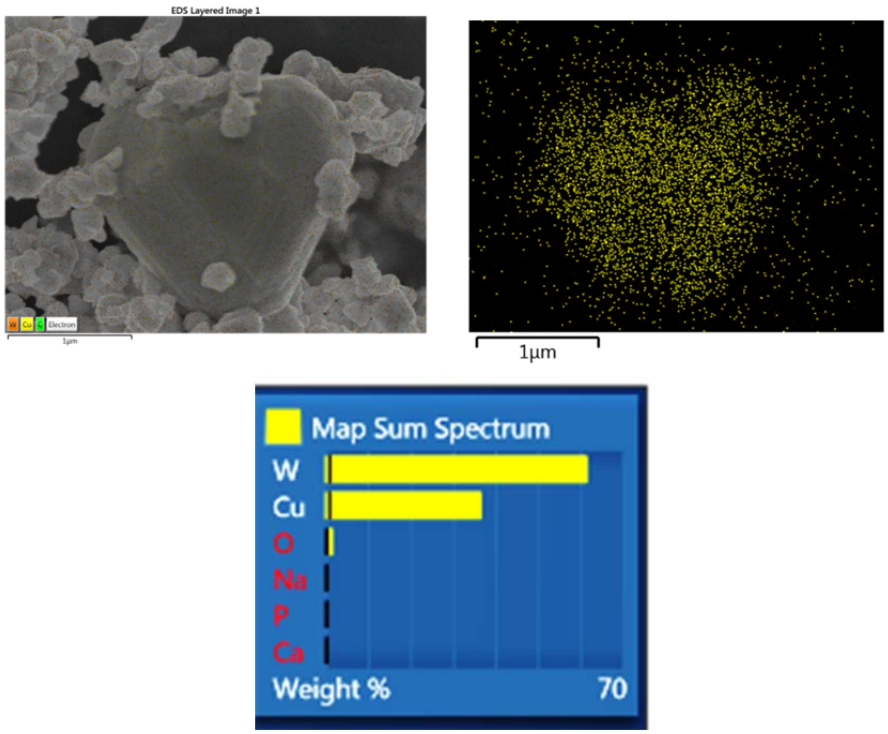

SI-F10: EDX analysis showing micrometer copper grains as well as the sum spectrum of the shown picture. Results are only representative for the shown pictures and therefore need to be seen as qualitative for the overall material.

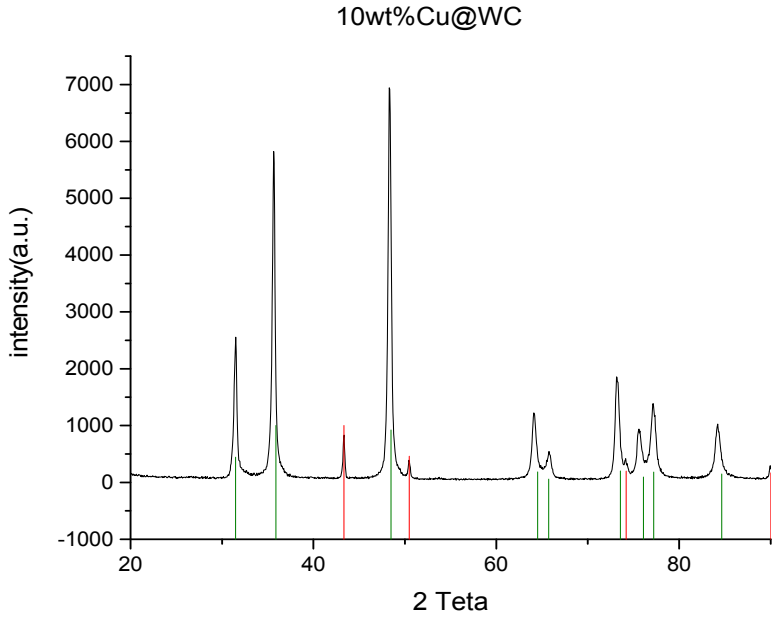

SI-F11: XRD diffractogram showing 10 wt% copper on tungsten carbide. Database PDF 4: Copper reference (Cu 00-004-0836) / WC reference (WC 01-077-4389)

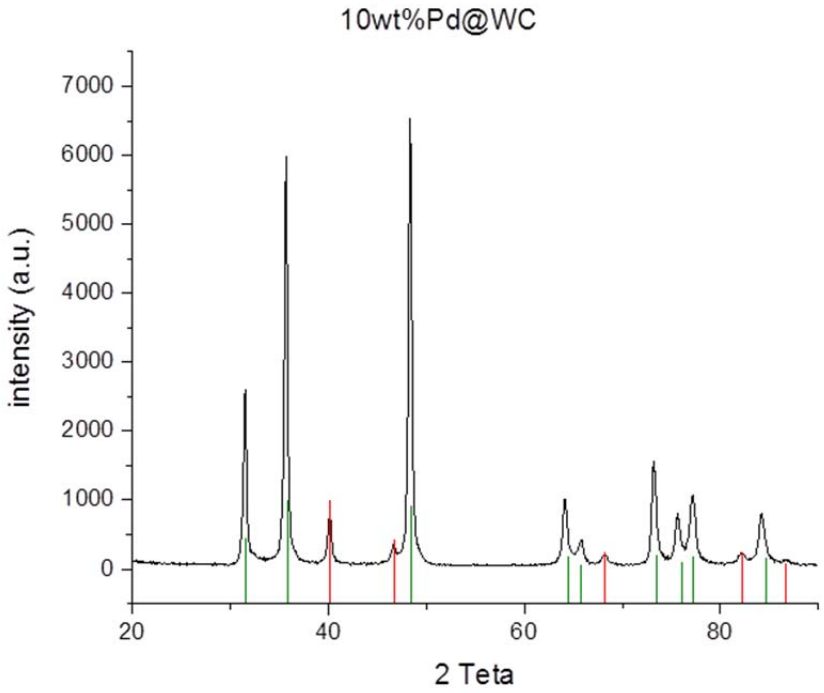

SI-F12: XRD diffractogram showing 10 wt% palladium on tungsten carbide. Database PDF 4: Palladium reference (Pd 00-005-0681) / WC reference (WC 01-077-4389)

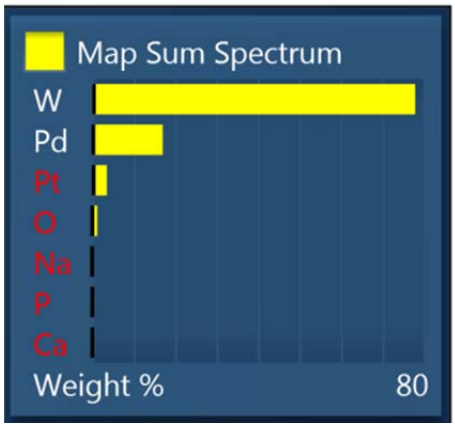

SI-F13: EDX mapping sum spectrum showing 10 wt% palladium on tungsten carbide. Results are only representative for the particular pictures and therefore need to be seen as qualitative for the overall material. Platinum is a result of the sputtering.

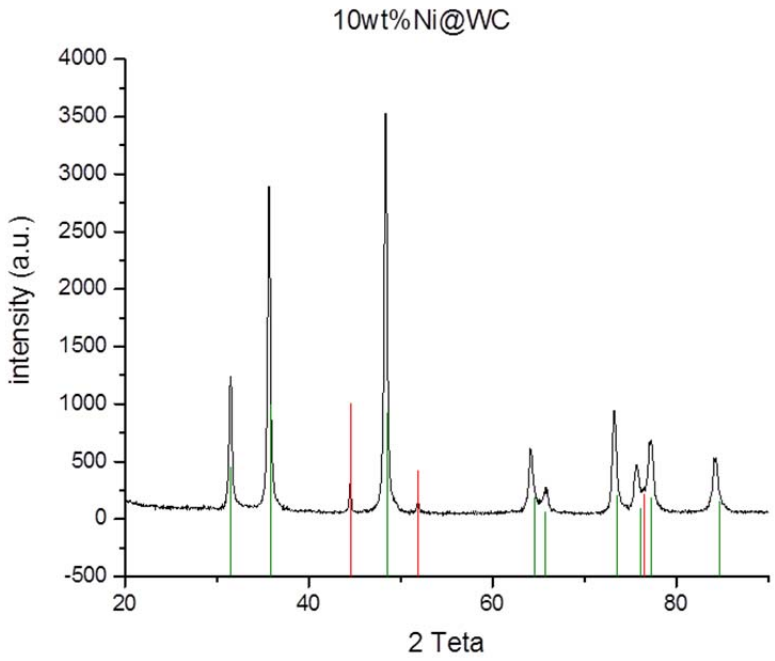

SI-F14: XRD diffractogram showing 10 wt% nickel on tungsten carbide. Database PDF 4: Nickel reference (Ni 00-004-0850) / WC reference (WC 01-077-4389)

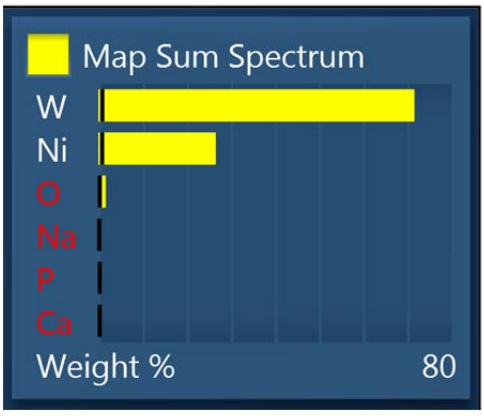

SI-F15: EDX mapping sum spectrum showing 10 wt% nickel on tungsten carbide. Results are only representative for the particular pictures and therefore need to be seen as qualitative for the overall material.

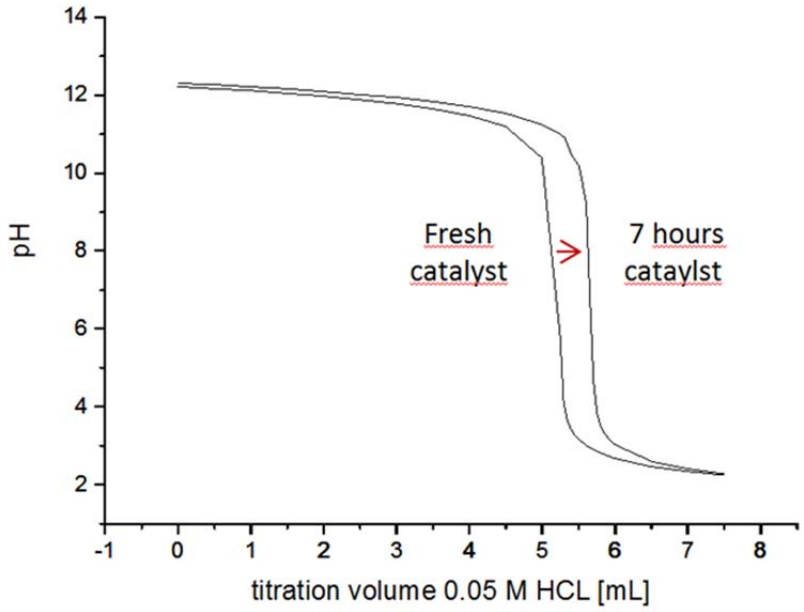

Concentration of acidic sites of fresh catalyst	4,25 meq g^{-1}
Concentration of acidic sites of 7 hours used catalyst	3,78 meq g^{-1}

We loose 0.478 meq g^{-1} (11%)

SI-F16: Decrease of acidic sites of Amberlyst 15 before and after a continuous 7 hour run.

Elemental Analysis	S [%]	S / C
Fresh Amberlyst 15	14.6	0.31
7 h Amberlyst 15	12.6	0.29
7 h Amberlyst 15 (Figure 43, B)	10.4	0.21

SI-F17: Sulfur to carbon ratio of Amberlyst 15 before and after a long time reaction.

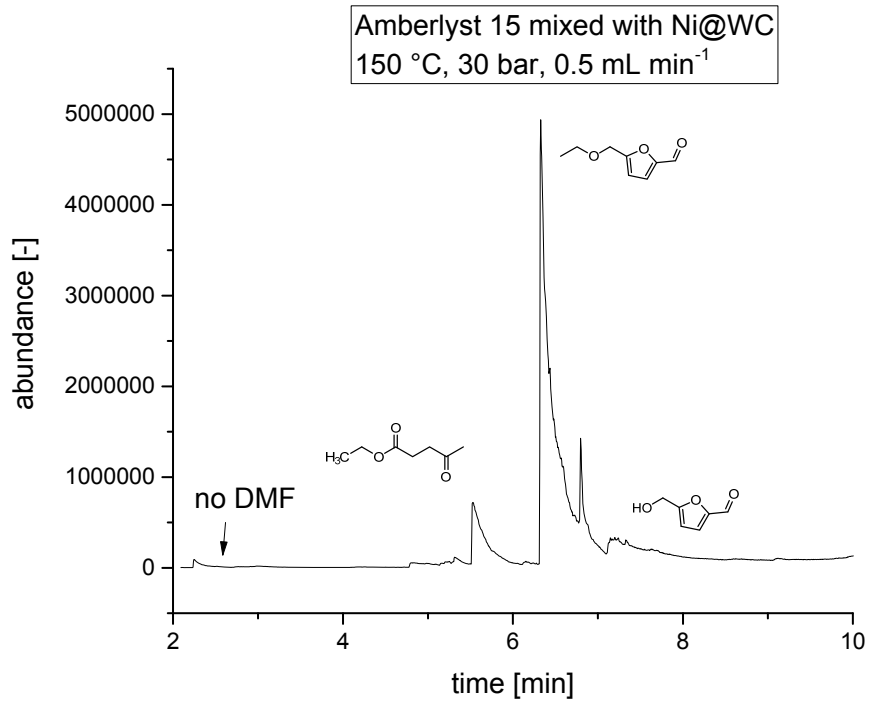

SI-F18: GC-MS results for the reactivity of the mixed column. Amberlyst 15 and Ni@WC were showing a dehydration reaction, but no hydrodeoxygenation. Amberlyst 15 has a temperature limit of 120 °C, and would degrade, applying 150 °C for a longer time period.

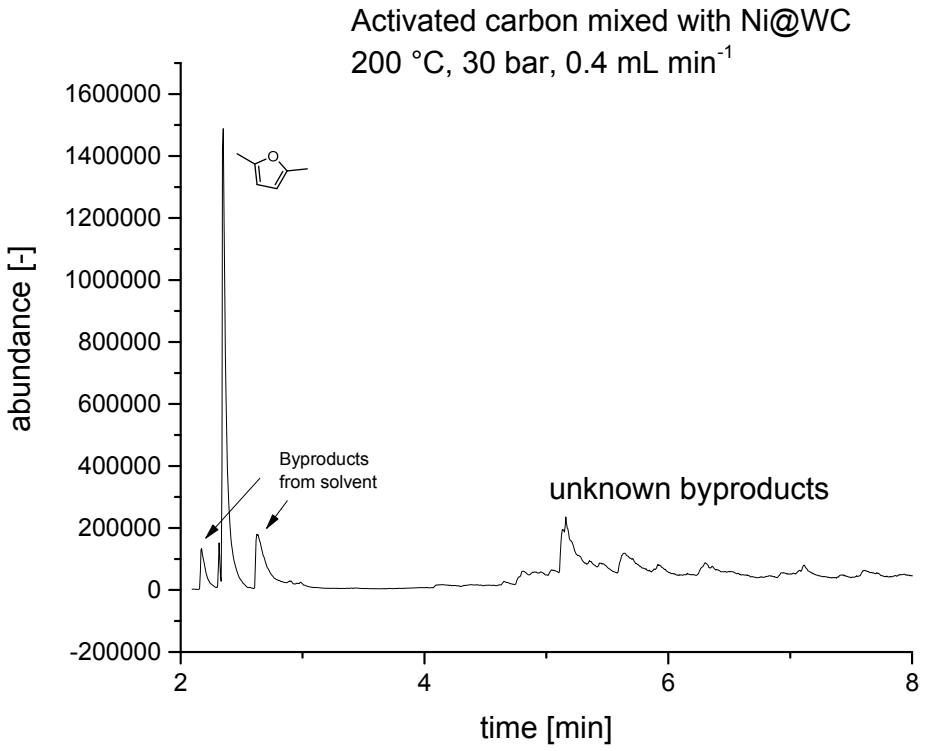

SI-F19: GC-MS result, for the mixed column using activated carbon as well as Ni@WC.

9. List of abbreviations

Abbreviation	Explanation
2,5-DMF	2,5-Dimethylfuran
5-HMF	5-Hydroxymethylfurfural
BET	Brunauer-Emmet-Teller
bp	Boiling point
Cu	Copper
DFT	Density Functional Theory
D_p	Particle diameter
EA	Elemental analysis
EDX	Energy dispersive X-ray spectroscopy
EL	Ethyllevulinate
EMF	5-Ethoxymethylfurfural
EtOH	Ethanol
FA	Formic acid
FDCA	2,5-Furandicarboxylic acid
FID	Flame Ionization detector
f_p	Friction factor
FT-IR	Fourier transform infrared spectroscopy
GC	Gas chromatograph
HCL	Hydrochloric acid
HDO	Hydrodeoxygenation
HOMO	Highest Occupied Molecular Orbital
HPLC	High-performance liwqid chromatography
ICP-OES	inductively coupled plasma optical emission spectrometry
L	Length of the catalytic bed
LUMO	Lowest Unoccupied Molecular Orbital
M	Molar, mol L^{-1}
meq g^{-1}	Mol equivalent per gram
MFC	Mass flow controller
MN	Metal nitride
MS	Mass spectrometer
NaOH	Sodium hydroxide
Ni	Nickel
NMR	Nuclear magnetic resonance
NP	Nanoparticle
p	Pressure
Pd	Palladium
Pt	Platinum
Q	Volume stream
R	Mass Specific Reaction Rate

RON	Reserach Octane Number
RT	Room temperature
SEM	Scanning electron microscopy
TEM	Transmission electron microscopy
v	Velocity
V	Volume
W	Tungsten (metallic form)
W_2C	Tungsten semi carbide
WC	Tungsten carbide
WO_3	Tungsten oxide
wt	weight percent
XRD	(wide angle) X-ray diffraction
Y	Yield
Δ	difference
Δp	Pressure difference
ρ	Density
τ	Residence time

10. List of publications

Braun M.; Esposito D., Hydrogenation Properties of Nanostructured Tungsten Carbide Catalysts in a Continuous-Flow Reactor, *ChemCatChem*, **2017**; DOI: 10.1002/cctc.201600927

Braun M.; Thach UD.; Prelot B.; Hesemann P.; Esposito D., Pd@ionosilica as heterogeneous hydrogenation catalyst for continuous flow reductive upgrade of cinnamaldehyde, *Journal of Chemical Technology and Biotechnology*, **2017**; DOI: 10.1002/jctb.5278

Braun M.; Antonietti M., Continuous flow process for the production of 2,5-dimethylfuran from fructose using (non-noble metal based) heterogeneous catalysis, *Green Chemistry*, **2017**, DOI: 10.1039/C7GC01055A

Chieffi G.; Braun M.; Esposito D., Continuous Reductive Amination of Biomass-Derived Molecules over Carbonized Filter Paper-Supported FeNi Alloy, *ChemSusChem*, **2015**; DOI: 10.1002/cssc.201500804

Mbaya Mani C.; Braun M.; Molinari V.; Antonietti M.; Fechler N., A high-throughput composite catalyst based on Nickel carbon cubes for the hydrogenation of 5-hydroxymethylfurfural to 2,5-dimethylfuran, *ChemCatChem*, **2017**, DOI: 10.1002/cctc.201700506

11. Acknowledgements

An dieser Stelle möchte ich mich bei einigen Menschen herzlichst bedanken, welche mich auf meiner „PhD – Reise“ begleitet haben. Während meinen 2.5 Jahren hier am Max-Planck-Institut in Golm sind aus vielen wissenschaftlichen Diskussionen nicht nur Paper, aus Stolpersteinen nicht nur akademische Straßen, sondern aus Kollegen auch gute Freunde geworden. Dieses interkulturelle Umfeld hat mir ermöglicht tolle Menschen über Sprachbarrieren und Ländergrenzen hinweg kennen zu lernen, wofür ich sehr dankbar bin. All diese Zeit hat mich gelehrt, dass man weit mehr erreichen kann, als man vielleicht am Anfang zu hoffen gewagt hat und das man gemeinsam die Welt ein wenig besser machen kann.

Besonderer Dank geht zuallererst an Prof. Markus Antonietti. Sein Enthusiasmus, seine Begeisterung für die Wissenschaft und Bioraffinerie und sein Wille etwas voran zu bringen, hat mich immer wieder inspiriert und mir zusätzlichen Antrieb verliehen. Vielen Dank für die Unterstützung und den steten Support!

Weiterer Dank geht natürlich an Dr. Davide Esposito. Als Mentor und Betreuer hast du mir immer wieder auf den richtigen Pfad geholfen und mich mit Input und Ratschlägen sehr gut beraten. Nicht nur wissenschaftlich, sondern auch freundschaftlich. Danke herzlichst dafür. Grazie mille ;)

Ich bin sehr dankbar, dass ich die schönen, aber auch schwierige Phasen mit so einem tollen Büro teilen durfte! Es hilft sehr, wenn man Freunde neben sich sitzen hat! Vielen Dank an all die Diskussionen, Hilfestellungen, das Lachen, aber auch das sich manchmal ärgern. Ein offenes Ohr von Menschen die den gleichen Weg gehen verstehen viele Dinge einfach am aller Besten! Danke an Mica, Vale, Narasimharao, Marius und Paolo!

Wissenschaftliches Arbeiten wäre auch nicht möglich ohne Kollegen, die auf so vielfältige Weise zur Arbeit beitragen. Sei es im wissenschaftlichen Sinne oder einfach durch ein offenes Ohr. Vielen Dank deshalb an die Bioraffineriegruppe mit Davide, Vale, Mica, Irina, Afro, Elliot, Marius und Llorenc!

Ohne die vielen Messungen und Auswertungen wäre diese Arbeit nicht zu schaffen gewesen. Deshalb auch ein großer Dank an all die helfenden Hände der Technikerinnen. Besonderen Dank an Irina, Regina, Marlies, Sylvia, Ingrid, Antje, Jessica, Ursula, Heike und Rona. Und ohne Bodo, seine guten Ideen und seine Basteleien würde hier auch manches schwieriger zu realisieren sein.

Eines meiner größten Hobbies war und ist das Laufen. Danke für das gemeinsame Training und die Wettkämpfe, Mica, Menny, Karo, Tom und natürlich Markus!

Und was wäre all die Arbeit, wenn man nicht auch ein wenig die Freizeit zusammen genießt. Deshalb vielen Dank an all die tollen Kollegen, die ich während meiner Zeit hier kennen lernen durfte. Während meiner Arbeit habe ich so viele hervorragende Wissenschaftler und vor allem Menschen kennen lernen dürfen, mit denen ich mal ein längeres, mal ein kürzeres Stück zusammen gegangen bin. An dieser Stelle sei ALLEN hierfür gedankt! Kollegen, Freunden und meiner „Berlin Family“.

Und all das, was ich mir über die Jahre vom Abitur bis zu diesem Meilenstein heute erarbeitet habe, wäre ohne die ständige Unterstützung meiner wunderbaren Familie nicht möglich gewesen! Vielen herzlichen Dank euch ALLEN. Ihr seid die Besten!

“Der Fortgang der wissenschaftlichen Entwicklung ist im Endeffekt eine ständige Flucht vor dem Staunen.”

Albert Einstein

12. Declaration

Die vorliegende Dissertation entstand im Zeitraum zwischen März 2015 und September 2017 am Max-Planck-Institut für Kolloid- und Grenzflächenforschung, unter der Betreuung von Prof. Dr. Markus Antonietti.

Hiermit erkläre ich, dass die vorliegende Arbeit selbstständig angefertigt und keine anderen als die angegebenen Hilfsmittel und Quellen verwendet wurden.

Max Braun

Potsdam, September 2017

13. References

[1] C. Econometrics*, Vol. 2017*, Cambridge Econometrics, **2016**.

[2] B. Kamm, M. Kamm, P. R. Gruber, S. Kromus, in *Biorefineries-Industrial Processes and Products*, Wiley-VCH Verlag GmbH, **2008**, pp. 1-40.

[3] J.-P. Wauquier, *Petroleum Refining: Crude oil, petroleum products, process flowsheets, Vol. 1*, Editions Technip, **1995**.

[4] R. Van Ree, E. Annevelink, Agrotechnology & Food Sciences Group, **2007**.

[5] T. Werpy, G. Petersen, ; National Renewable Energy Lab., Golden, CO (US), **2004**, p. Medium: ED; Size: 76 pp. pages.

[6] aM. Kröger, U. Prüße, K.-D. Vorlop, *Topics in Catalysis* **2000**, *13*, 237-242; bB. Girisuta, L. P. B. M. Janssen, H. J. Heeres, *Chemical Engineering Research and Design* **2006**, *84*, 339-349.

[7] L. Atanda, M. Konarova, Q. Ma, S. Mukundan, A. Shrotri, J. Beltramini, *Catalysis Science & Technology* **2016**, *6*, 6257-6266.

[8] T. M. Quigley, A. S. Mackenzie, *Nature* **1988**, *333*, 549-552.

[9] M. Gross, *Current Biology* **2014**, *24*, R583-R585.

[10] *Reference Reviews* **2010**, *24*, 19-19.

[11] R. B. Jackson, A. Vengosh, J. W. Carey, R. J. Davies, T. H. Darrah, F. O'Sullivan, G. Pétron, *Annual Review of Environment and Resources* **2014**, *39*, 327-362.

[12] D. J. Anderson, C. F. Kirkvold, P. Pisio, Google Patents, **1976**.

[13] P. McKendry, *Bioresource Technology* **2002**, *83*, 55-63.

[14] P. McKendry, *Bioresource Technology* **2002**, *83*, 37-46.

[15] E. E. Harris, *Advances in Carbohydrate Chemistry* **1949**, *4*, 153-188.

[16] V. Molinari, C. Giordano, M. Antonietti, D. Esposito, *Journal of the American Chemical Society* **2014**, *136*, 1758-1761.

[17] D. M. Alonso, J. Q. Bond, J. A. Dumesic, *Green Chemistry* **2010**, *12*, 1493-1513.

[18] a*Chemistry & Industry* **2013**, *77*, 20-23; bS. G. Newman, K. F. Jensen, *Green Chemistry* **2013**, *15*, 1456-1472.

[19] P. Anastas, N. Eghbali, *Chemical Society Reviews* **2010**, *39*, 301-312.

[20] A. Mountraki, M. Tsakalova, A. Panteli, A. I. Papoutsi, A. C. Kokossis, *Industrial & Engineering Chemistry Research* **2016**, *55*, 3478-3492.

[21] P. Bhaumik, P. L. Dhepe, in *Biomass Sugars for Non-Fuel Applications*, The Royal Society of Chemistry, **2016**, pp. 1-53.

[22] B. Saha, M. M. Abu-Omar, *ChemSusChem* **2015**, *8*, 1133-1142.

[23] R. Daniel, H. Xu, C. Wang, D. Richardson, S. Shuai, *Applied Energy* **2012**, *98*, 59-68.

[24] X. Tong, Y. Ma, Y. Li, *Applied Catalysis A: General* **2010**, *385*, 1-13.

[25] H. Joshi, B. R. Moser, J. Toler, W. F. Smith, T. Walker, *Biomass and Bioenergy* **2011**, *35*, 3262-3266.

[26] M. Wayman, A. Dzenis, *The Canadian Journal of Chemical Engineering* **1984**, *62*, 699-705.

[27] N. Mosier, C. Wyman, B. Dale, R. Elander, Y. Y. Lee, M. Holtzapple, M. Ladisch, *Bioresource Technology* **2005**, *96*, 673-686.

[28] A. A. Rosatella, S. P. Simeonov, R. F. M. Frade, C. A. M. Afonso, *Green Chemistry* **2011**, *13*, 754-793.

[29] R.-J. van Putten, J. C. van der Waal, E. de Jong, C. B. Rasrendra, H. J. Heeres, J. G. de Vries, *Chemical Reviews* **2013**, *113*, 1499-1597.

[30] M. E. Baumgardner, T. L. Vaughn, A. Lakshminarayanan, D. Olsen, M. A. Ratcliff, R. L. McCormick, A. J. Marchese, *Energy & Fuels* **2015**, *29*, 7317-7326.

[31] D. A. Rothamer, J. H. Jennings, *Fuel* **2012**, *98*, 203-212.

[32] L. Petrus, M. A. Noordermeer, *Green Chemistry* **2006**, *8*, 861-867.

[33] Y. Roman-Leshkov, C. J. Barrett, Z. Y. Liu, J. A. Dumesic, *Nature* **2007**, *447*, 982-985.
[34] E. B. Fitzherbert, M. J. Struebig, A. Morel, F. Danielsen, C. A. Brühl, P. F. Donald, B. Phalan, *Trends in Ecology & Evolution* **2008**, *23*, 538-545.
[35] D. Pimentel, *Natural Resources Research* **2003**, *12*, 127-134.
[36] S. Zhong, R. Daniel, H. Xu, J. Zhang, D. Turner, M. L. Wyszynski, P. Richards, *Energy & Fuels* **2010**, *24*, 2891-2899.
[37] Y. Roman-Leshkov, C. J. Barrett, Z. Y. Liu, J. A. Dumesic, *Nature* **2007**, *447*, 982-985.
[38] M. Malenshek, D. B. Olsen, *Fuel* **2009**, *88*, 650-656.
[39] P. J. Jessup, Google Patents, **1989**.
[40] F. Cherubini, *Energy Conversion and Management* **2010**, *51*, 1412-1421.
[41] K. Tong, M. J. Gleeson, G. Rong, F. You, *Biomass and Bioenergy* **2014**, *60*, 108-120.
[42] R. E. Blankenship, D. M. Tiede, J. Barber, G. W. Brudvig, G. Fleming, M. Ghirardi, M. R. Gunner, W. Junge, D. M. Kramer, A. Melis, T. A. Moore, C. C. Moser, D. G. Nocera, A. J. Nozik, D. R. Ort, W. W. Parson, R. C. Prince, R. T. Sayre, *Science (New York, N.Y.)* **2011**, *332*, 805-809.
[43] H. Xu, C. Wang, in *Biofuels from Lignocellulosic Biomass*, Wiley-VCH Verlag GmbH & Co. KGaA, **2016**, pp. 105-129.
[44] V. K. Varshney, S. Naithani, in *Cellulose Fibers: Bio- and Nano-Polymer Composites: Green Chemistry and Technology* (Eds.: S. Kalia, B. S. Kaith, I. Kaur), Springer Berlin Heidelberg, Berlin, Heidelberg, **2011**, pp. 43-60.
[45] M. B. Sticklen, *Nat Rev Genet* **2008**, *9*, 433-443.
[46] R. Vanholme, B. Demedts, K. Morreel, J. Ralph, W. Boerjan, *Plant Physiology* **2010**, *153*, 895-905.
[47] J. Zakzeski, P. C. A. Bruijnincx, A. L. Jongerius, B. M. Weckhuysen, *Chemical Reviews* **2010**, *110*, 3552-3599.
[48] H. Wang, M. Tucker, Y. Ji, *Journal of Applied Chemistry* **2013**, *2013*, 9.
[49] A. Fukuoka, P. L. Dhepe, *Angewandte Chemie* **2006**, *118*, 5285-5287.
[50] X. Tan, W. Deng, M. Liu, Q. Zhang, Y. Wang, *Chemical Communications* **2009**, 7179-7181.
[51] M. Mascal, E. B. Nikitin, *Angewandte Chemie* **2008**, *120*, 8042-8044.
[52] J. B. Binder, J. J. Blank, A. V. Cefali, R. T. Raines, *ChemSusChem* **2010**, *3*, 1268-1272.
[53] W. Yang, A. Sen, *ChemSusChem* **2010**, *3*, 597-603.
[54] R. Taylor, L. Nattrass, G. Alberts, P. Robson, C. Chudziak, A. Bauen, I. Libelli, G. Lotti, M. Prussi, R. Nistri, E4tech/Re-CORD/Wageningen UR, **2015**.
[55] G. Rothenberg, in *Catalysis*, Wiley-VCH Verlag GmbH & Co. KGaA, **2008**, pp. 39-75.
[56] E. E. Santiso, A. M. George, C. H. Turner, M. K. Kostov, K. E. Gubbins, M. Buongiorno-Nardelli, M. Sliwinska-Bartkowiak, *Applied Surface Science* **2005**, *252*, 766-777.
[57] D. Astruc, F. Lu, J. R. Aranzaes, *Angewandte Chemie International Edition* **2005**, *44*, 7852-7872.
[58] A. S. Kashin, V. P. Ananikov, *The Journal of Organic Chemistry* **2013**, *78*, 11117-11125.
[59] H. Häkkinen, S. Abbet, A. Sanchez, U. Heiz, U. Landman, *Angewandte Chemie International Edition* **2003**, *42*, 1297-1300.
[60] X. Zhou, W. Xu, G. Liu, D. Panda, P. Chen, *Journal of the American Chemical Society* **2010**, *132*, 138-146.
[61] M. Comotti, W.-C. Li, B. Spliethoff, F. Schüth, *Journal of the American Chemical Society* **2006**, *128*, 917-924.
[62] J. Yang, Y. Xie, R. Wang, B. Jiang, C. Tian, G. Mu, J. Yin, B. Wang, H. Fu, *ACS Applied Materials & Interfaces* **2013**, *5*, 6571-6579.
[63] A. K. Singh, Q. Xu, *ChemCatChem* **2013**, *5*, 652-676.
[64] P. J. Dyson, P. G. Jessop, *Catalysis Science & Technology* **2016**, *6*, 3302-3316.
[65] S. S. Y. Tan, D. R. MacFarlane, in *Ionic Liquids* (Ed.: B. Kirchner), Springer Berlin Heidelberg, Berlin, Heidelberg, **2010**, pp. 311-339.
[66] R. Porta, M. Benaglia, A. Puglisi, *Organic Process Research & Development* **2016**, *20*, 2-25.

[67] H. D. B. Jenkins, in *Chemical Thermodynamics at a Glance*, Blackwell Publishing Ltd, **2008**, pp. 160-163.
[68] S. Belletante, L. Montastruc, S. Negny, S. Domenech, *Biochemical Engineering Journal* **2016**, *116*, 195-209.
[69] G. A. Somorjai, K. R. McCrea, J. Zhu, *Topics in Catalysis* **2002**, *18*, 157-166.
[70] W. Boerjan, J. Ralph, M. Baucher, *Annual review of plant biology* **2003**, *54*, 519-546.
[71] J. Pérez, J. Muñoz-Dorado, T. de la Rubia, J. Martínez, *International Microbiology* **2002**, *5*, 53-63.
[72] C. Li, X. Zhao, A. Wang, G. W. Huber, T. Zhang, *Chemical Reviews* **2015**, *115*, 11559-11624.
[73] H. Yang, R. Yan, H. Chen, D. H. Lee, C. Zheng, *Fuel* **2007**, *86*, 1781-1788.
[74] O. A. T. Mafe, N. Pensupa, E. M. Roberts, C. Du, in *Renewable Resources for Biorefineries*, The Royal Society of Chemistry, **2014**, pp. 117-145.
[75] D. Murzin, P. Dhepe, K. Seshan, G. Kraus, P. Fardim, J. H. Clark, J. Kovensky, R. Leino, P. Seidl, *Biomass Sugars for Non-fuel Applications*, Royal Society of Chemistry, **2015**.
[76] C. E. Wyman, S. R. Decker, M. E. Himmel, J. W. Brady, C. E. Skopec, L. Viikari, *Polysaccharides: structural diversity and functional versatility* **2005**, *1*, 1023-1062.
[77] L. Hobbs, in *Starch (Third Edition)*, Academic Press, San Diego, **2009**, pp. 797-832.
[78] R. S. Assary, T. Kim, J. J. Low, J. Greeley, L. A. Curtiss, *Physical Chemistry Chemical Physics* **2012**, *14*, 16603-16611.
[79] M. Graglia, N. Kanna, D. Esposito, *ChemBioEng Reviews* **2015**, *2*, 377-392.
[80] B. Kamm, M. Kamm, M. Schmidt, T. Hirth, M. Schulze, in *Biorefineries-Industrial Processes and Products*, Wiley-VCH Verlag GmbH, **2008**, pp. 97-149.
[81] W. L. Faith, *Industrial & Engineering Chemistry* **1945**, *37*, 9-11.
[82] M. J. Taherzadeh, K. Karimi, *BioResources* **2007**, *2*, 472-499.
[83] F. Bergius, *Industrial & Engineering Chemistry* **1937**, *29*, 247-253.
[84] A. J. Ragauskas, C. K. Williams, B. H. Davison, G. Britovsek, J. Cairney, C. A. Eckert, W. J. Frederick, J. P. Hallett, D. J. Leak, C. L. Liotta, *Science (New York, N.Y.)* **2006**, *311*, 484-489.
[85] E. Farnetti, R. Di Monte, J. Kašpar, *Inorganic and bioinorganic chemistry* **2009**, *2*, 50.
[86] P. J. Denny, M. V. Twigg, *Studies in Surface Science and Catalysis* **1980**, *6*, 577-599.
[87] G. Eigenberger, *Fixed-Bed Reactors*, Wiley Online Library, **2000**.
[88] C. Mbaya Mani, M. Braun, V. Molinari, M. Antonietti, N. Fechler, *ChemCatChem* **2017**, n/a-n/a.
[89] R. Farra, A. Rinaldi, M. Greiner, J. Cao, R. Schlögl, M.-G. Willinger, in *European Microscopy Congress 2016: Proceedings*, Wiley-VCH Verlag GmbH & Co. KGaA, **2016**.
[90] M. Zabeti, W. M. A. Wan Daud, M. K. Aroua, *Fuel Processing Technology* **2009**, *90*, 770-777.
[91] P. Gupta, S. Paul, *Catalysis Today* **2014**, *236*, 153-170.
[92] A. Primo, F. Neatu, M. Florea, V. Parvulescu, H. Garcia, *Nature communications* **2014**, *5*, 5291.
[93] G. Brieger, T. J. Nestrick, *Chemical Reviews* **1974**, *74*, 567-580.
[94] H. S. Fogler, **1999**.
[95] O. Levenspiel, *The chemical reactor omnibook, Vol. 3*, OSU book stores Oregon, USA, **1996**.
[96] Y. Nakagawa, S. Liu, M. Tamura, K. Tomishige, *ChemSusChem* **2015**, *8*, 1114-1132.
[97] S. De, J. Zhang, R. Luque, N. Yan, *Energy & Environmental Science* **2016**, *9*, 3314-3347.
[98] J. Zhao, C. Zhou, C. He, Y. Dai, X. Jia, Y. Yang, *Catalysis Today* **2016**, *264*, 123-130.
[99] L. Hu, L. Lin, S. Liu, *Industrial & Engineering Chemistry Research* **2014**, *53*, 9969-9978.
[100] J. S. Lee, K. Ogawa, *JOURNAL OF CHEMICAL ENGINEERING OF JAPAN* **1994**, *27*, 691-693.
[101] R. S. Subramanian, *Clarkson University* **2004**.
[102] A. Züttel, *Naturwissenschaften* **2004**, *91*, 157-172.
[103] K.-K. Cheng, X.-B. Zhao, J. Zeng, J.-A. Zhang, *Biofuels, Bioproducts and Biorefining* **2012**, *6*, 302-318.
[104] F. K. Kazi, A. D. Patel, J. C. Serrano-Ruiz, J. A. Dumesic, R. P. Anex, *Chemical Engineering Journal* **2011**, *169*, 329-338.

[105] R. F. Tester, J. Karkalas, X. Qi, *Journal of Cereal Science* **2004**, *39*, 151-165.
[106] J. Deng, T. Xiong, H. Wang, A. Zheng, Y. Wang, *ACS Sustainable Chemistry & Engineering* **2016**, *4*, 3750-3756.
[107] R. Xing, Y. Liu, Y. Wang, L. Chen, H. Wu, Y. Jiang, M. He, P. Wu, *Microporous and Mesoporous Materials* **2007**, *105*, 41-48.
[108] R. Kunin, E. A. Meitzner, J. A. Oline, S. A. Fisher, N. Frisch, *I&EC Product Research and Development* **1962**, *1*, 140-144.
[109] M. Sevilla, A. B. Fuertes, *Carbon* **2009**, *47*, 2281-2289.
[110] M. Toda, A. Takagaki, M. Okamura, J. N. Kondo, S. Hayashi, K. Domen, M. Hara, *Nature* **2005**, *438*, 178-178.
[111] M. Hurtta, I. Pitkänen, J. Knuutinen, *Carbohydrate Research* **2004**, *339*, 2267-2273.
[112] H. Sugisawa, H. Edo, *Journal of Food Science* **1966**, *31*, 561-565.
[113] I. S. Fagerson, *Journal of Agricultural and Food Chemistry* **1969**, *17*, 747-750.
[114] J.-B. Donnet, *Carbon black: science and technology*, CRC Press, **1993**.
[115] A. Primo, A. Forneli, A. Corma, H. García, *ChemSusChem* **2012**, *5*, 2207-2214.
[116] X. Y. Liu, M. Huang, H. L. Ma, Z. Q. Zhang, J. M. Gao, Y. L. Zhu, X. J. Han, X. Y. Guo, *Molecules (Basel, Switzerland)* **2010**, *15*, 7188-7196.
[117] N. Jiang, R. Huang, W. Qi, R. Su, Z. He, *BioEnergy Research* **2012**, *5*, 380-386.
[118] R. Nie, X. Peng, H. Zhang, X. Yu, X. Lu, D. Zhou, Q. Xia, *Catalysis Science & Technology* **2017**, *7*, 627-634.
[119] S. Navalon, A. Dhakshinamoorthy, M. Alvaro, H. Garcia, *Chemical Reviews* **2014**, *114*, 6179-6212.
[120] Z. Z. Fang, X. Wang, T. Ryu, K. S. Hwang, H. Y. Sohn, *International Journal of Refractory Metals and Hard Materials* **2009**, *27*, 288-299.
[121] M. S. El-Eskandarany, T. Konno, K. Sumiyama, K. Suzuki, M. Omori, T. Hirai, M. Ishikuro, K. Takada, *Metallurgical and Materials Transactions A* **1996**, *27*, 4210-4213.
[122] F. Harnisch, G. Sievers, U. Schröder, *Applied Catalysis B: Environmental* **2009**, *89*, 455-458.
[123] R. Ooms, M. Dusselier, J. A. Geboers, B. Op de Beeck, R. Verhaeven, E. Gobechiya, J. A. Martens, A. Redl, B. F. Sels, *Green Chemistry* **2014**, *16*, 695-707.
[124] S. Ramanathan, S. T. Oyama, *The Journal of Physical Chemistry* **1995**, *99*, 16365-16372.
[125] D. Ham, J. Lee, *Energies* **2009**, *2*, 873.
[126] I. Lee, F. Delbecq, R. Morales, M. A. Albiter, F. Zaera, *Nat Mater* **2009**, *8*, 132-138.
[127] E. Gross, *Studies in Surface Science and Catalysis* **2017**, *177*, 57-84.
[128] W. C. Conner, J. L. Falconer, *Chemical Reviews* **1995**, *95*, 759-788.
[129] A. Kurlov, A. Gusev, *Inorganic Materials* **2006**, *42*, 121-127.
[130] A. Primo, H. García, in *New and Future Developments in Catalysis*, Elsevier, Amsterdam, **2013**, pp. 425-449.
[131] Y. Xi, L. Huang, R. C. Forrey, H. Cheng, *RSC Advances* **2014**, *4*, 39912-39919.
[132] C. Giordano, C. Erpen, W. Yao, M. Antonietti, *Nano letters* **2008**, *8*, 4659-4663.
[133] C. B. Rodella, D. H. Barrett, S. F. Moya, S. J. A. Figueroa, M. T. B. Pimenta, A. A. S. Curvelo, V. Teixeira da Silva, *RSC Advances* **2015**, *5*, 23874-23885.
[134] R. V. Jones, L. Godorhazy, N. Varga, D. Szalay, L. Urge, F. Darvas, *Journal of Combinatorial Chemistry* **2006**, *8*, 110-116.
[135] M. Braun, D. Esposito, *ChemCatChem* **2017**, *9*, 393-397.
[136] J. Stachurski, J. M. Thomas, *Catalysis Letters* **1988**, *1*, 67-72.
[137] R. D. Cortright, M. Sanchez-Castillo, J. A. Dumesic, *Applied Catalysis B: Environmental* **2002**, *39*, 353-359.
[138] V. Molinari, M. Antonietti, D. Esposito, *Catalysis Science & Technology* **2014**, *4*, 3626-3630.
[139] M. Braun, M. Antonietti, *Green Chemistry* **2017**, *19*, 3813-3819.
[140] X. Tiancun, A. Lidun, Z. Weimin, S. Shishan, X. Guoxin, *Catalysis Letters* **1992**, *12*, 287-296.
[141] G.-Y. Jeong, A. K. Singh, S. Sharma, K. W. Gyak, R. A. Maurya, D.-P. Kim, *NPG Asia Mater* **2015**, *7*, e173.

[142] G. Tian, H. Xu, R. Daniel, *DMF-a new biofuel candidate*, InTech, **2011**.
[143] N. Li, W. Wang, M. Zheng, T. Zhang, *Catalytic Hydrogenation for Biomass Valorization* **2014**, 22.
[144] M. A. Sánchez, G. C. Torres, V. A. Mazzieri, C. L. Pieck, *Journal of Chemical Technology & Biotechnology* **2017**, *92*, 27-42.
[145] T. Thananatthanachon, T. B. Rauchfuss, *Angewandte Chemie International Edition* **2010**, *49*, 6616-6618.
[146] S. Murat Sen, C. A. Henao, D. J. Braden, J. A. Dumesic, C. T. Maravelias, *Chemical Engineering Science* **2012**, *67*, 57-67.
[147] A. Boisen, T. B. Christensen, W. Fu, Y. Y. Gorbanev, T. S. Hansen, J. S. Jensen, S. K. Klitgaard, S. Pedersen, A. Riisager, T. Ståhlberg, J. M. Woodley, *Chemical Engineering Research and Design* **2009**, *87*, 1318-1327.
[148] C. Triebl, V. Nikolakis, M. Ierapetritou, *Computers & Chemical Engineering* **2013**, *52*, 26-34.
[149] R. P. Anex, A. Aden, F. K. Kazi, J. Fortman, R. M. Swanson, M. M. Wright, J. A. Satrio, R. C. Brown, D. E. Daugaard, A. Platon, G. Kothandaraman, D. D. Hsu, A. Dutta, *Fuel* **2010**, *89*, S29-S35.
[150] Y. Qian, L. Zhu, Y. Wang, X. Lu, *Renewable and Sustainable Energy Reviews* **2015**, *41*, 633-646.
[151] G. W. Festel, *Chemical Engineering & Technology* **2008**, *31*, 715-720.